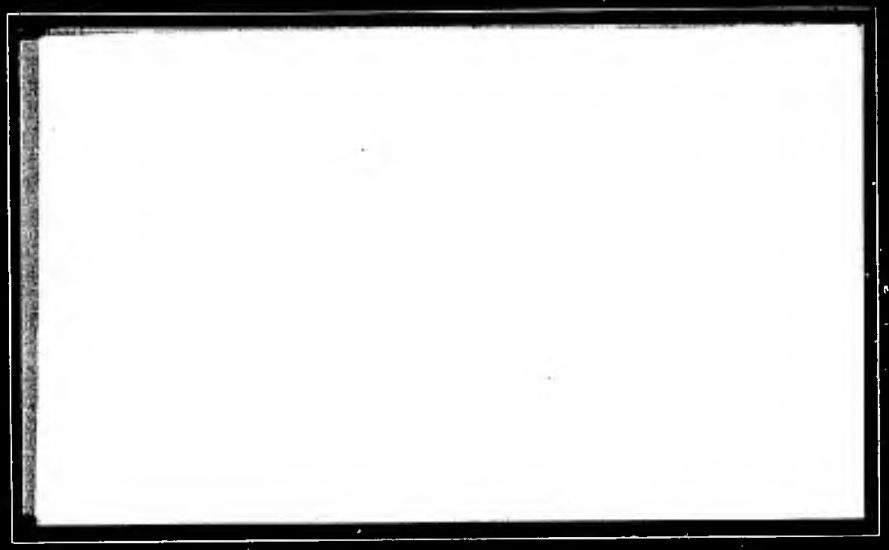

Microwave Laboratory

W. W. HANSEN LABORATORIES OF PHYSICS

STANFORD UNIVERSITY · STANFORD, CALIFORNIA

THE STIMULATED RAMAN EFFECT AND ITS APPLICATION AS A TUNABLE LASER

by

H. E. Puthoff

M. L. Report No. 1547

Technical Report
Contract Nonr 225(48)
June 1967

Microwave Laboratory
W. W. Hansen Laboratories of Physics
Stanford University
Stanford, California

ABSTRACT

The stimulated Raman effect provides an efficient means for producing coherent optical signals throughout the visible and infrared portion of the spectrum using a single laser source as exciter and either a crystal or a cell containing a gas or liquid as the target. The Raman-shifted output retains the high-intensity well-collimated monochromatic properties of the original laser. The objectives of the research program presented here were to investigate those aspects of the Raman effect relevant to the possibility of constructing a tunable Raman laser in which continuous tuning over tens of angstroms could be expected.

The approach used in the theoretical development is unique in certain respects, and therefore worthy of special mention. Originating with work by Jaynes and developed and applied extensively by Pantell and co-workers, the method is based on the density matrix formulation. It differs from that in general use in the literature, however, in that the expectation values of operators of interest are formed by the trace prescription $p = \langle \mu \rangle = Tr(\rho\mu)$ and substituted into the density matrix equations before they are solved. As a result, the differential equations to be solved are in terms of macroscopic variables of interest such as polarization, and thereby lend themselves readily to physical interpretation.

The theory of the tunable Raman effect is developed and it is shown that for tuning to occur, (a) the medium must lack a center of symmetry, (b) the vibrational transition involved in the Raman scattering event must be not only Raman active but also infrared absorbing, and (c) angular separation between the Raman and exciting laser beams is necessary. Tuning is accomplished by adjustment of the angle between the Raman and laser beams by rotation of a resonator for the Raman beam which is off axis relative to the laser beam. In the Raman scattering process, wave vector conservation (i.e., phase matching) determines the wave vector of the vibrational wave, which in turn determines the operating point on the vibrational dispersion characteristic and hence controls the frequency.

The tuning concept is verified experimentally by the measurement of a 50 Å tuning characteristic of an infrared-absorbing optical vibrational mode (628 cm^{-1}) in the crystal lithium niobate ($LiNbO_3$), accomplished by means of spontaneous Raman scattering of a He-Ne gas laser beam. The application of this technique provided, in addition to the tuning characteristic of interest, a plot of the dispersion characteristic of the vibrational mode of the crystal, a material property of interest in its own right.

The application of the tunable Raman effect as a tunable Raman laser operating above threshold is considered. The theory and design is based on the use of an off-axis resonator system in which the Raman and laser beams are not collinear. The tunable laser is shown to be a threshold device which provides for the conversion of power at the laser frequency into power at the Raman frequency in accordance with the usual parametric device Manley-Rowe relationships. Experimental verification of the theory and design is presented in terms of a study reported in detail elsewhere which demonstrates that the stimulated Raman effect in an off-axis resonator system behaves as predicted.

The results of the experimental study of the tuning characteristic of $LiNbO_3$ and the generation of stimulated Raman emission in an off-axis resonator, when taken together, indicate that the construction of a tunable Raman laser based on the 628 cm^{-1} transition in $LiNbO_3$ is feasible. Under present state-of-the-art conditions an estimated laser pump power $\sim$ 4 Mw/cm^2 for a crystal $\sim$ 0.5 cm long is required to reach threshold.

In summary, the main contributions of this study consist of the analysis of the tunable Raman effect, the measurement of the tuning and dispersion characteristics of an optical mode in the crystal $LiNbO_3$, and the presentation of the theory, design, and feasibility of the construction of a tunable Raman laser.

The tuning concept is verified experimentally by the measurement of a 50 Å tuning characteristic of an infrared-absorbing optical vibrational mode (628 cm^{-1}) in the crystal lithium niobate ($LiNbO_3$), accomplished by means of spontaneous Raman scattering of a He-Ne gas laser beam. The application of this technique provided, in addition to the tuning characteristic of interest, a plot of the dispersion characteristic of the vibrational mode of the crystal, a material property of interest in its own right.

The application of the tunable Raman effect as a tunable Raman laser operating above threshold is considered. The theory and design is based on the use of an off-axis resonator system in which the Raman and laser beams are not collinear. The tunable laser is shown to be a threshold device which provides for the conversion of power at the laser frequency into power at the Raman frequency in accordance with the usual parametric device Manley-Rowe relationships. Experimental verification of the theory and design is presented in terms of a study reported in detail elsewhere which demonstrates that the stimulated Raman effect in an off-axis resonator system behaves as predicted.

The results of the experimental study of the tuning characteristic of $LiNbO_3$ and the generation of stimulated Raman emission in an off-axis resonator, when taken together, indicate that the construction of a tunable Raman laser based on the 628 cm^{-1} transition in $LiNbO_3$ is feasible. Under present state-of-the-art conditions an estimated laser pump power ~ 4 Mw/cm^2 for a crystal ~ 0.5 cm long is required to reach threshold.

In summary, the main contributions of this study consist of the analysis of the tunable Raman effect, the measurement of the tuning and dispersion characteristics of an optical mode in the crystal $LiNbO_3$, and the presentation of the theory, design, and feasibility of the construction of a tunable Raman laser.

ACKNOWLEDGEMENTS

I would like to begin by stating that in the course of this work it has become increasingly clear to the author that all human endeavor is truly a joint enterprise, for it is the mutual interaction and stimulation which makes it all worthwhile.

I wish especially to acknowledge that Professor R. H. Pantell served not only as my advisor, but also as a friend and counselor from whom I learned much, both technically and in the broader sense, and I shall always be grateful for our association.

I also wish to thank my co-worker Mr. B. G. Huth for his many creative contributions throughout this work and to express to him that I have always found our collaboration to be both encouraging and fruitful.

To Professor S. E. Harris I would like to express my appreciation for our many discussions which always proved to be stimulating and rewarding. I am also grateful to Professor R. L. White for his suggestions concerning clarification and emphasis which grew out of his reading of the manuscript.

It is also a pleasure to acknowledge the invaluable technical assistance of Mr. M. A. Chacon in assembling together experimental apparatus, and Messrs. Robert Griffin and Forrest Futtere in preparing various optical components and samples, and I wish to thank Messrs. R. Feigelson and E. Lean for supplying the crystals used in this work. I am also indebted to Mr. Norman Bettini and the drafting room for their part in the preparation of the drawings and figures. I would like especially to acknowledge the fine work of Mrs. Julie Spranza who executed most of the figures.

I also wish to express my sincere appreciation to Mrs. R. Caulk who typed the first draft and to Dr. A. S. Braun and Mmes. Iona Williams, Suzanne Wise, Betty Dutton, and Pauline Brady who provided not only technical skills but also a sense of esprit de corps in the preparation of the final manuscript. I wish to single out especially Mrs. Williams for her generous spirit which was overwhelmingly apparent in the tireless effort put forth during last-minute typing of the major portion of the manuscript.

Finally, I wish to thank my wife Jan, whose loving contribution to my life insures that any contribution of mine is a product of a joint venture.

TABLE OF CONTENTS

LIST OF FIGURES

CHAPTER I

INTRODUCTION

A. RAMAN EFFECT

In 1928 Raman and Krishnan, in a series of light-scattering experiments with liquids and gaseous vapors, observed that a certain small percentage of the light experienced a substantial frequency shift (~ several hundred angstroms) during the scattering process.[1] In the same year the effect was observed independently by Landsberg and Mandelstam in work with crystals.[2] In their experiments the frequency shifts were found to correspond to the natural vibrational resonances of the scattering substance under consideration. From this observation it was inferred that nonlinearities in the polarizability of the material were responsible for a "mixing" action which beat together the input radiation and natural resonances to produce sum and difference frequencies. Such a process is illustrated in Fig. 1.1. The phenomenon has become known as the Raman effect and is now a basic tool in spectroscopic work.

1. Stimulated Raman Effect

Interest in the Raman effect has increased sharply in the last few years as intense laser sources have become available. One reason is that the effect is now more readily observable and therefore more useful as a tool in studying the properties of materials. The primary reason, however, lies in the fact that the shifted lines can themselves participate in stimulated processes characteristic of lasers and thus provide new sources of coherent optical radiation. This latter effect has been designated the stimulated Raman effect.

The stimulated Raman effect was discovered in 1962 in an experiment by Woodbury and Ng in which they observed an unexpected emission line at 7670 Å in the output of a Q switched ruby laser (6943 Å).[3] By its

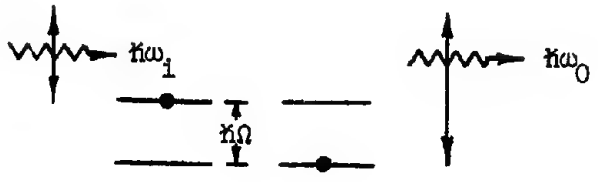

(a) Sum-frequency production

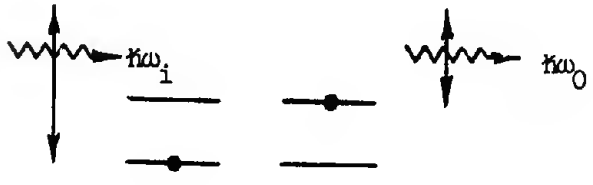

(b) Difference-frequency production

FIG. 1.1--The Raman effect is a nonlinear light-scattering process which beats together the input radiation field and natural resonances of the medium to produce photons at the sum and difference frequencies. The above figure indicates how photons in the incident beam are converted into such output photons with an accompanying change in the state of excitation of the medium. The length of a vertical arrow corresponds to the energy carried by the given photon.

intensity and collimation it was apparent that the new line resulted from stimulated emission, although the wavelength corresponded to no known transition in ruby. The effect was correctly interpreted by Eckhardt, et al., as resulting from stimulated Raman emission from molecular vibrations in the nitrobenzene-filled Kerr cell used for Q-switching.[4] A detailed step-by-step description of the discovery and its interpretation was presented at the Third International Quantum Electronics Conference held in Paris, January, 1963, and is available in the Conference Proceedings.[5] The original discovery was soon followed by the observation of stimulated Raman emission from several other materials including other liquids, both organic[6] and inorganic,[7] crystals,[8] and gases.[9] Concurrent with the early experimental work, the theory was developed by Hellwarth[3,10,11] and others[12,13] to explain the stimulated effect which is illustrated in Fig. 1.2.

Whereas ordinary Raman scattering efficiencies are of the order of 10^{-6} scattered photons per incident photon, the stimulated effect has yielded laser-to-Raman conversion efficiencies as high as 30% in organic liquids[5] and efficiences approaching unity are theoretically possible.[11] The stimulated Raman effect thus provides an efficient means for producing coherent optical signals throughout the visible and infrared spectrum in a selectively-controlled manner using only a single laser source as exciter, and either a crystal or a cell containing a liquid or gas as the target. To date more than 100 coherent lines have been observed,[14,15] and the range of frequencies covered extends considerably beyond the simple Raman shifts because of iterative and parametric processes in which the initially-generated Raman line itself acts as a pump source for further shifts. A current list of materials from which stimulated Raman scattering has been observed is included as Appendix A.

2. Self-Focusing Phenomenon

Following initial work in the stimulated Raman effect, which was directed primarily toward the search for new materials and the development of the theory, more quantitative studies were undertaken in an effort to determine Raman scattering cross-sections from stimulated experiments. It was found that in almost all of the studies with organic liquids the

FIG. 1.2--In the stimulated Raman effect, the conversion of input radiation to radiation at the difference frequency takes place in the presence of other photons at the difference frequency. The newly-generated photons are emitted "in step with" the Raman radiation already present, i.e., as a coherent wave with the same phase and direction.

experimentally-determined cross sections were one to two orders of magnitude greater[16-23] than those expected on the basis of low-level spontaneous Raman scattering experiments.[24,25] Exceptions to this were experiments with off-axis resonators in which the Raman and laser beams were not collinear,[26,27] and an experiment in which the Raman cell was pumped by a diffuse laser beam.[28] In these latter experiments gains consistent with theory were observed.

Several ideas were put forth to explain the above-mentioned discrepancy,[23] and a series of experiments by workers in several laboratories finally revealed that the anomalous gain effect was due to self-focusing and self-trapping of the optical beams.[29-41] In this phenomenon the index of refraction increases in regions of high intensity due to the Kerr effect or the electrostrictive effect. The increase in the index of refraction then produces self-perpetuating lens effects which result in the formation of intense filaments 5–80 microns in diameter. As a result, the effective intensity is much greater than one would expect in the absence of self-focusing, resulting in a lowered threshold requirement for stimulated Raman emission. In fact, in self-focusing liquids threshold depends not so much on the strength of the Raman scattering cross-section as on the self-focusing properties of the liquid. It has been shown unequivocally by Wang[34] that the power required to reach threshold is simply that power required to bring the so-called "self-focusing" length just inside the far end of the Raman cell (see Fig. 1.3). Although a bonus from the standpoint of reduced thresholds and increased power outputs, the self-focusing phenomenon makes it extremely difficult to study the stimulated Raman effect quantitatively in self-focusing liquids.

3. Stimulated Raman Effect in an Optical Resonator

If such studies were to be made, it was clear that it would be necessary to employ an experimental technique which in some manner would average out the effects of self-focusing. An investigation undertaken by a Stanford group (Huth, Karlov, Pantell, and Puthoff) showed that the use of an off-axis resonator provides just such a technique,[42-46] This explains the results of early experimental work with off-axis systems[26,27]

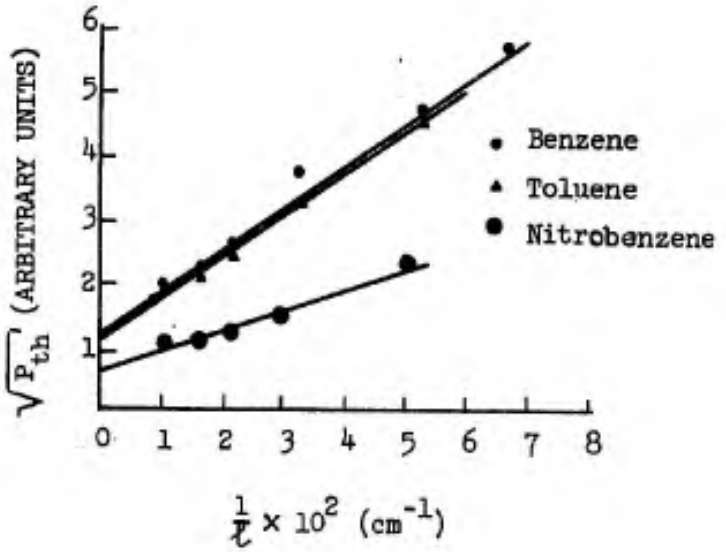

FIG. 1.3--From self-focusing theory, the threshold power for the formation of filaments in a liquid column of length ℓ is given by

$$\sqrt{P_{th}} = \alpha + \beta/\ell \quad ,$$

where α and β are constants. Thus if the threshold for stimulated Raman emission corresponds to the threshold for filament formation, a plot of the square root of the threshold laser power for stimulated emission versus $1/\ell$ should yield straight lines, and such is seen to be the case.

in which reasonable agreement between theory and experiment was obtained as far as threshold was concerned. In the Stanford work, analysis indicated that an off-axis system would respond to a spatial average of the laser intensity, and this was confirmed by threshold-to-saturation agreement between theory and experiment over a large range of experimental conditions. Typical results from this study are shown in Fig. 1.4.

4. Nanosecond Pulse Generation

Examination of the cavity output with a high-speed photodetector during work with the off-axis cavity system at Stanford revealed fine structure characteristic of interference between adjacent axial cavity modes space ~ c/2L apart. For the one-meter cavity under consideration the spacing was 144 MHz. Such interference resulted in a periodic ripple pattern as shown in Fig. 1.5. Since the initial phases of the cavity modes are random, the interference pattern was different each time the experiment was repeated. The observation of such a pattern suggested the application of a well-known technique used to obtain nonosecond and subnanosecond spikes of optical power from laser cavities, namely, the insertion of a modulator to couple modes.[47-54] The experiment, carried out by Pantell, Puthoff, Huth, and Kohn, resulted in the first observation of mode coupling in something other than a laser cavity, namely, the coupling of adjacent axial modes in an external Raman resonator, shown in Fig. 1.6.[44,55,56] The observation of such coupling in connection with the stimulated Raman effect means that the production of nanosecond and subnanosecond spikes of coherent oscillation throughout the visible and infrared spectrum is now possible, due to the large number of frequencies obtainable from a host of materials by means of the stimulated Raman effect.

5. Tunable Raman Laser

In addition to providing coherent radiation at various discrete frequencies, it was suggested independently by Loudon[57] and by Pantell and Puthoff[58] that the stimulated Raman effect should also be capable of acting as a continuously-tunable source of coherent radiation. All that is required is:

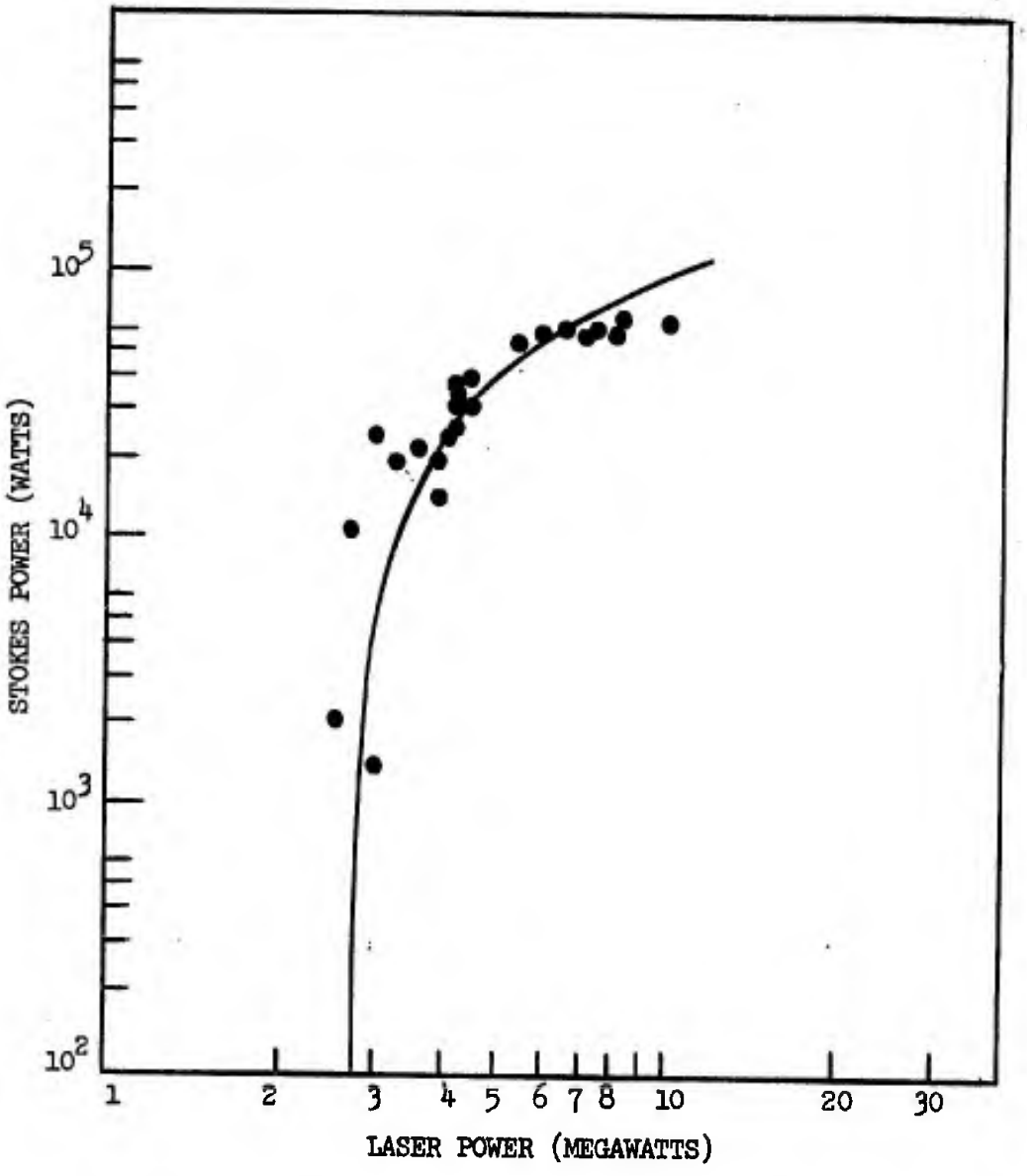

FIG. 1.4--Comparison of theory and experiment. Stokes output power is plotted as a function of laser power for a 20 cm cell of benzene showing the scatter of experimental data. The solid line is the theoretical curve.

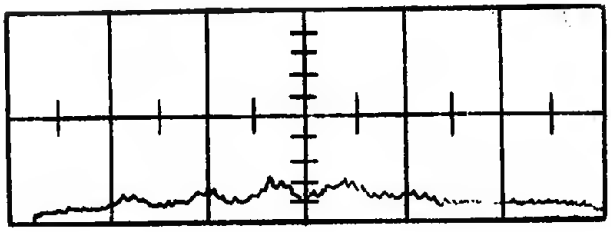

FIG. 1.5--Power output from the Stokes resonator in the absence of the modulator. The time scale is 10 nsec/div; time increases to the right.

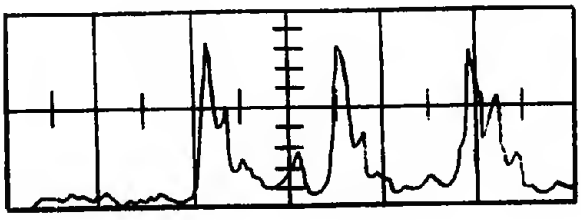

FIG. 1.6--Power output from the Stokes resonator with the modulator on. The time scale is 5 nsec/div; time increases to the right.

(1) the vibrational transition involved in the Raman scattering event must be infrared active, i.e., capable of absorbing radiation at the vibrational frequency,

(2) the medium must lack a center of symmetry, and

(3) stimulated Raman emission is forced to take place at some angle other than collinear with the laser beam, e.g., by the use of an off-axis resonator separate from the laser cavity enclosing the Raman medium.

That these factors conspire to yield the possibility of a tunable Raman laser is apparent when one considers the dispersion characteristic or ω_v-k_v diagram associated with an infrared-absorbing transition, such as an infrared-active optical vibrational mode of a crystal. A mode of this type is a mixture of mechanical vibration and electromagnetic radiation with the result that the dispersion curve is partly phonon-like partly photon-like in nature,[59] as shown in Fig. 1.7. This is due to the strong coupling between the mechanical vibrations and electromagnetic radiation in the region where their frequencies and wave vectors are nearly identical. The quanta associated with such mixed modes are sometimes called polaritons.[60] The dispersion properties of such a mode have been described in detail by Huang[61,62] for the single-resonance lossless case, and an extension to the multimode lossy case has been carried out by Barker.[63]

In the region of large k_v most of the energy in the lattice mode is mechanical rather than electromagnetic, and the difference between the laser and Stokes frequencies is simply the transverse optical mode vibrational frequency. As the region of lower k_v is approached, most of the energy in the lattice mode is electromagnetic rather than mechanical, and in this region the frequency associated with the optical mode is sensitively dependent on the phonon wave vector k_v. Since this correspondence exists between the wave vector and optical mode frequency, control of k_v during the Raman scattering process results in the control of the Stokes frequency, since the latter is the difference between the frequency of the incident light and that of the optical mode. Control of the wave vector is accomplished by adjusting the angle between the laser and Stokes beams which, by conservation of wave vector, controls k_v (see Fig. 1.8). In summary then, the Stokes light is tunable as a result of dispersion by adjustment of k_v which determines the operating point on the dispersion characteristic.

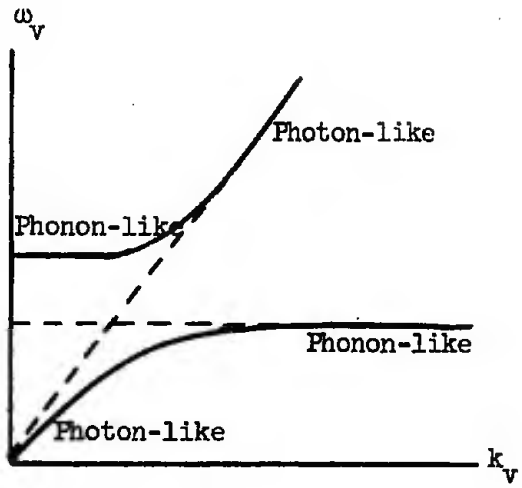

FIG. 1.7--Dispersion characteristic of infrared active optical vibrational mode of a crystal.

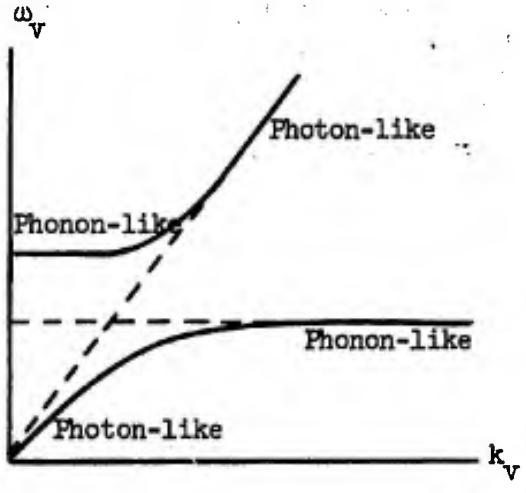

FIG. 1.7--Dispersion characteristic of infrared active optical vibrational mode of a crystal.

The theory of the tunable Raman laser was developed in detail and published by Puthoff, Pantell, and Huth.[64-66] It was the possibility of such a device that provided the motivation for the extensive work with resonators and off-axis systems at Stanford. With but a few exceptions, work in other laboratories has not involved the use of a separate cavity for the Raman medium since stimulated Raman emission is relatively easy to obtain either by placement of the Raman material inside the laser cavity or by placement external to the laser cavity where emission is generated on a single-pass basis.

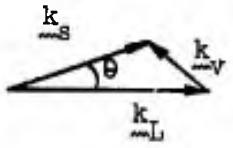

FIG. 1.8--Control of vibrational wave vector k_v by adjustment of angle θ between laser and Stokes beams.

Of primary importance in the experimental verification of the concept of a tunable Raman laser are a series of experiments carried out at Bell Laboratories[67-69] and at Stanford[70] in which the dispersion characteristic of an optical phonon branch of a given crystal is mapped out by means of the Raman effect. In these experiments a cw laser beam of low power, $<$ 100 milliwatts, passes through the crystal producing Raman scattering. The rapid variation of ω_v with k_v in the low-k_v region of the dispersion characteristic results in an observed tunable output for scattering in the near-forward direction (0-15°), and from this information the dispersion characteristic can be constructed. The results of these studies are shown in Fig. 1.9. The measured tuning range in wave numbers is given by the frequency span covered (ordinate). With a He-Ne laser as the exciting source, the tuning of the Stokes output in the experiments cited covered the ranges listed in Table I.1.

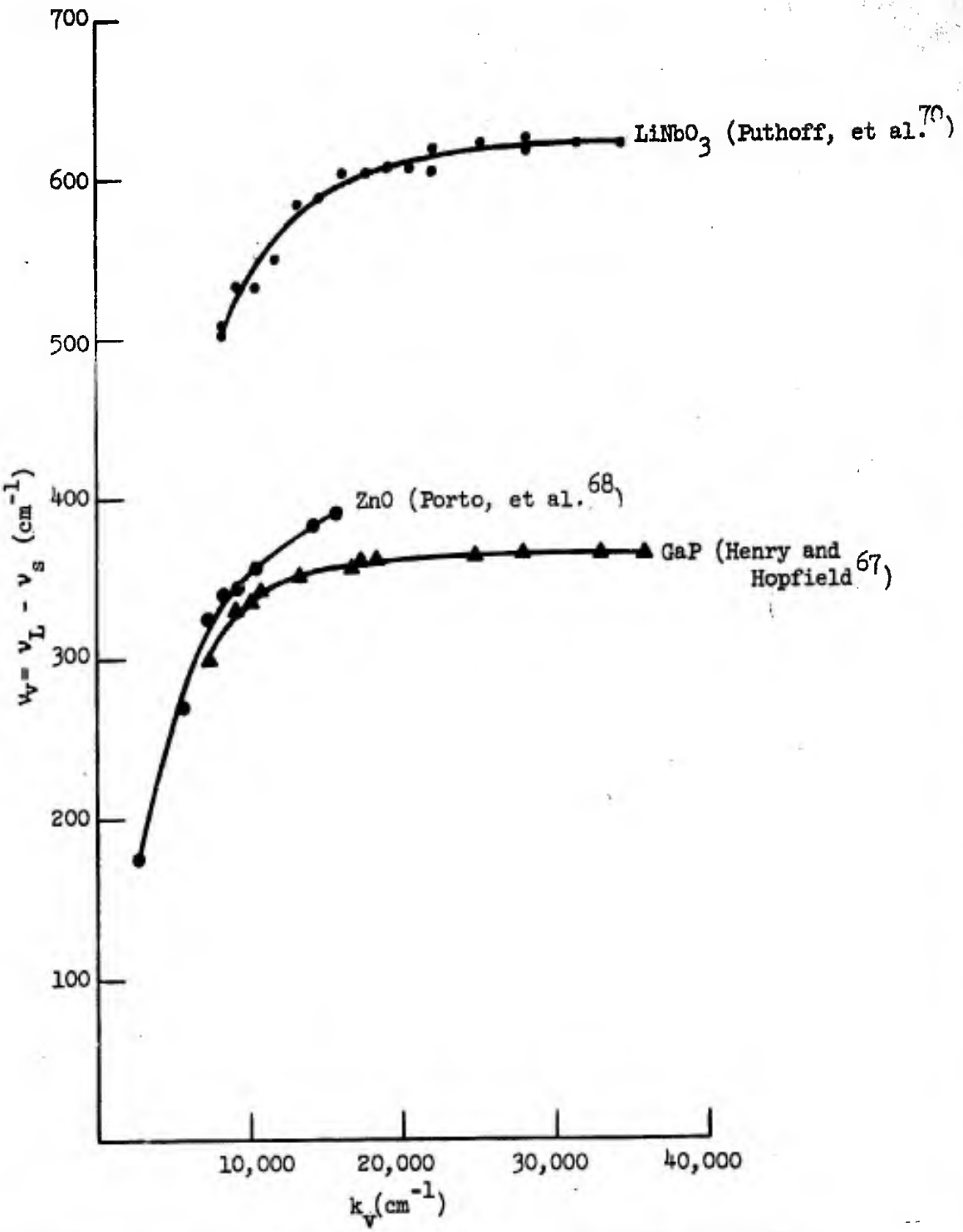

FIG. 1.9--Optical mode dispersion characteristics for several crystals as inferred from Raman scattering experiments. The variation of frequency with k_v exhibits the tunability of the Stokes output.

TABLE I.1

Crystal	Observed Stokes Wavelengths	Observed Tuning Range
$LiNbO_3$	6536 Å - 6586 Å	50 Å
ZnO	6399 Å - 6489 Å	90 Å
GaP	6450 Å - 6478 Å	28 Å

B. RESEARCH AND CONCLUSIONS

The material covered in this work, much of which was alluded to in the previous section, may now be specifically outlined. The objectives of the research program were to investigate those aspects of the Raman effect that were unexplored or not fully understood and, in particular, to concentrate on those features pertinent to the evaluation of the stimulated Raman effect as a source of tunable coherent optical radiation.

Chapter II begins with a classical description of the Raman effect which serves as a general introduction. This is then followed by a quantum mechanical treatment.

The approach used in the quantum analysis is unique in certain respects and therefore worthy of special mention. Originating with work by Jaynes[71,72] and developed extensively and applied to several problems by Pantell and co-workers, the method is based on the density matrix formulation. It differs from that in general use in the literature, however, in that the expectation values of operators of interest are formed by the trace prescription $p = \langle \mu \rangle = Tr\ (\rho\mu)$ and substituted into the density matrix equations <u>before</u> they are solved. As a result, the differential equations to be solved are in terms of macroscopic variables of interest such as polarization, and thereby lend themselves readily to physical interpretation.

In its application, the approach can be summarized succinctly as follows:

(1) a perturbation hamiltonian for the problem of interest is introduced into the equations of motion of the density matrix;

(2) expectation values of pertinent observables are formed by the trace prescription;

(3) by successive differentiation of the expectation values and substitution from the equation of motion of the density matrix, a set of differential equations in terms of the variables of interest are obtained;

(4) if it is necessary to take into account the modification of the driving fields by the response of the medium, then the system of equations is closed by the addition of a field or circuit equation driven by the expectation values of the variables describing the medium. In this way both the effect of the fields on the quantized medium and the reaction of the medium back on the fields is included. In view of the high occupation numbers of macroscopically observable fields, the fields can usually be treated classically, although this is not a necessary restriction.

Application of the approach described above yields a set of coupled nonlinear differential equations which describe the behavior of a quantized medium in the presence of, for example, a driving radiation field. The equations are in terms of classical variables such as the expectation values of polarization, nonlinear polarizability, and energy. The whole constitutes a self-consistent descriptive approach. The contribution of the author with regard to this method lies in its application to the description of the Raman and parametric effects of interest, presented in Chapter II.

Chapter III consists of a general survey of the physical significance of the equations of motions derived in Chapter II. Included is a discussion of symmetry and parity considerations and the manner in which they determine which effects may occur. In particular, the conditions affecting the tunability of a Stokes signal are discussed. It is shown that if the vibration is not infrared active, then tuning is not possible. If the vibration is infrared active, however, then tuning is possible provided

the medium does not possess a center of symmetry, e.g., liquids are eliminated from consideration. The results can be summarized in the form of a table as shown below.

Raman Active	Infrared Active	Centrosymmetric Medium	Tunable	Example
X		X		Benzene(992 cm^{-1})
X	X	X		Water(3450 cm^{-1})
X	X		X	$LiNbO_3$(628 cm^{-1})

In Chapter IV the theory of the tunable Stokes effect is presented. In the development it is shown that the tunable Raman effect can be considered to be a "pure" Raman process when the difference between the laser and Raman frequencies is resonant with the vibrational frequency, and a resonance-dominated parametric process when it is not. Even in the parametric region, however, the strength of the effect is determined by the strength of the on-resonance Raman effect, and therefore the two effects are not independent. In particular, it is found that the properties of the medium are describable in terms of three susceptibility tensors, a second rank vibrational tensor χ_v, a third rank parametric tensor χ_P, and a fourth rank Raman tensor χ_R. In the case of a well-ordered medium such as a crystal, they are interrelated by an expression of the form

$$|\chi_P|^2 = \chi_v \chi_R \quad .$$

Expressions are then derived for the Stokes gain in terms of the susceptibility tensors, the results of which can be summarized as shown in Fig. 1.10. An important result of this chapter is that in a crystal the Raman and resonant parametric gains are shown to be nearly identical, indicating that broadband high-gain tuning can be achieved. Also included in Chapter IV is a discussion of how the theoretical results derived on a semiclassical basis may be extended to cover non-stimulated, that is, spontaneous, measurements.

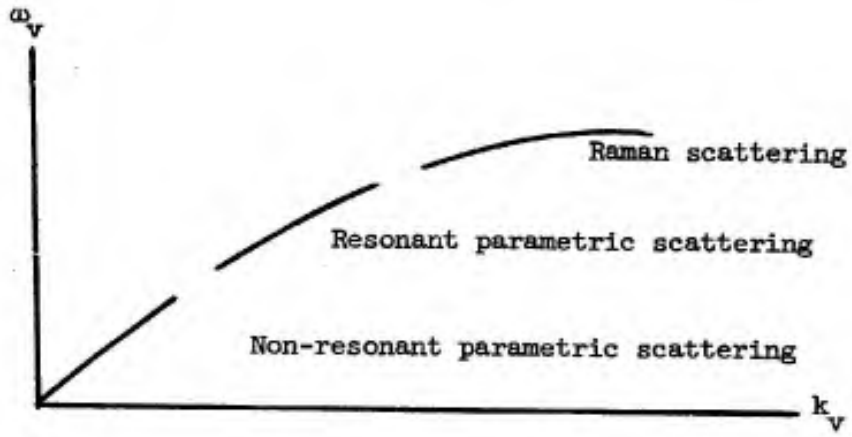

	Phase-matching req'd.	Gain
Raman scattering	No	$g = K I_L$
Resonant parametric scattering	Yes	$g = K I_L$
Non-resonant parametric scattering	Yes	$g = K\sqrt{I_L}$

FIG. 1.10--Processes dominant in Stokes scattering from various regions of a dispersion characteristic. For the processes near resonance, the gain is proportional to the laser intensity.

Presented in Chapter V is the theory of the tunable Raman laser which is shown to be a threshold device which provides for the conversion of laser power into Stokes power in accordance with the Manley-Rowe relationships when operated well above threshold.

Chapter VI presents the results of an experimental program. One part consists of a study reported in detail elsewhere[46] which demonstrates that the stimulated Raman effect in an off-axis resonator system behaves as predicted. Benzene was used as a medium and a Q-switched ruby laser as the source. Although the particular vibration studied is not infrared active and therefore does not allow the Stokes output to be tuned, it does permit verification of the design considerations since the theory is shown to be applicable to both cases. In the second part, the measurement of a 50 Å tuning characteristic of the 628 cm^{-1} optical mode in the crystal $LiNbO_3$ is presented, based on spontaneous scattering of a low-level He-Ne gas laser beam. From the scattering information a plot of the dispersion characteristic in the polariton region is constructed. Chapter VI ends with consideration of calculations which indicate that the construction of a tunable Raman laser based on the 628 cm^{-1} transition in $LiNbO_3$ is feasible, provided a crystal and components with characteristics corresponding to the best of the state-of-the-art can be assembled together. The construction of such a device in the future is envisioned as high quality crystals become available. A summary of the results of the thesis work is presented in Chapter VII.

In the material presented here the figures are assigned a more organic role than is usually the case in technical manuscripts. Whenever possible, relevant portions of the text are presented in the captions of the figures to which the text refers as opposed to being contained in the main body of material. It is hoped that such a procedure serves to integrate the presentation more fully.

CHAPTER II

THEORY

A. CLASSICAL TREATMENT

1. General Considerations

The basic properties of Raman scattering from molecular vibrations can be easily understood with the aid of a relatively simple classical picture. An individual molecule from which scattering takes place typically consists of two or more nuclei bonded together and surrounded by an electron cloud, as shown in Fig. 2.1.

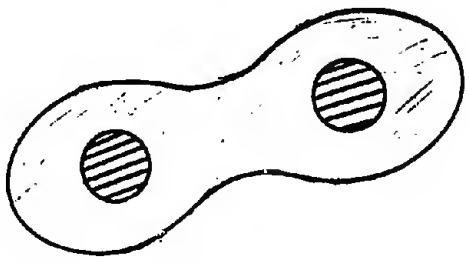

FIG. 2.1--Non-vibrating molecule consisting of nuclei surrounded by electron cloud.

If an incident radiation field in the visible or near infrared portion of the spectrum is allowed to interact with the molecule, an electric dipole moment p is induced,

$$p = \alpha E = \alpha \tilde{E} \cos \omega t \qquad (2.1)$$

where α is the electronic polarizability of the molecule. The dipole moment results from the displacement of the electron charge cloud with respect to the nuclei. In this interaction the relatively light electron cloud follows the incident field while to a first approximation the heavier nuclei remain stationary. Assuming the nuclei remain stationary, the electron polarizability α is simply a constant characteristic of the molecule. It is this constant which accounts for the index of refraction of a medium composed of such molecules.

The assumption that the nuclei remain stationary is not quite correct, however, for some of the energy absorbed by the electrons is transferred to the nuclei due to the motion of the electron cloud. As a result, the nuclei begin to oscillate about their equilibrium positions as shown in Fig. 2.2.

As the nuclei oscillate, two effects can occur. First, a dipole moment μ may be generated if separation of charge takes place during the vibration. If this occurs, the molecule is capable of interacting directly with infrared radiation at the vibrational frequency, and the molecule is said to be infrared active. Secondly, it is reasonable to expect that the electronic polarizability α may change as the nuclear configuration changes, and this indeed is observed to be the case. The situation can be expressed mathematically by expanding the electronic polarizability α in a Taylor's series in terms of normal mode vibrational coordinates q_i ,

$$\alpha = \alpha_0 + \sum_i \left(\frac{\partial \alpha}{\partial q_i}\right)_0 q_i + \ldots = \alpha_0 + \sum_i \left(\frac{\partial \alpha}{\partial q_i}\right)_0 \tilde{q}_i \cos \omega_i t + \ldots \quad . \tag{2.2}$$

Substitution of (2.2) into (2.1) then yields

$$p = \alpha_0 \tilde{E} \cos \omega t + \frac{1}{2} \sum_i \left(\frac{\partial \alpha}{\partial q_i}\right)_0 \tilde{q}_i \tilde{E} \left[\cos(\omega+\omega_i)t + \cos(\omega-\omega_i)t\right] + \ldots \quad . \tag{2.3}$$

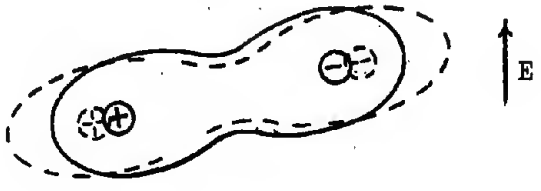

FIG. 2.2--Vibrating molecule. The vibrations are induced by energy transferred to the nuclei by the motion of the electron cloud. The frequency of oscillation of the nuclei corresponds not to the frequency of the oscillating electron cloud which is identical with that of the applied field, but rather to an infrared vibrational frequency which in general corresponds to one or more of the natural or normal-mode frequencies of the molecular vibrations, although these frequencies may be pulled in those cases where infrared radiation fields are present which can drive the molecular vibrations off resonance. For typical structures (organic liquids such as benzene and chloroform, or crystals such as lithium niobate or diamond) the molecular vibrations lie in the 3-30μ portion of the infrared spectrum and are determined by the atomic weights, bond strengths, and symmetries of the molecule.

From Eq. (2.3) we see that as the molecule vibrates, changes in the electronic polarizability lead to dipole moments which give rise to pairs of emission lines, one above and one below the excitation frequency. Each is displaced by an amount corresponding to a vibrational frequency. It is the generation of these displaced lines which constitutes the Raman effect. The lower frequency emission lines are designated Stokes lines, the higher the anti-Stokes, as indicated in Fig. 2.3. In ordinary, non-stimulated, Raman scattering the intensities of the displaced lines are typically six orders of magnitude below the intensity of the exciting line. For the case of stimulated Raman emission, however, conversion efficiencies approaching 100% are possible.

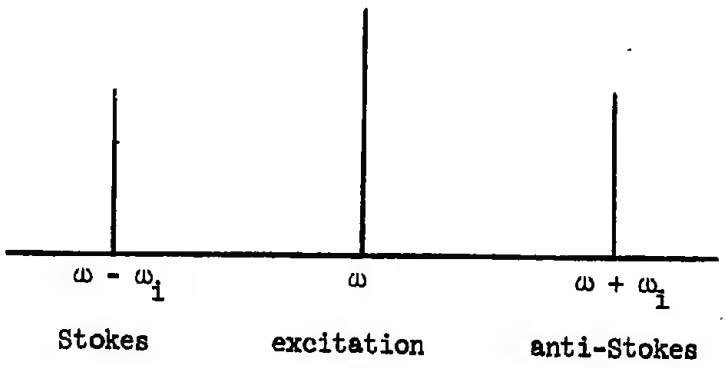

FIG. 2.3--Raman effect – generation of displaced emission lines. The terms "Stokes" and "anti-Stokes" follows from Stokes' law in fluorescence studies which states that emission lines generally are lower in frequency than excitation lines.

The intensities of the Raman lines, whether stimulated or non-stimulated, depend strongly on the type of bonding. They are usually much higher for covalent than for ionic bonds.[73] This results from the fact that the Raman intensity resulting from a vibration depends on how much the polarizability changes with displacement during the vibration, i.e., $(\partial\alpha/\partial q_i)_0$. In the case of a covalent bond, valence electrons

are shared by the atoms, and a change of the distance between the nuclei strongly affects the polarizability. In the case of ionic bonding, however, each electron is essentially under the influence of only one nucleus and the change in polarizability during the vibration is small. This tendency toward mutual exclusion between a strong Raman effect and a strong infrared effect at the vibrational frequency renders the choice of materials for use in a tunable Raman laser a matter of compromise, since, as we shall see later, it would be preferable that both effects were strong.

In Eq. (2.2) for the expansion of the polarizability α in terms of vibrational coordinates q_i, only the first order terms in q_i were retained. The process described is therefore called the first-order Raman effect. In certain media (crystals for which each lattice point is a center of symmetry, e.g., NaCl) the first order term vanishes identically because of symmetry considerations.[74,75] In this case the next higher order term, which constitutes the second-order Raman effect, may be considered.[76] This effect is weaker by several orders of magnitude and therefore will not be discussed further.

2. Hamiltonian

Based on considerations stated in the previous section, an interaction hamiltonian is chosen of the form

$$\mathcal{H} = - \mu_i(\underset{\sim}{q})\, E_i - \frac{1}{2}\, \alpha_{ij}(\underset{\sim}{q})\, E_j E_i \quad , \tag{2.4}$$

where summation over repeated subscripts is understood. The first term is of the form of the potential energy of a dipole in an electric field, and accounts for the dipole moment associated with the molecular vibrations. The second term is of the form of the potential energy stored in a polarizable medium and accounts for the dipole moments associated with the electronic vibrations. The corresponding total dipole moment is found from

$$p_i^{tot} = - \frac{\partial \mathcal{H}}{\partial E_i} = \mu_i(\underset{\sim}{q}) + \alpha_{ij}(\underset{\sim}{q})\, E_j \quad . \tag{2.5}$$

In deriving (2.5) from (2.4), use is made of the symmetry property $\alpha_{ji} = \alpha_{ij}$, a restriction imposed by energy considerations.[77]

B. QUANTUM MECHANICAL TREATMENT

1. Introduction

In the remainder of this chapter we consider the stimulated Raman effect from the quantum mechanical point of view. This phenomenon is for the most part investigated using the semiclassical approach in which the fields are treated classically and the medium is treated quantum mechanically. Unless one is interested in noise phenomena this approach is justified in view of the high occupation numbers of macroscopically-observable fields. A high state of excitation implies that large quantum numbers are involved, and this in turn by the correspondence principle of quantum mechanics implies that the fields can be expected to behave classically. The restriction to a semiclassical approach is relaxed in Section IV, E, where the phenomenon of spontaneous Raman emission is considered.

2. Placzek's Approximation

In the discussion of the Raman effect from the classical point of view, a hamiltonian (2.4) was evolved in which the infrared and Raman activity of a molecule are described in terms of a molecular dipole moment μ and an electronic polarizability α , both dependent on the vibrational coordinate q .

In passing from the classical to the quantum mechanical picture, the representation of an electronic polarizability which is parametrically dependent on the vibrational coordinate q is handled by means of Placzek's approximation. Placzek's approximation is based on the fact that although it is the electrons which interact with the incident radiation, the energy absorbed is transferred to the nuclei which then perform small oscillations about fixed positions. Therefore, the polarizability must be expressible as a power series in the vibrational amplitudes with the matrix elements calculable in terms of the energy states of the nuclei. The power series

approach can be carried out in terms of what is called the adiabatic approximation (discussed thoroughly in Sections 14, 20, and 40 of reference 76). A brief description of the adiabatic approximation which summarizes the points of interest for our application is presented below.

In the adiabatic approximation the wave functions for the system are written in the form

$$\psi_{nv}(x,X) = \chi_{nv}(X)\, \varphi_n(x,X) \quad , \tag{2.6}$$

where $\chi_{nv}(X)$ is a wave function for the nuclei and $\varphi_n(x,X)$ is the wave function for the electrons moving in the field of the nuclei held fixed in an arbitrary configuration X . The symbol n is the electronic quantum number and v is the quantum number for the nuclear motion. Therefore, the first factor is associated with the nuclear motion, and the second factor is of a form which corresponds to the approximation that during the nuclear motion the electrons move as though the nuclei were fixed in their instantaneous positions. The approximation is termed "adiabatic" because the electrons follow the nuclear motion adiabatically. In an adiabatic motion, an electron does not make transitions from one electronic state to others; instead, an electronic state is itself progressively deformed by the nuclear displacements.

The significance of the approach as far as purposes here are concerned is that it justifies the technique of calculating the matrix elements of the electronic polarizability using as basis eigenstates the two <u>vibrational</u> levels, with the electrons assumed to remain in the electronic ground state. The matrix elements of the hamiltonian (2.4) are therefore given by

$$\mathcal{H}_{nm} = -(\mu_i)_{nm} E_i - \tfrac{1}{2}(\alpha_{ij})_{nm} E_j E_i \quad ,$$

where n and m take on the values 1 and 2 corresponding to the ground and first excited state of a two-level vibrational system.

A second result of interest obtained from the adiabatic analysis is that the matrix elements of the polarizability consist of products of dipole matrix elements, indicating that the polarizability operator is of even parity with regard to X .

3. Equations of Motion for the Quantized Medium

In this section we derive the equations of motion which describe infrared and Raman effects resulting from the interaction of a classical electromagnetic field and a two-level vibrational system. The approach followed is the modified density matrix approach described in Section I.C.

It is assumed that the medium consists of a collection of molecules, or unit cells in the case of a crystal, each of which possesses a pair of vibrational eigenstates separated in energy by $E_2 - E_1 = \hbar\Omega$, as shown in Fig. 2.4.

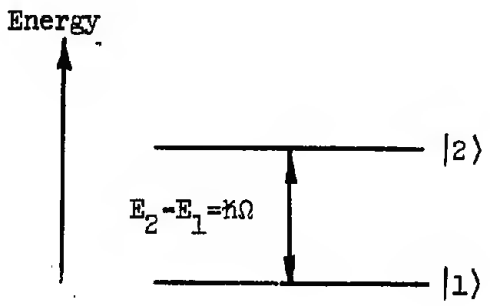

FIG. 2.4--Energy level diagram for two-level vibrational system.

Taking into account the discussion of the previous section, we choose for our purposes a molecular hamiltonian of the form

$$\mathcal{H} = \mathcal{H}_0 + \mathcal{H}' \quad .$$

Here $\mathcal{H}_0$ is the hamiltonian in the absence of the electric field. The operator $\mathcal{H}_0$ satisfies the eigenvalue equation

$$\mathcal{H}_0|n\rangle = E_n|n\rangle \quad , \qquad n = 1, 2$$

and $\mathcal{H}'$ is the interaction hamiltonian

$$\mathcal{H}' = -\mu_i(\underset{\sim}{q})\, E_i - \frac{1}{2}\alpha_{ij}(\underset{\sim}{q})\, E_j E_i \quad , \tag{2.7}$$

where $\alpha_{ij}(\underset{\sim}{q})$ is here taken to represent that part of the electronic polarizability resulting from the nuclear motion; i.e., α^0_{ij} in Eq. (2.2), which is that part of the electronic polarizability that is independent of nuclear motion, has been subtracted out. The effects of α^0_{ij} are taken into account by assigning an index of refraction to the medium. The subscripts i, j refer to coordinate directions, and summation over repeated subscripts is understood.

With the vibrational eigenstates $|1\rangle$ and $|2\rangle$ used as basis vectors, the interaction hamiltonian (2.7) assumes the following matrix form:

$$\mathcal{H}' \rightarrow \begin{pmatrix} -(\mu_i)_{11}\, E_i - \frac{1}{2}(\alpha_{ij})_{11}\, E_j E_i & -(\mu_i)_{12}\, E_i - \frac{1}{2}(\alpha_{ij})_{12}\, E_j E_i \\ -(\mu_i)^*_{12}\, E_i - \frac{1}{2}(\alpha_{ij})^*_{12}\, E_j E_i & -(\mu_i)_{22}\, E_i - \frac{1}{2}(\alpha_{ij})_{22}\, E_j E_i \end{pmatrix} . \tag{2.8}$$

The complex conjugates which appear in (2.8) satisfy the requirement that $\mathcal{H}'$, which corresponds to a physical observable, must be represented by a hermitian operator.

To obtain equations of motion for variables of interest, we begin with the equation of motion for the density matrix as applied to a two-level system in contact with an environment characterized by relaxation times T_1 and T_2,[78]

$$i\hbar\, \dot{\rho}_{nm} - \hbar\omega_{nm}\, \rho_{nm} + \frac{i\hbar}{T_2}\, \rho_{nm} = [\mathcal{H}', \rho]_{nm} \qquad n \neq m = 1,2 \quad , \tag{2.9}$$

$$i\hbar\, \dot{\rho}_{nn} + \frac{i\hbar}{T_1}\, (\rho_{nn} - \rho^e_{nn}) = [\mathcal{H}', \rho]_{nn} \qquad n = 1,2 \quad . \tag{2.10}$$

Here T_2 is the "transverse", "dipole-dipole", or "spin-spin" relaxation time associated with the dephasing of one molecular vibration relative to another, and determines the linewidth transition $2/T_2$; T_1 is the "longitudinal" or "spin-lattice" or "dipole-lattice" relaxation time, which is a measure of how much time is required for a perturbed system to exchange energy with its environment in order to reach equilibrium.

In discussing the Raman effect, it is permissible to treat the ρ_{nn}, which correspond to the level populations, as constants, since the change in populations due to the Raman effect is negligible.[11] Therefore, it may be assumed that the solution to (2.10) is given by $\rho_{nn} = \rho^e_{nn}$ set by the thermal Boltzmann distribution. In particular, at room temperature we have $\rho^e_{11} - \rho^e_{22} \approx \rho^e_{11} \approx 1$ for infrared transitions.

Substitution of the interaction hamiltonian (2.8) into the equation of motion for the off-diagonal density matrix element ρ_{21} yields

$$i\hbar\,\dot{\rho}_{21} + \frac{i\hbar}{T_2}\,\rho_{21} - \hbar\Omega\,\rho_{21} = [-(\mu_i)^*_{12}\,E_i - \tfrac{1}{2}(\alpha_{ij})^*_{12}\,E_jE_i](\rho_{11}-\rho_{22})^e \quad , \tag{2.11}$$

where small correction terms to the frequency Ω have been dropped. Since the density operator is hermitian, we have in addition the relationship $\rho_{12} = \rho^*_{21}$.

At this point the approach often used consists of solving the differential equation for the density matrix elements by means of some approximation procedure such as the equating of like frequency terms on either side of the equation. After a solution is obtained, the transition to a classical observable, such as the dipole moment, is then made by calculating the expectation value of the corresponding operator, e.g.,

$$\langle \mu_i \rangle = \mathrm{Tr}(\rho\mu_i) \quad . \tag{2.12}$$

However, the procedure can be reversed to good advantage. That is, the trace prescription (2.12) can be applied first and then, by successive differentiation with respect to time followed by substitution from the density matrix equation (2.11), a differential equation in terms of the

classical variable of interest is obtained. An equation of this type lends itself readily to physical interpretation and is often useful both in helping to understand the basic processes at work and in guiding the approximation procedures to be used.

One of the observables of interest is the expectation value of the electric dipole operator μ_i , given by

$$\begin{aligned}\langle\mu_i\rangle &= \mathrm{Tr}(\rho\mu_i) \\ &= [\rho_{11}(\mu_i)_{11} + \rho_{22}(\mu_i)_{22}] + [\rho_{21}(\mu_i)_{12} + \text{c.c.}] \\ &= \langle\mu_i\rangle_{\text{perm}} + \langle\mu_i'\rangle \quad .\end{aligned}$$

In the above expression c.c. denotes the complex conjugate. The dipole moment consists of a permanent dipole $\langle\mu_i\rangle_{\text{perm}}$ and a fluctuating component $\langle\mu_i\rangle$. It is the latter that is of interest as far as interaction with infrared or optical fields is concerned. By successive differentiation of the above expression for $\langle\mu_i\rangle$ with substitution from (2.11), the following differential equation for the fluctuating component of the dipole moment is obtained:

$$\begin{aligned}\langle\ddot{\mu}_i'\rangle + \gamma\langle\dot{\mu}_i'\rangle + \Omega^2\langle\mu_i'\rangle &= \frac{\Omega}{\hbar}[2(\mu_i)_{12}(\mu_j)^*_{12}E_j \\ &\quad + (\mu_i)_{12}(\alpha_{jk})^*_{12}E_kE_j](\rho_{11}-\rho_{22})^e \quad ,\end{aligned} \tag{2.13}$$

where $\gamma = 2/T_2$. In the derivation leading to the above expression, use was made of the inequality $\Omega^2 \gg (1/T_2)^2$ and the fact that the quantities $(\mu_i)_{12}(\mu_j)^*_{12}$ and $(\mu_i)_{12}(\alpha_{jk})^*_{12}$ are real. The reality proofs are presented in Appendix B.

In precisely the same manner the expectation value of the time-varying component of the polarizability is found to satisfy the differential equation

$$\begin{aligned}\langle\ddot{\alpha}_{ij}'\rangle + \gamma\langle\dot{\alpha}_{ij}'\rangle + \Omega^2\langle\alpha_{ij}'\rangle &= \frac{\Omega}{\hbar}[2(\alpha_{ij})_{12}(\mu_k)^*_{12}E_k \\ &\quad + (\alpha_{ij})_{12}(\alpha_{k\ell})^*_{12}E_\ell E_k](\rho_{11}-\rho_{22})^e \quad .\end{aligned} \tag{2.14}$$

In the derivation of the above equation it is necessary to show that $(\alpha_{ij})^*_{12}\,(\alpha_{k\ell})_{12}$ is real (also presented in Appendix B).

Once the solutions to (2.13) and (2.14) are obtained, the time-varying dipole moment can be determined from

$$p_i' = \langle \mu_i' \rangle + \langle \alpha_{ij}' \rangle E_j \quad . \tag{2.15}$$

Assuming there are η molecules or unit cells per unit volume, each contributing a dipole moment $\underset{\sim}{p}'$ in accordance with the above expression, one then determines the macroscopic polarization $\underset{\sim}{P}'$ by summing the contributions from each molecule. In the summation, care must be taken to note that the matrix element products appearing in (2.13) and (2.14) will in general vary from molecule to molecule depending on the orientation of the molecule with respect to the fixed coordinate system in which the matrix elements are calculated. Therefore in the summation an average over all possible orientations results. Carrying out the summation over a unit volume, we obtain in place of (2.13)-(2.15)

$$\ddot{M}_i + \gamma \dot{M}_i + \Omega^2 M_i = \frac{\Omega(N_1-N_2)^e}{\hbar} \left[2(\mu_i)_{12} (\mu_j)^*_{12} E_j + \overline{(\mu_i)_{12}(\alpha_{jk})^*_{12}} E_k E_j \right] , \tag{2.16}$$

$$\ddot{Q}_{ij} + \gamma \dot{Q}_{ij} + \Omega^2 Q_{ij} = \frac{\Omega(N_1-N_2)^e}{\hbar} \left[2(\alpha_{ij})_{12}(\mu_k)^*_{12} E_k + \overline{(\alpha_{ij})_{12}(\alpha_{k\ell})^*_{12}} E_\ell E_k \right] \tag{2.17}$$

and

$$P_i' = M_i + Q_{ij} E_j \quad , \tag{2.18}$$

where $M_i = \Sigma\langle \mu_i' \rangle$, $Q_{ij} = \Sigma\langle \alpha_{ij}' \rangle$, $P_i' = \Sigma p_i'$, and the overbar indicates orientational averaging. In addition, the population difference $(N_1-N_2)^e = \eta(\rho_{11}-\rho_{22})^e$ has been introduced, where η is the number of molecules or unit cells per unit volume.

The equations of motion for the vibrational dipole moment μ and electronic polarizability Q describe the behavior of the medium in the presence of an electromagnetic field. In order to close the system of equations it is necessary to include a field equation which takes into account the effects of the medium back on the field. The appropriate wave equation, derived from Maxwell's equations, is

$$\nabla \times (\nabla \times \underset{\sim}{E}^{mac}) + \frac{1}{c^2} \underset{\approx}{\epsilon}_{\infty} \cdot \frac{\partial^2 \underset{\sim}{E}^{mac}}{\partial t^2} = -\frac{4\pi}{c^2} \frac{\partial^2 \underset{\sim}{P}^{,source}}{\partial t^2} . \quad (2.19)$$

In the above expression the macroscopic field has been labeled as such in order to distinguish it from the local fields acting on the individual molecules or unit cells, as they are not necessarily identical. The quantity $\underset{\approx}{\epsilon}_{\infty}$ is the dielectric tensor of the medium due to transitions not explicitly accounted for in the polarization source term $\underset{\sim}{P}^{,source}$.

The differences between the local and macroscopic fields, and between the actual polarization and the polarization source term that drives the macroscopic field equation are due to the influence of nearby polarizable matter on the local electric field seen by a given molecule or unit cell. Such polarization effects can be ignored only in two cases. One case is that of a dilute gas in which there are no nearby neighbors to influence the local field, which is then identical with the macroscopic field. The other case is that of valence electrons in semiconductors and metals where the electronic wavefunctions are spread throughout the crystal rather than being localized at a given molecule or unit cell, and, therefore, sample the macroscopic rather than the local field.[79] For these two cases $\underset{\sim}{E}^{mac}$ can be taken equal to the local electric field $\underset{\sim}{E}$ and $\underset{\sim}{P}^{,source}$ can be taken equal to the polarization $\underset{\sim}{P}'$ calculated from the matter equations. For all other media a distinction between local and macroscopic fields is made by introducing what are known as Lorentz local field correction factors.

The procedure for determining the Lorentz correction factors analytically is well-known in principle but difficult if not impossible to carry out in practice in materials of complex geometries such as anisotropic crystals.[80] However, the overall result of such a calculation, were it to be carried out, is simply to introduce constant (tensor) factors as multipliers of the matrix element products which appear in (2.16) and (2.17) with a relabeling of the fields, moments, and polarizations as macroscopic variables compatible with the field equation. Therefore, we can proceed with the understanding that the matter and field equations (2.16) – (2.19) are compatible (the labels can be dropped), provided the bar indicating orientational averaging also includes the introduction of Lorentz correction factors.

4. Summary

Equations (2.16) – (2.19) comprise a self-consistent descriptive approach capable of accounting for the infrared and Raman effects resulting from the interaction of an electromagnetic field with a two-level vibrational system. In this interaction we see that the fluctuating components of the dipole moment μ and polarizability α act as harmonic oscillators of frequency Ω driven by the electric fields which are present. The description of the processes of interest by equations of this form has the clarity of a classical phenomenological description and yet retains in an explicit form the information resulting from quantum mechanical considerations, in the form of the matrix element coefficients which couple the fields to the oscillators. As an example of the use of information obtained at the quantum mechanical level, knowledge of the parity of the eigenstates can be applied to determine whether certain coefficients vanish in a particular case. These points are taken up in more detail in the following chapter.

CHAPTER III

EQUATIONS OF MOTION – GENERAL INTERPRETATION-SYMMETRY AND PARITY CONSIDERATIONS

A. INTRODUCTION

In this chapter we consider the physical significance of the set of coupled equations and examine the restrictions imposed by symmetry and parity considerations. To simplify the notation we assume all polarizations and fields to be polarized in one direction; therefore, the coordinate subscripts may be dropped. No loss of information is incurred by this procedure as the results can be generalized by reference back to the fully-subscripted equations (2.16)-(2.19). With this simplification (2.16)-(2.19) reduce to

$$\ddot{M} + \gamma\dot{M} + \Omega^2 M = \frac{\Omega(N_1 - N_2)^e}{\hbar}\left[2\,\overline{|\mu_{12}|^2}\,E + \overline{\mu_{12}\alpha_{21}}\,E^2\right] , \quad (3.1)$$

$$\ddot{Q} + \gamma\dot{Q} + \Omega^2 Q = \frac{\Omega(N_1 - N_2)^e}{\hbar}\left[2\,\overline{\mu_{12}\alpha_{21}}\,E + \overline{|\alpha_{12}|^2}\,E^2\right] , \quad (3.2)$$

$$P' = M + QE , \quad (3.3)$$

$$\nabla \times (\nabla \times E) + \frac{\epsilon_\infty}{c^2}\frac{\partial^2 E}{\partial t^2} = -\frac{4\pi}{c^2}\frac{\partial^2 P'}{\partial t^2} . \quad (3.4)$$

Of primary interest to begin with is the difference between Raman scattering from infrared-active and from non-infrared active vibrations, for it is this difference which determines whether a tunable laser based on the stimulated Raman effect is possible in principle. In order to delineate the difference, we consider the qualitative aspects of Raman scattering from such vibrations.

B. NON-INFRARED-ACTIVE CASE; $|\mu_{12}| = 0$, $|\alpha_{12}| \neq 0$

When there is no dipole moment μ associated with a vibration of interest, i.e., $|\mu_{12}| = 0$, then the vibration does not interact with an infrared field at the vibrational frequency. This case applies to the majority of the transitions for which the stimulated Raman effect has been observed. The often-studied 992 cm^{-1} vibration in benzene is a case in point.

In general, if the vibrational eigenstates are states of the same parity, then we have $|\mu_{12}| = 0$, $|\alpha_{12}| \neq 0$; and if they are of opposite parity, $|\mu_{12}| \neq 0$, $|\alpha_{12}| = 0$. Therefore, a mutual exclusion rule for Raman and infrared activity exists when the eigenstates are of a definite parity. For molecules or unit cells which possess a center of symmetry the eigenstates have a definite parity, and therefore fall into this category.[81] For states of mixed parity, it is possible for both $|\mu_{12}|$, $|\alpha_{12}| \neq 0$.

Under the condition $|\mu_{12}| = 0$, Eqs. (3.1)-(3.4) reduce to

$$\ddot{Q} + \gamma\dot{Q} + \Omega^2 Q = \frac{\Omega(N_1 - N_2)^e}{\hbar} \overline{|\alpha_{12}|^2} E^2 \quad , \qquad (3.5)$$

$$P' = QE \quad , \qquad (3.6)$$

$$\nabla \times (\nabla \times E) + \frac{\epsilon_\infty}{c^2} \frac{\partial^2 E}{\partial t^2} = -\frac{4\pi}{c^2} \frac{\partial^2 P'}{\partial t^2} \quad . \qquad (3.7)$$

Examination of the above equations reveals that

(a) no infrared dipole moment M is generated at the vibrational frequency;

(b) if propagating fields at the laser and Stokes frequencies are present, each of the form $\frac{1}{2} e^{i(\omega t - \mathbf{k}\cdot\mathbf{r})} + \text{c.c.}$, a vibrational Q wave of frequency $\omega_v = \omega_L - \omega_s = \Omega$ and wave vector $\mathbf{k}_v = \mathbf{k}_L - \mathbf{k}_s$ is generated;

(c) the vibrational Q wave, by mixing with the laser wave as indicated in the polarization equation (3.6), generates in turn a field at the Stokes frequency, thereby rendering self-consistent the original assumption of a Stokes field;

(d) no polarization P' is generated at the vibrational frequency, and therefore an electromagnetic wave near the vibrational frequency propagates as a simple wave through a medium of refractive index $n = \sqrt{\epsilon_\infty}$.

Since the vibrational Q wave and infrared field E are uncoupled in the vicinity of the vibrational transition, the traveling-wave solutions to (3.5) and (3.7) are represented by the uncoupled dispersion curves shown in Fig. 3.1.

The conservation of frequency and wave vector during the Raman scattering process yields a closed vector relationship on the dispersion diagram as illustrated in Fig. 3.2. From the diagram it is apparent that the generation of a Stokes wave of frequency $\omega_s = \omega_L - \Omega$ with any k value, i.e., in any direction, is allowed. Therefore, Raman scattering involving a non-infrared-active vibration is a process for which phase matching (k conservation) is automatically assured for Stokes wave propagation in any direction. This is due to the ability of the non-dispersive vibrational wave to assume any k value required to take up the difference between given laser and Stokes k values.

C. INFRARED-ACTIVE CASE I; $|\mu_{12}| \neq 0$, $|\alpha_{12}| \neq 0$, $\overline{\mu_{12}\alpha_{21}} \neq 0$

Here we consider the general case where the vibration is infrared-active, and therefore capable of absorbing and radiating electromagnetic

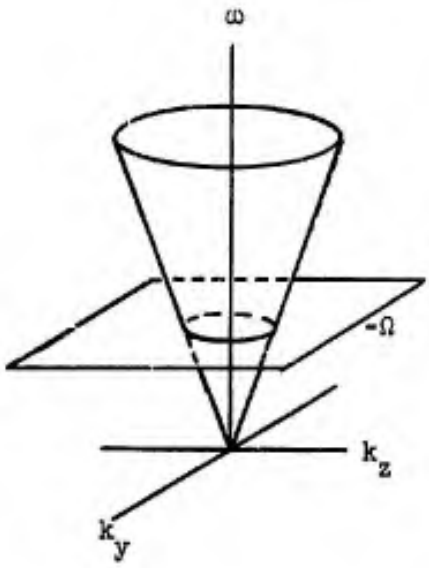

FIG. 3.1--Dispersion characteristics for non-infrared-active case. The inverted cone is the locus of vectors representing the propagation of electromagnetic energy with $k = \omega\sqrt{\epsilon}/c$. The flat plane corresponds to the propagation of an optical vibrational wave Q of frequency Ω and an arbitrary k value dictated by the driving term in (3.5).

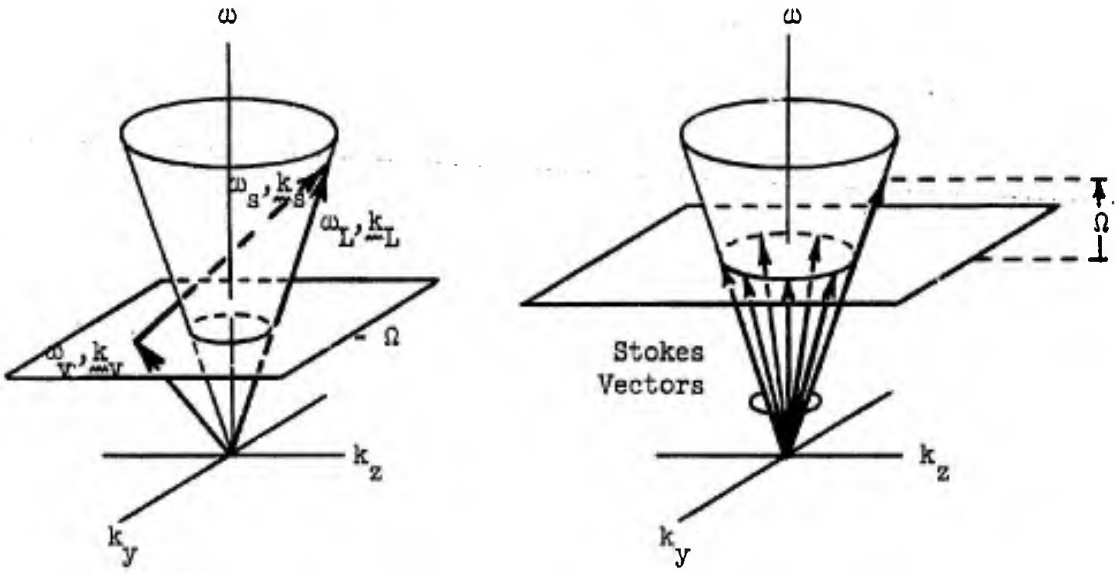

FIG. 3.2--Conservation of frequency and wave vector in the Raman scattering process involving a non-infrared-active vibration. The conservation conditions

$$\omega_L = \omega_v + \omega_s$$

$$\underset{\sim}{k}_L = \underset{\sim}{k}_v + \underset{\sim}{k}_s$$

imply a closed vector relationship on the dispersion diagram as shown in (a). Conservation of ω requires that the projections of the dispersion vectors on the vertical axis sum to zero, while conservation of $\underset{\sim}{k}$ requires closure of the horizontal projections. The locus of possible Stokes vectors is found by subtracting the dispersion characteristic of the vibrational wave (the plane) from a point on the dispersion characteristic which represents the ω, k of the input laser light. The result is as shown in (b). Only those Stokes vectors which terminate on the intersection of the two surfaces satisfy the frequency-wave vector relationships.

energy at the vibrational frequency. This is the case of interest as far as the possibility of the construction of a tunable Raman laser is concerned. The 628 cm^{-1} optical vibrational mode in $LiNbO_3$ chosen for study in this work (Chapter VI) provides an example.

Since $|\mu_{12}|$, $|\alpha_{12}| \neq 0$, the full set of equations (3.1)-(3.4) applies. Examination reveals that

(a) an infrared dipole moment M is generated at the vibrational frequency, driven by the product of the laser and Stokes fields and coupled to an infrared field;

(b) the dipole moment M , in turn, generates an infrared field at the vibrational frequency through the polarization term;

(c) the vibrational Q wave is driven both by the product of the laser and Stokes fields, and by the infrared field: the fact that the vibrational Q wave is coupled to the infrared field permits the vibration to be "tuned" in accordance with the infrared dispersion characteristic, leading to tuning of the Stokes wave;

(d) the vibrational Q wave mixes with the laser wave in the polarization equation to generate in turn a field at the Stokes frequency;

(e) the polarization P′ generated at the vibrational frequency by the resonant dipole moment M drives the field equation, leading to the normal absorption and dispersion effects associated with resonance.

It is useful at this point to examine (e) in some detail, for it is the resonance dispersion characteristic which permits tuning of the Stokes output. Ignoring for the moment the Stokes and laser fields present, the infrared effects are determined by the equations

$$\ddot{M} + \gamma\dot{M} + \Omega^2 M = \frac{\Omega(N_1 - N_2)^e}{\hbar} \, 2 \, \overline{|\mu_{12}|^2} \, E \quad , \qquad (3.8)$$

$$P' = M \quad , \qquad (3.9)$$

and

$$\nabla \times (\nabla \times \mathbf{E}) + \frac{\epsilon_\infty}{c^2} \frac{\partial^2 \mathbf{E}}{\partial t^2} = -\frac{4\pi}{c^2} \frac{\partial^2 \mathbf{P}'}{\partial t^2} \quad . \tag{3.10}$$

If the field $\mathbf{E}$ is assumed to be of the form

$$\mathbf{E} = \frac{\tilde{\mathbf{E}}_v}{2} e^{i(\omega_v t - k_v^o z)} + \text{c.c.} \quad ,$$

and the other variables are defined in a similar manner, the following dispersion relation is obtained:

$$k_v^{o2} = \frac{\omega_v^2 \epsilon_v}{c^2} \quad , \tag{3.11}$$

where ϵ_v is the complex dielectric constant (see Fig. 3.3). The superscript "zero" on the propagation constant is to distinguish this case from others later on where perturbation effects due to laser and Stokes fields will be taken into account.

An optical vibrational mode is a mixture of a vibrational wave and and electromagnetic wave. The dispersion characteristic is therefore that of a coupled mode system, partly mechanical, partly electromagnetic in nature. As a result, the dispersion curve is partly phonon-like, partly photon-like, as illustrated in Fig. 3.4.[82] The region within a few linewidths of resonance where ϵ_v has an imaginary part has been ignored in these diagrams for clarity.

The quanta associated with such mixed modes are sometimes called polaritons.[83] The dispersion properties of this type of mode have been described in detail by Huang[84,85] for the single-resonance lossless case, and an extension to the multimode lossy case has been carried out by Barker.[86]

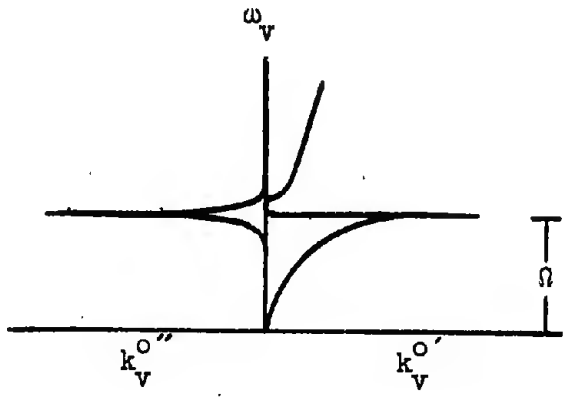

FIG. 3.3--Dispersion characteristic of infrared-active vibration, given by

$$k_v^{o2} = \frac{\omega_v^2 \epsilon_v}{c^2} \quad ,$$

where ϵ_v is the complex dielectric constant

$$\epsilon_v = \epsilon_\infty^v + \frac{\Omega^2 \Delta \epsilon}{\Omega^2 - \omega_v^2 + i\omega_v \gamma} \quad .$$

In the above expression γ is the linewidth, ϵ_∞^v is the frequency-independent contribution to the dielectric constant from higher-lying transitions, and $\Delta\epsilon$ is the contribution to the dielectric constant from this vibration as one passes through resonance, given by

$$\Delta\epsilon = \frac{8\pi(N_1 - N_2)^e \overline{|\mu_{12}|^2}}{\hbar\Omega} \quad .$$

Since ϵ_v is complex, the propagation constant k_v^o is also complex, and thus k_v^o can be written

$$k_v^o = k_v^{o'} + ik_v^{o''} \quad .$$

The real and imaginary parts of k_v^o determine the dispersion and absorption properties, respectively, of the transition under consideration.

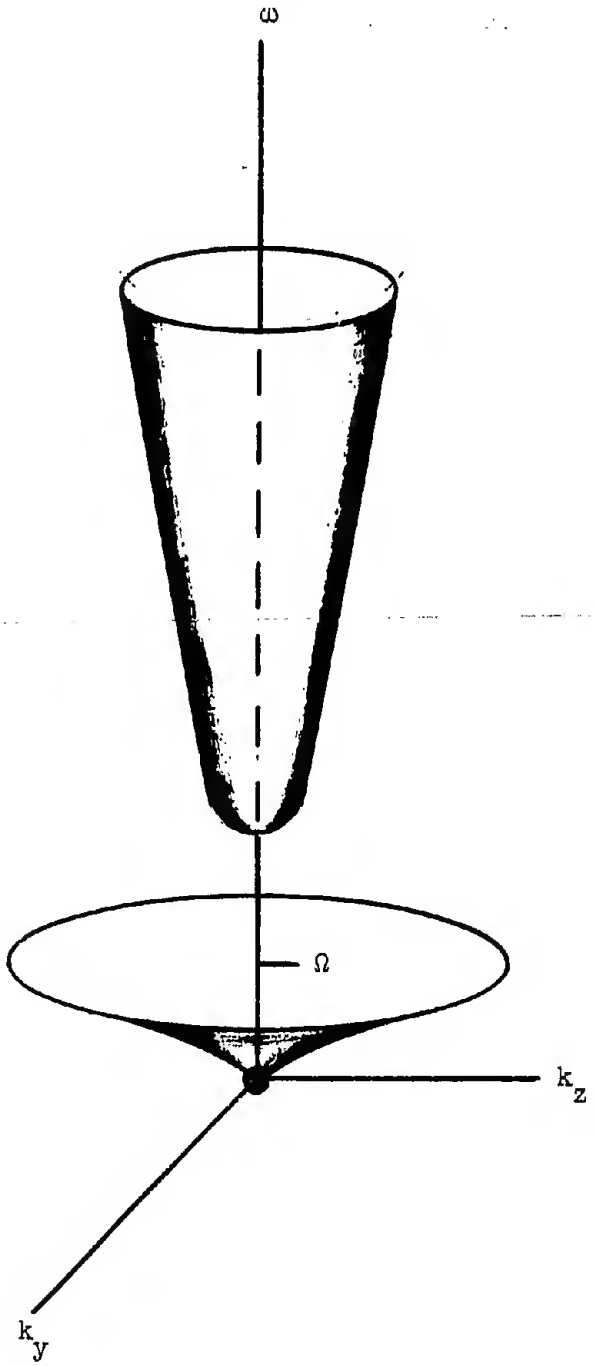

FIG. 3.4--Dispersion characteristic for infrared-active case. Coupling between the electromagnetic waves and optical vibrations gives rise to two surfaces separated by a gap. The lower surface represents a coupled wave which is purely electromagnetic in character near the origin but becomes purely vibrational near the edge of the flared region. The character of the waves represented by the upper surface is reversed, being primarily vibrational near the ω axis and primarily electromagnetic in the region away from the axis.

As far as the Raman scattering process is concerned, the vibrational Q wave, through the first term in Eq. (3.2), can follow the infrared field and thus the dispersion characteristic. Conservation of frequency and wave vector then yields a closed vector relationship on the dispersion diagram which results in the locus of possible Stokes vectors shown in Fig. 3.5. In the region of large k_v the mixed mode is predominantly mechanical rather than electromagnetic, and the difference between the laser and Stokes frequencies is simply the transverse optical mode vibrational frequency Ω . In the region of lower k_v , most of the energy in the mode is electromagnetic rather than mechanical, and the mixed-mode frequency is sensitively dependent on k_v . In this latter region the Stokes frequency, given by the difference between the frequency of the incident laser beam and that of the mixed mode, can be controlled by the choice of allowed wave vectors. In practice, tuning of the Stokes output is accomplished by varying the angle between k_L and k_s by rotation of a Stokes resonator relative to the direction of the laser beam. The design of a tunable Raman laser based on the above considerations is presented in the following chapter.

D. INFRARED-ACTIVE CASE II; $|\mu_{12}| \neq 0$, $|\alpha_{12}| \neq 0$, $\overline{\mu_{12}\alpha_{21}} = 0$

This case differs from the previous in that the orientational average of the matrix element product $\mu_{12}\alpha_{21}$ is zero, although the matrix element product itself exists on a molecule-to-molecule basis. This occurs, for example, in an isotropic fluid composed of anisotropic molecules, each of which possesses a vibrational transition which is simultaneously Raman and infrared active. The 3450 cm^{-1} vibrational transition in H_2O provides an example.[81] That the orientational average of $\mu_{12}\alpha_{21}$ must vanish in an isotropic fluid is due to symmetry considerations. From (3.1) it is seen that the matrix element product of interest relates the dipole moment to the square of the electric field. Since an isotropic fluid is centrosymmetrical, inversion through the center of symmetry must leave the system unchanged. Such an operation

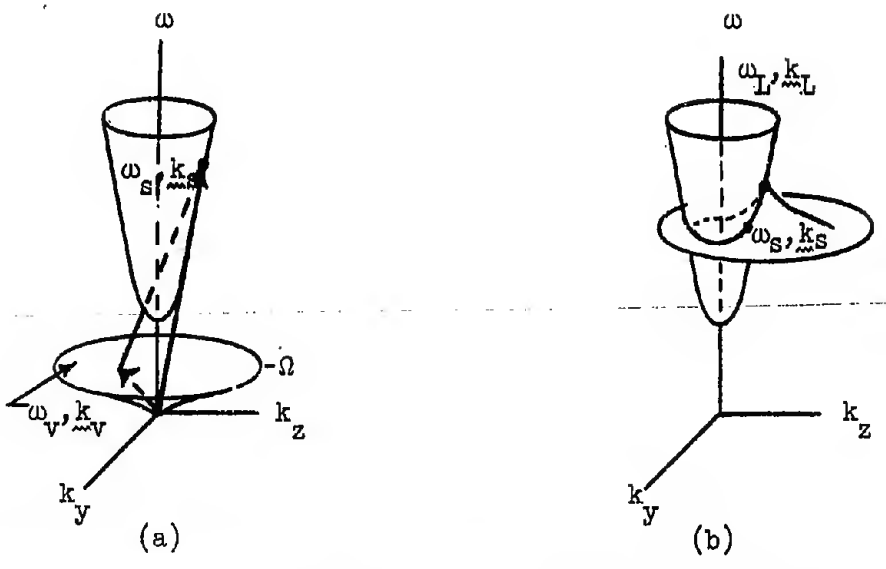

FIG. 3.5--Conservation of frequency and wave vector in the Raman scattering process involving an infrared-active vibration. The conservation conditions

$$\omega_L = \omega_v + \omega_s$$

$$\underset{\sim}{k}_L = \underset{\sim}{k}_v + k_s$$

imply a closed vector relationship as shown in (a). The locus of possible Stokes vectors is found by subtracting the dispersion characteristic of the vibrational wave (lower surface of (a)) from a point on the dispersion characteristic which represents the ω,k of the input laser light. The result is shown in (b). Only those Stokes vectors which terminate on the intersection of the two surfaces satisfy the frequency-wave vector relationships.

applied to the term of interest, however, leaves the square of the field unchanged while reversing the moment in direction. Since the latter is contradictory to the centrosymmetric assumption, the coefficient $\overline{\mu_{12}\alpha_{21}}$ must vanish.

Under the condition $\overline{\mu_{12}\alpha_{21}} = 0$, Eqs. (3.1)-(3.4) reduce to

$$\ddot{M} + \gamma\dot{M} + \Omega^2 M = \frac{\Omega(N_1-N_2)^e}{\hbar} \, 2 \, \overline{|\mu_{12}|^2} \, E \quad ,$$

$$\ddot{Q} + \gamma\dot{Q} + \Omega^2 Q = \frac{\Omega(N_1-N_2)^e}{\hbar} \, \overline{|\alpha_{12}|^2} \, E^2 \quad ,$$

$$P' = M + QE$$

$$\nabla \times (\nabla \times E) + \frac{\epsilon_\infty}{c^2} \frac{\partial^2 E}{\partial t^2} = -\frac{4\pi}{c^2} \frac{\partial^2 P'}{\partial t^2} \quad .$$

By virtue of the infrared activity, the dispersion relationships of the previously-discussed infrared active case (Section C) still apply. By virtue of the Raman activity, a vibrational Q wave is generated by the product of laser and Stokes waves. However, the two phenomena are independent. The application of a laser wave and the subsequent production of a Stokes wave does not serve to excite a macroscopic vibrational dipole moment M which would lead to an infrared field E . Therefore, the vibrational Q wave and infrared wave are uncoupled with the result that the vibrational wave does not follow the infrared dispersion characteristic. Thus the tuning phenomenon discussed in the previous case is not possible even though the Raman and infrared effects may occur independently.

CHAPTER IV

THEORY OF THE TUNABLE STOKES EFFECT

A. INTRODUCTION

The theory of the tunable Stokes effect is developed here, and it is shown that the generation of Stokes light occurs by means of two separate but interrelated phenomena.. One is a "pure" Raman process of the type which occurs in any Raman-active medium regardless of whether or not the medium is infrared active. This phenomenon occurs in the region of the dispersion characteristic where the vibrations are predominantly mechanical in nature (see Fig. 4.1). The other is a parametric process which requires that an infrared wave be generated in the scattering process which can subsequently mix with the laser wave to produce a Stokes difference-frequency output. This method of generation predominates in the region of the dispersion characteristic which is primarily electromagnetic.

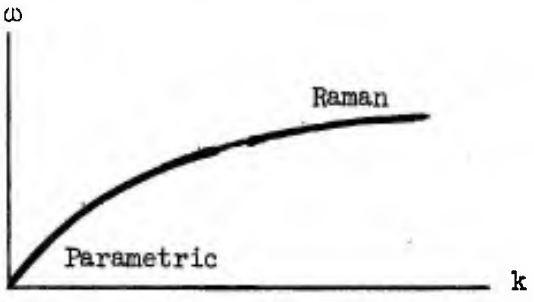

FIG. 4.1--Dispersion characteristic of an infrared-active optical vibration. The regions in which the parametric and Raman processes each predominate in the generation of Stokes light are shown.

The two types of scattering processes are found to be related through the susceptibility tensors which govern the interactions. Both are threshold processes which lead to stimulated emission provided losses can be overcome.

B. VIBRATIONAL, PARAMETRIC, AND RAMAN SUSCEPTIBILITIES

We now consider the solution to the equations of motion (3.1) – (3.4). If the dipole moment M is assumed to have a solution of the form

$$M = \frac{\tilde{M}_v}{2} e^{i\omega_v t} + \text{c.c.} \quad ,$$

and the other variables are defined in a similar manner, where v, L, and s refer to the vibrational, laser, and Stokes frequencies, the steady-state solutions to (3.1) – (3.4) can be written

$$\tilde{P}_v' = \chi_v \tilde{E}_v + \chi_P^* \tilde{E}_L \tilde{E}_s^* \quad , \tag{4.1}$$

$$\tilde{P}_s' = \chi_P \tilde{E}_v^* \tilde{E}_L + \chi_R |\tilde{E}_L|^2 \tilde{E}_s \quad , \tag{4.2}$$

$$\tilde{P}_L' = \chi_P^* \tilde{E}_v \tilde{E}_s + \chi_R^* \tilde{E}_L |\tilde{E}_s|^2 \quad , \tag{4.3}$$

$$\nabla \times (\nabla \times \tilde{E}_\nu) - \frac{\omega_\nu^2 \epsilon_\infty^\nu}{c^2} \tilde{E}_\nu = \frac{4\pi\omega_\nu^2}{c^2} \tilde{P}_\nu' \quad , \quad \nu = v,s,L \quad . \tag{4.4}$$

The quantities χ_v , χ_R , and χ_P are what shall be termed the vibrational, Raman, and parametric susceptibilities, defined by

$$\chi_v = \frac{\Omega(N_1 - N_2)^e}{\hbar D_v} \overline{2|\mu_{12}|^2} \quad , \tag{4.5}$$

and

$$\chi_R = \frac{1}{2} \frac{\Omega(N_1 - N_2)^e}{\hbar D_v^*} \overline{|\alpha_{12}|^2} \quad , \tag{4.6}$$

$$\chi_P = \frac{\Omega(N_1 - N_2)^e}{\hbar D_v^*} \overline{\mu_{12}\alpha_{21}} \quad , \tag{4.7}$$

where D_v is the resonance denominator

$$D_v = \Omega^2 - \omega_v^2 + i\,\omega_v\,\gamma \quad .$$

With the solution to the equations of motion (3.1) – (3.4) written in the above form, processes of interest can be discussed in terms of the susceptibilities.

The vibrational susceptibility χ_v is a second-rank tensor property which relates the polarization at the vibrational frequency to the field at the same frequency. This tensor therefore accounts for the absorption and dispersion properties of the medium due to the vibrational transition. Comparison of (3.12), (3.13), and (4.5) indicates that the complex dielectric constant in the vicinity of the vibrational transition can be written in the familiar form

$$\epsilon_v = \epsilon_\infty^v + 4\pi\chi_v \quad . \tag{4.8}$$

The Raman susceptibility χ_R is a fourth rank tensor property which accounts for the "pure" Raman scattering process. Since this process depends on the matrix $|\alpha_{12}|$ resulting from the deformation of the molecule or unit cell during vibration, this type of scattering is also known as deformation potential scattering.

The parametric susceptibility χ_p is a third rank tensor property which accounts for the generation of a Stokes wave by a parametric interaction involving a vibrational and a laser wave. Since this process

depends on the matrix element $\mu_{12}\alpha_{21}$, and therefore on the generation of a dipole moment and infrared field, this type of scattering is known as electromagnetic or polar scattering.

The parametric interaction is of vital importance, for it is this process which is primarily responsible for the tunability of the Stokes output. Since the process is characterized by a third rank tensor, it cannot occur in a medium with a center of symmetry, as discussed in Section III B.4, since third rank tensors vanish identically in such media.

Comparison of Eqs. (4.5) – (4.7) yields the important relationship

$$|\chi_p|^2 \leq \chi_v \chi_R \quad . \tag{4.9}$$

The equality holds in the case of a well-ordered single-crystalline substances where the orientational average of the product of μ and α is equal to the product of the averages. The above relationship indicates that the polar or electromagnetic scattering which takes place in the parametric process is determined by the product of the infrared and Raman activities of the vibrational mode. Therefore, the generation of Stokes output by the parametric process, although separate from the Raman process, is nonetheless intimately connected to the Raman process through the susceptibility tensors.[87]

C. COUPLED-WAVE INTERACTION

The gain experienced by a wave at the Stokes frequency in the presence of vibrational and laser waves is obtained by considering the coupled-wave interaction of the three fields. We consider the laser field, which acts as a pump source for the Raman and parametric interactions, to be a known fixed wave which propagates through the medium without depletion. The appropriate coupled-wave equations for the Stokes and vibrational waves, obtained from Eqs. (4.1) – (4.4), are

$$\nabla \times (\nabla \times \tilde{E}_v^*) - \frac{\omega_v^2 \epsilon_v^*}{c^2} \tilde{E}_v^* = \frac{4\pi\omega_v^2}{c^2} \chi_p \tilde{E}_L^* \tilde{E}_s \quad , \tag{4.10}$$

and

$$\nabla \times (\nabla \times \tilde{E}_s) - \frac{\omega_s^2 \epsilon_\infty^s}{c^2} \tilde{E}_s = \frac{4\pi\omega_s^2}{c^2} (\chi_P \tilde{E}_v^* \tilde{E}_L + \chi_R |\tilde{E}_L|^2 \tilde{E}_s) \quad , \quad (4.11)$$

where, as before, the complex dielectric constant in the region of the vibrational transition, ϵ_v , is given by (4.8).

Traveling-wave solutions to (4.10) and (4.11) are found by assuming[1]

$$\tilde{E}_\nu = \tilde{\tilde{E}}_\nu e^{-i\underline{k}_\nu \cdot \underline{r}} \quad , \quad \nu = v, L, s \quad . \quad (4.12)$$

The result (derived in Appendix C) is an expression for the Stokes propagation constant k_s ,

$$k_s = \frac{\omega_s \sqrt{\epsilon_\infty^s}}{c} + \frac{2\pi\omega_s \chi_R |\tilde{\tilde{E}}_L|^2}{c\sqrt{\epsilon_\infty^s}} + \frac{8\pi^2 \omega_v^2 \omega_s \chi_P^2 |\tilde{\tilde{E}}_L|^2}{c^3 \sqrt{\epsilon_\infty^s} (k_v^{*2} - k_v^{o*2})} \quad , \quad (4.13)$$

where

$$\underline{k}_L = \underline{k}_s + \underline{k}_v^* \quad . \quad (4.14)$$

---

[1] A moment's reflection will reveal that in order to obtain real traveling-wave solutions of the form

$$E = \frac{1}{2} \tilde{\tilde{E}} e^{i(\omega t - \underline{k} \cdot \underline{r})} + \text{c.c.}$$

by a two-step process which begins with

$$E = \frac{1}{2} \tilde{E} e^{i\omega t} + \text{c.c.} \quad ,$$

the form (4.12) is the necessary second step.

The first term in (4.13) is the ordinary dispersion term for the propagation of a wave at frequency ω_s in the absence of coupling to other waves. The second and third terms are perturbation terms in k_s arising from Raman and parametric interactions, respectively. The imaginary parts of the last two terms lead to gain at the Stokes frequency. In the interest of simplicity, we consider the Raman and parametric terms separately. This is in keeping with one of the major results to be derived, namely that the contribution from each term predominates in a different region of the ω-k dispersion characteristic.

D. STOKES GAIN

1. Raman Gain

Ignoring the parametric term in (4.13) and expressing the Raman susceptibility in the form $\chi_R = \chi_R' + i\chi_R''$, we find that the imaginary part of the Stokes propagation constant $k_s = k_s' + ik_s''$ is given by

$$k_s'' = \frac{2\pi\omega_s \chi_R'' |\tilde{E}_L|^2}{c\sqrt{\epsilon_\infty^s}} \tag{4.15}$$

Therefore, the Stokes gain due to the Raman term, $\alpha = k_s''$, can be written

$$\boxed{\alpha_R = \frac{4\pi^2 \chi_R'' |\tilde{E}_L|^2}{n_s \lambda_s}, \quad \text{RAMAN GAIN}} \tag{4.16}$$

where n_s is the Stokes refractive index $n_s = \sqrt{\epsilon_\infty^s}$ and λ_s is the Stokes free-space wavelength $\lambda_s = 2\pi c/\omega_s$. The gain is seen to be proportional to the laser intensity. Since the Raman susceptibility χ_R has the frequency dependence shown in Fig. 4.2, the Raman gain is maximum at the vibrational frequency $\omega_v = \Omega$, and falls off rapidly outside the linewidth. Therefore, Raman output, when observed, is expected to occur near the vibrational frequency Ω.

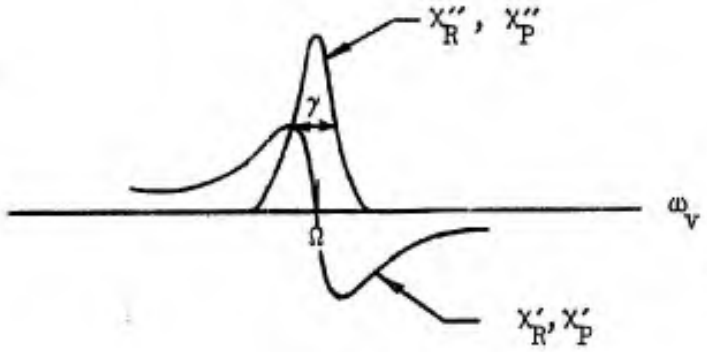

FIG. 4.2--Frequency dependence of Raman and parametric susceptibilities as obtained from Eqs. (4.6) and (4.7).

2. Parametric Gain

Ignoring the Raman term in (4.13), the imaginary part of the Stokes propagation constant k_s is given by

$$k_s'' = \mathrm{Im}\left[\frac{8\pi^2 \omega_v^2 \omega_s \chi_P^2 |\tilde{E}_L|^2}{c^3\sqrt{\epsilon_\infty^s}\,(k_v^{*2} - k_v^{o*2})}\right] . \qquad (4.17)$$

Examination of the above equation reveals that the contribution to the Stokes gain by the parametric term differs in kind from that of the Raman term in that the gain depends on the vibrational propagation constant k_v. It is also apparent from the form of the denominator that the gain will be maximized under the condition that the vibrational propagation constant set up in the parametric process closely matches the propagation constant for infrared radiation, i.e., a phase-matching condition must be met. Therefore, it is necessary to consider in some detail the implications of the complex wave vector conservation requirement given by (4.14). The considerations which follow yield considerable insight into the behavior of the parametric process.

The Stokes and vibrational propagation constants $\underset{\sim}{k}_s$ and $\underset{\sim}{k}_v^*$ each have real and imaginary parts, while the laser propagation constant $\underset{\sim}{k}_L$ is assumed to be strictly real since laser depletion is being ignored. Therefore, upon separation of real and imaginary parts, (4.14) yields

$$\underset{\sim}{k}_L = \underset{\sim}{k}_s' + \underset{\sim}{k}_v' \quad , \tag{4.18}$$

$$\underset{\sim}{k}_s'' = \underset{\sim}{k}_v'' \quad . \tag{4.19}$$

Conservation of the imaginary parts indicates that the growth constants of the Stokes and vibrational waves are the same. Therefore, the buildup of a Stokes wave is accompanied by the generation of infrared radiation if the vibration is infrared active. Conservation of the real parts indicates that the real part of the vibrational propagation constant, k_v' , is determined by the vector relationships shown in Fig. 4.3.

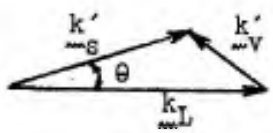

FIG. 4.3--Wave vector conservation (real parts). The vibrational propagation constant k_v' is determined from the law of cosines,

$$k_v'^2 = k_L^2 + k_s'^2 - 2k_L k_s' \cos\theta \quad . \tag{4.20}$$

A plot of (4.20) yields a family of curves for various angles which can be plotted on the infrared dispersion characteristic of Fig. 3.3, repeated here as Fig. 4.4. It is apparent from the figure that the propagation constant k_v' which satisfies the conservation condition (4.20) is not necessarily the same as the infrared wave propagation constant $k_v^{o\prime}$. In particular, for very large k_v' values, a considerable

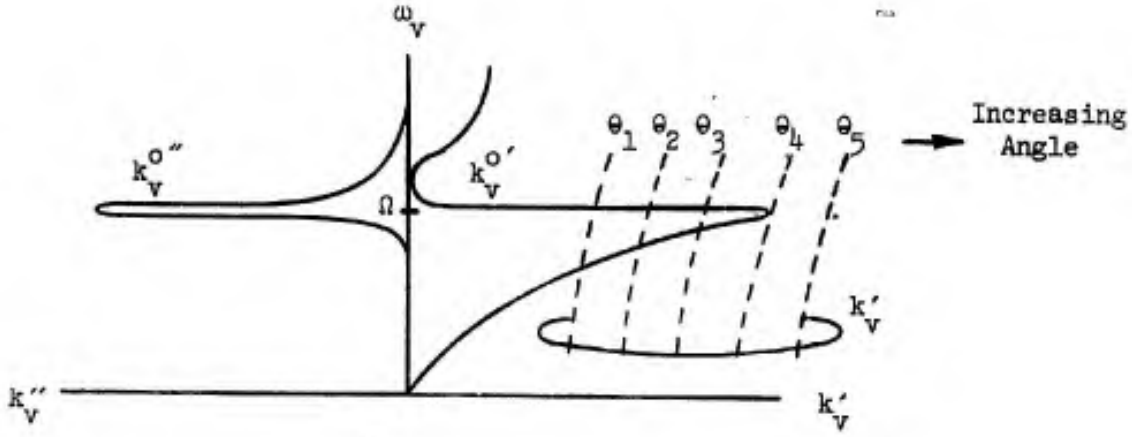

FIG. 4.4--Vibrational propagation constant k_v . The solid curve represents the infrared wave propagation constant k_v^o obtained from infrared absorption and dispersion measurements in the absence of laser and Stokes fields. The dotted curves indicate the values of k'_v which satisfy the wave vector conservation requirement during Stokes generation.

difference between the two must exist, since the infrared dispersion characteristic does not extend into the large k_v' region. It is useful in the discussion of the parametric interaction to express this in terms of a complex mismatch term, defined by

$$k_v = k_v^o + \Delta k_v \quad . \tag{4.21}$$

Substitution of (4.21) into (4.17) then yields for the imaginary part of the Stokes propagation constant

$$k_s'' = \mathrm{Im}\left\{ \frac{8\pi^2 \omega_v^2 \omega_s \chi_P^2 |\tilde{\tilde{E}}_L|^2}{c^3 \sqrt{\epsilon_\infty^s} \left[(k_v^{o*} + \Delta k_v^*)^2 - k_v^{o*2} \right]} \right\} \quad . \tag{4.22}$$

In the region of very large k_v' , the real part of the mismatch term, $\Delta k_v'$, must be large, as indicated by the previous discussion. Since this term appears in the denominator, the parametric term is relatively weak in this region where the angle between Stokes and laser beams is large. Therefore, for large beam angle separation, the predominant gain mechanism is the Raman rather than the parametric effect, and emission at the vibrational frequency Ω occurs.

By the nature of the denominator, it is necessary that the mismatch term Δk_v be minimized for a high parametric gain. To minimize Δk_v , we look for solutions where $\Delta k_v \ll k_v^o$. Under this assumption, (4.22) reduces to

$$k_s'' = \mathrm{Im}\left[\frac{4\pi^2 \omega_s \omega_v \chi_P^2 |\tilde{\tilde{E}}_L|^2}{c^2 \sqrt{\epsilon_\infty^s} \sqrt{\epsilon_v^*}} \frac{1}{\Delta k_v' - i\Delta k_v''} \right] . \tag{4.23}$$

In the region below resonance $(\omega_v < \Omega)$ we can, to a first order approximation, assume that both χ_P and ϵ_v^* are real; therefore, the parametric gain given by the imaginary part of k_s arises solely from the imaginary part of the mismatch term. If the denominator is rationalized,

it is clear that the gain is maximized under the condition $\Delta k_v' = 0$, that is, along the $\omega_v - k_v'$ infrared dispersion characteristic.

From the conservation condition (4.19) and mismatch definition (4.21), we have the additional relationship

$$\Delta k_v'' = k_s'' + \alpha_v \quad , \tag{4.24}$$

where $\alpha_v \triangleq |k_v^{o''}|$ is the loss constant for infrared wave propagation. Substituting the above into (4.23) and assuming the phase-matching condition $\Delta k_v' = 0$, we obtain the final expression

$$k_s''^2 + \alpha_L k_s'' - \alpha_P^2 = 0 \quad , \tag{4.25}$$

where

$$\alpha_P^2 = \frac{4\pi^2 \omega_s \omega_v \chi_P'^2 |\tilde{\tilde{E}}_L|^2}{c^2 \sqrt{\epsilon_\infty^s} \sqrt{\epsilon_v}} \quad . \tag{4.26}$$

The solution to (4.25) is given by

$$k_s'' = \frac{\alpha_v}{2} \left[\sqrt{1 + 4\left(\frac{\alpha_P}{\alpha_v}\right)^2} - 1 \right] . \tag{4.27}$$

a. Non-resonant parametric gain.

In the region far below resonance, the infrared loss term $\alpha_v = |k_v^{o''}|$ is vanishingly small as is seen in Fig. 4.4. Under this condition, (4.27) yields for the non-resonant parametric gain the expression $k_s'' = \alpha_P$, which can be written

$$\boxed{\alpha_P = \frac{4\pi^2 \chi_P' |\tilde{\tilde{E}}_L|}{\sqrt{n_s n_v \lambda_s \lambda_v}} \quad \begin{matrix} \text{NON-RESONANT} \\ \text{PARAMETRIC} \\ \text{GAIN} \end{matrix}} \quad . \tag{4.28}$$

The non-resonant parametric gain is seen to be proportional to the square root of the laser intensity, rather than to the intensity as is the case for Raman gain. Such behavior is typical of non-resonant parametric processes. Figure 4.2 can be consulted to obtain the frequency dependence of χ_P' . Far below resonance the gain is seen to be essentially constant.

b. Resonant parametric gain.

As resonance is approached, a region is entered in which, although still outside the linewidth, the infrared loss term α_v predominates over the parametric gain α_P . In this region where $\alpha_v \gtrsim \alpha_P$, (4.27) yields for the resonant parametric gain $\alpha_{PR} = k_s''$ the expression

$$\boxed{\alpha_{PR} = \frac{\alpha_P^2}{\alpha_v} = \frac{16\pi^4 \chi_P''^2 |\tilde{E}_L|^2}{n_s n_v \lambda_s \lambda_v \alpha_v}} \quad \text{RESONANT PARAMETRIC GAIN} \quad . \quad (4.29)$$

In contrast to the non-resonant parametric gain, the parametric gain on the approach to resonance is proportional to the laser intensity, as is the Raman gain. The compensating frequency effects of χ_P' (Fig. 4.2) and $\alpha_v = |k_v^{o\prime\prime}|$ (Fig. 3.3) serve to keep the parametric gain flat until resonance is approached to within approximately a linewidth.

3. Comparison of Raman and Parametric Gains

It is apparent from the discussion of the preceding section that the construction of a tunable Raman laser must depend on the parametric effect for tuning outside the linewidth, since the Raman gain drops drastically. Therefore, it is of interest to determine the relative strengths of the resonant Raman gain and the parametric gain near resonance. A derivation of the ratio of the two is carried out in Appendix D with the result

$$\frac{\alpha_{PR}}{\alpha_R(\Omega)} \approx \frac{\sqrt{\epsilon_\infty^v}}{n_v} \frac{\chi_P''^2(\Omega)}{\chi_P''(\Omega)|\chi_v''(\Omega)|} \quad . \quad (4.30)$$

That is, the ratio of the parametric to the Raman gain is given essentially by the ratio of the square of the resonant parametric susceptibility to the product of the resonant Raman and vibrational susceptibilities. The factor in front is the ratio of the index of refraction above the transition to that at the operating frequency ω_v, a ratio slightly less than unity.

The importance of the above result lies in the fact that for a well-ordered crystal the susceptibility ratio is unity [see Eq. (4.9)]. Therefore, in such a medium, tuning outside the Raman linewidth is permitted by means of the parametric effect with a gain essentially equal to the Raman gain.

4. Summary

The result of the solution to the coupled-wave problem can be summarized by stating that in a medium which is simultaneously Raman and infrared active, a Stokes wave in the presence of a laser beam propagates as

$$\tilde{E}_s = \tilde{\mathcal{E}}_s e^{-ik_s z} = \tilde{\mathcal{E}}_s e^{-i(k_s' + ik_s'')z} .$$

Multiplication of the above by its complex conjugate yields

$$|\tilde{E}_s|^2 = |\tilde{\mathcal{E}}_s|^2 e^{2k_s'' z}$$

Therefore, the Stokes intensity $I_s = |\tilde{E}_s|^2$ satisfies the growth equation

$$\frac{dI_s}{dz} = g_s I_s , \qquad (4.31)$$

where the Stokes power gain $g_s = 2k_s''$ is given by an equation of the form

$$g_s = K \sqrt{I_L}$$

for the non-resonant parametric case, and

$$g_s = K I_L \tag{4.32}$$

for the Raman and resonant-parametric cases.

If the intensities $I_{s,L} = |\tilde{E}_{s,L}|^2$ are re-expressed in terms of the power per unit area

$$\frac{\mathcal{P}}{A} = \frac{cn}{8\pi}|\tilde{E}|^2 \quad ,$$

then the gain coefficient K for the Raman effect is given by

$$K = \frac{64\pi^3 \chi_R''(\Omega)}{cn_L n_s \lambda_s} \quad , \tag{4.33}$$

and the gain coefficient K for the resonant parametric effect in the case of a well-ordered crystal is given by $\sqrt{\epsilon_\infty^v / n_v}$ times the above.

E. SPONTANEOUS EMISSION EFFECTS

Up to this point a semi-classical approach has been used throughout. That is, while the medium has been treated from a quantum mechanical view-point, the fields have been created as classical variables. As a result, only induced or stimulated emission processes have been considered. Spontaneous emission processes, which can be taken into account mathematically by field quantization, have been ignored. However, spontaneous Raman scattering and parametric scattering are the processes which are observed in low-level light-scattering experiments.

The effects of spontaneous emission can, however, be introduced in a straightforward manner into results derived on the basis of the semi-classical approach. As an example, we consider equations (4.31) and (4.33) derived for Stokes propagation in the Raman case. These equations relate the Stokes and laser intensities $I_{s,L} = |\tilde{E}_{s,L}|^2$. If the

variables

$$\eta_\nu = \frac{V}{\hbar\omega_\nu} \frac{\epsilon_\nu^\infty |\tilde{E}_\nu|^2}{8\pi}$$

are introduced, where V is an arbitrary volume, (4.31) and (4.33) can be written in the form

$$\frac{d\eta_s}{dz} = g_s \eta_s \quad , \tag{4.34}$$

$$g_s = K' \eta_L \quad , \tag{4.35}$$

where

$$K' = \frac{8\pi\hbar\omega_L}{V\epsilon_L^\infty} K \quad .$$

Thus far, the variable η_ν is simply the energy contained in a volume V associated with a traveling-wave mode at frequency ν, divided by the energy per photon. As such η_ν is a classical variable. However, it can be shown[78] that when fields are quantized, expressions derived on a semi-classical basis remain valid provided η_ν is replaced by $(\eta_\nu + 1)$, where η_ν is now identified as the number of photons in the given traveling-wave mode, and the addition of the 1 represents the "extra photon" in the mode which accounts for spontaneous emission effects. For the example at hand, (4.34) and (4.35) are therefore to be replaced by

$$\frac{d\eta_s}{dz} = g_s (\eta_s + 1) \quad , \tag{4.36}$$

$$g_s = K' (\eta_L + 1) \quad . \tag{4.37}$$

Of importance to our applications is the interpretation that considerations based on a semiclassical approach can be applied to a spontaneous event, since the latter can be thought of as a stimulated event due to the presence of a single photon. For the generation of spontaneous Stokes light by an applied laser source, for example, the solution to (4.36) and (4.37) yields (taking $\eta_s(0) = 0$, $\eta_L(0) \gg 1$)

$$\eta_s(\Delta z) = K' \eta_L \Delta z \quad .$$

That is, the number of photons spontaneously emitted into a given Stokes mode is linearly proportional to the intensity of the laser beam, the length of the scattering material, and the gain coefficient derived on the basis of a semiclassical approach.

F. CONVERSION RELATIONSHIP FOR RAMAN AND RESONANT PARAMETRIC EFFECTS

The preceding results indicate that the resonant Raman and near-resonant parametric effects both lead to gains proportional to the laser intensity. Since each effect predominates in a different region of the dispersion characteristic, the effects can be treated separately.

In the case where the Raman effect predominates, the Stokes polarization (Eq. 4.2) for the maximum gain resonant case is given by

$$\tilde{P}_s' = i \chi_R''(\Omega) |\tilde{E}_L|^2 \tilde{E}_s \quad .$$

In the case where the parametric effect predominates, the Stokes polarization, given by

$$\tilde{P}_s' = \chi_p \tilde{E}_v^* \tilde{E}_L \quad ,$$

can be reduced to the form

$$\tilde{P}_s' = i \frac{4\pi^2 \chi_p'^2(\omega_v)}{n_v \lambda_v \alpha_v} |\tilde{E}_L|^2 \tilde{E}_s \quad .$$

Proof of the above follows simply by the elimination of $\tilde{E}_v^*$ and use of approximations in a manner identical to that used in deriving the resonant parametric gain.

The importance of this result lies in the fact that in the application of the results of this chapter to the design of a tunable Raman laser, all derivations can proceed mathematically on the basis of the Raman term alone with the relization that in the parametric region the results can be converted by the equivalence relation

$$\chi_R''(\Omega) \Longleftrightarrow \frac{4\pi^2 \chi_P'^2(\omega_v)}{n_v \lambda_v \alpha_v} \quad . \tag{4.38}$$

For the crystal case where the susceptibility ratios in (4.30) cancel, the above reduces to

$$\chi_P''(\Omega) \Longleftrightarrow \frac{\sqrt{\epsilon_\infty^v}}{n_v} \chi_R''(\Omega) \quad . \tag{4.39}$$

CHAPTER V

THEORY OF A TUNABLE RAMAN LASER

A. PROPOSED DESIGN

We summarize here the results obtained thus far which are pertinent to the design of a tunable Raman laser.

(1) The passage of a laser beam through a medium which possesses an optical mode that is simultaneously Raman and infrared-active results in a resonant parametric gain mechanism for Stokes waves of frequency $\omega_s = \omega_L - \omega_v$, where ω_v is in the vicinity of the vibrational transition frequency Ω.

(2) For any given Stokes frequency, the gain is optimized at a phase matching angle θ such that wave-vector conservation (Fig. 4.3) places the vibrational operating point on the infrared dispersion characteristic.

(3) The resonant parametric gain in the region of interest is a constant which, in a crystal, is approximately equal to the resonant Raman gain.

Based on the above three points, a proposed design for the construction of a tunable Raman laser is as shown in Fig. 5.1. Tuning is achieved through control of the angle θ.

B. THEORY

As a result of the simplification stated in Section IV, F, the theory of the tunable Raman laser can be developed on the basis of the pure Raman effect followed by the conversion (4.3).

The geometry is as shown in Fig. 5.1. The laser beam makes a single pass through the system, while the Stokes fields are generated in the form of cavity modes. For the latter we choose in place of the traveling wave equation (4.4) an alternative representation based on a normal mode expansion.

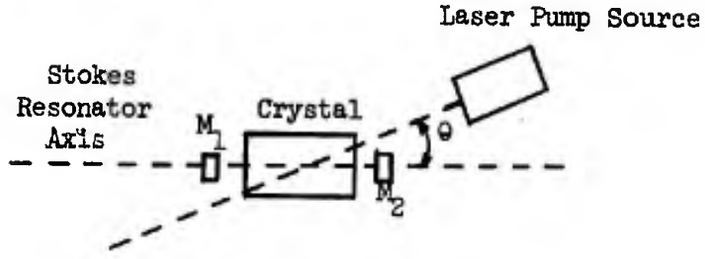

FIG. 5.1--Tunable Raman laser design. The off-axis resonator system allows the angle θ between laser and Stokes beams to be controlled. Mirrors M_1 and M_2 provide for multiple passes through the crystal. If the small-signal gain per round trip pass exceeds the loss, then appreciable Stokes fields can build up within the resonator and thus provide significant output.

For a single longitudinal mode, the appropriate expression is[88]

$$\ddot{E}_s + \frac{1}{\tau_{ph}} \dot{E}_s + \omega_s^2 E_s = -\frac{4\pi}{n_s^2} u_a \int \ddot{P}'_s \, u_a \, dV \quad , \tag{5.1}$$

where the integration is carried out over the resonator volume, assumed to be filled by the Raman medium. The quantity u_a is an orthonormal resonator mode given by

$$u_a = \sqrt{\frac{2}{LA}} \sin \frac{m\pi z}{L} \quad , \tag{5.2}$$

where m is an integer, L is the length of the resonator, and A is the cross-sectional area of the cavity Stokes beam. The quantities τ_{ph} and ω_s are the resonator photon lifetime and resonant frequency, respectively.

The equation for the laser beam is that appropriate to a traveling wave, given by (4.4),

$$\nabla \times (\nabla \times \tilde{E}_L) - \frac{\omega_L^2 n_L^2}{c^2} \tilde{E}_L = \frac{4\pi\omega_L^2}{c^2} \tilde{P}'_L \quad , \tag{5.3}$$

where $n_L^2 = \epsilon_\infty^L$.

Under steady-state conditions, the field equations are driven by the polarization source terms given by (4.2) and (4.3),

$$\tilde{P}'_s = i\chi''_R(\Omega) \, |\tilde{E}_L|^2 \, \tilde{E}_s \tag{5.4}$$

and

$$\tilde{P}'_L = -i\chi''_R(\Omega) \, \tilde{E}_L \, |\tilde{E}_s|^2 \quad . \tag{5.5}$$

Here $\tilde{P}'_s$ represents the driving term for the Stokes resonator and is proportional to the laser intensity; $\tilde{P}'_L$ is proportional to the Stokes intensity and introduces depletion loss at the laser frequency due to energy conversion.

An expression can now be obtained for $\tilde{E}_L$ as a function of z by substituting (5.5) into (5.3) and ignoring in the integration the

rapidly-varying spatial variation inherent in $|\tilde{E}_s|^2$ due to the form of the resonator mode given by (5.2). That is, $|\tilde{E}_s|^2$ is replaced by its average value $|\tilde{E}_s|^2/LA$, where $|\tilde{E}_s|^2$ is the magnitude of the cavity mode. Multiplication of the result by its complex conjugate yields an expression for the depletion of laser intensity,

$$|E_L|^2 = |\tilde{E}_L(x,y)|^2 \, e^{-\frac{8\pi^2 \chi_R''(\Omega) |\tilde{E}_s|^2}{n_L \lambda_L L A} z} \quad . \tag{5.6}$$

Substitution of (5.4) and (5.6) into (5.1) then yields an important relationship between a normalized laser power V and a normalized Stokes power U, namely

$$V = \frac{U}{1-e^{-U}} \quad , \tag{5.7}$$

where

$$V = \frac{8\pi^2 \tau_{ph} c \chi_R''(\Omega)}{n_s^2 \lambda_s A} \int |\tilde{E}_L(x,y)|^2 \, dA \tag{5.8}$$

and

$$U = \frac{8\pi^2 \chi_R''(\Omega) |\tilde{E}_s|^2}{n_L \lambda_L A} \quad . \tag{5.9}$$

The form of the integral on the right hand side of (5.8) indicates that a cavity mode is driven by a spatial average of the laser intensity. Therefore, the power generated in a Stokes mode depends only on the average intensity rather than on the specific intensity distribution. As a result, the presence of "hot spots" in the laser beam due to filamenting or self-focusing phenomena does not alter the value of the integrals.

Expressions (5.8) and (5.9) can be rewritten in terms of powers as

$$V = \frac{64\pi^3 \tau_{ph} \chi_R''(\Omega)}{n_L n_s^2 \lambda_s} \frac{P_L}{A} \quad , \tag{5.10}$$

$$U = \frac{64\pi^3 \tau_R \chi_R''(\Omega)}{\lambda_L n_L n_s^2} \frac{P_s}{A} \quad . \tag{5.11}$$

In these expressions P_L is the input laser power, P_s is the total Stokes power coupled out of the cavity, τ_R is the resonator lifetime determined solely by the mirror reflectivities, and τ_{ph} is the total photon lifetime taking into account scattering, absorption, and mirror losses.

In the derivation of the above it was assumed that the Raman and laser beams overlap throughout the cavity. However, when the laser is rotated to an angle θ with respect to the resonator axis, the interaction volume may be decreased as a result of the geometry. In this case the integration in (5.1) is carried out over the interaction volume only with the result that on the right hand side of (5.10) and (5.11) a multiplying factor β must be included, where β is given by

$$\beta = \sqrt{\frac{4A}{\pi L^2}} \quad \text{cosec } \theta$$

for those values of θ which yield $\beta < 1$, and is unity elsewhere.

Figure 5.2 is a plot of (5.7) and shows the general system behavior in terms of normalized powers. Threshold occurs at $V = 1$, and P_L at threshold can be calculated from (5.10). When the input laser power is much larger than threshold, the ratio P_s/P_L approaches the Manley-Rowe limit reduced by the factor τ_{ph}/τ_R which represents the amount of energy lost and therefore not available as useful output. That is, for

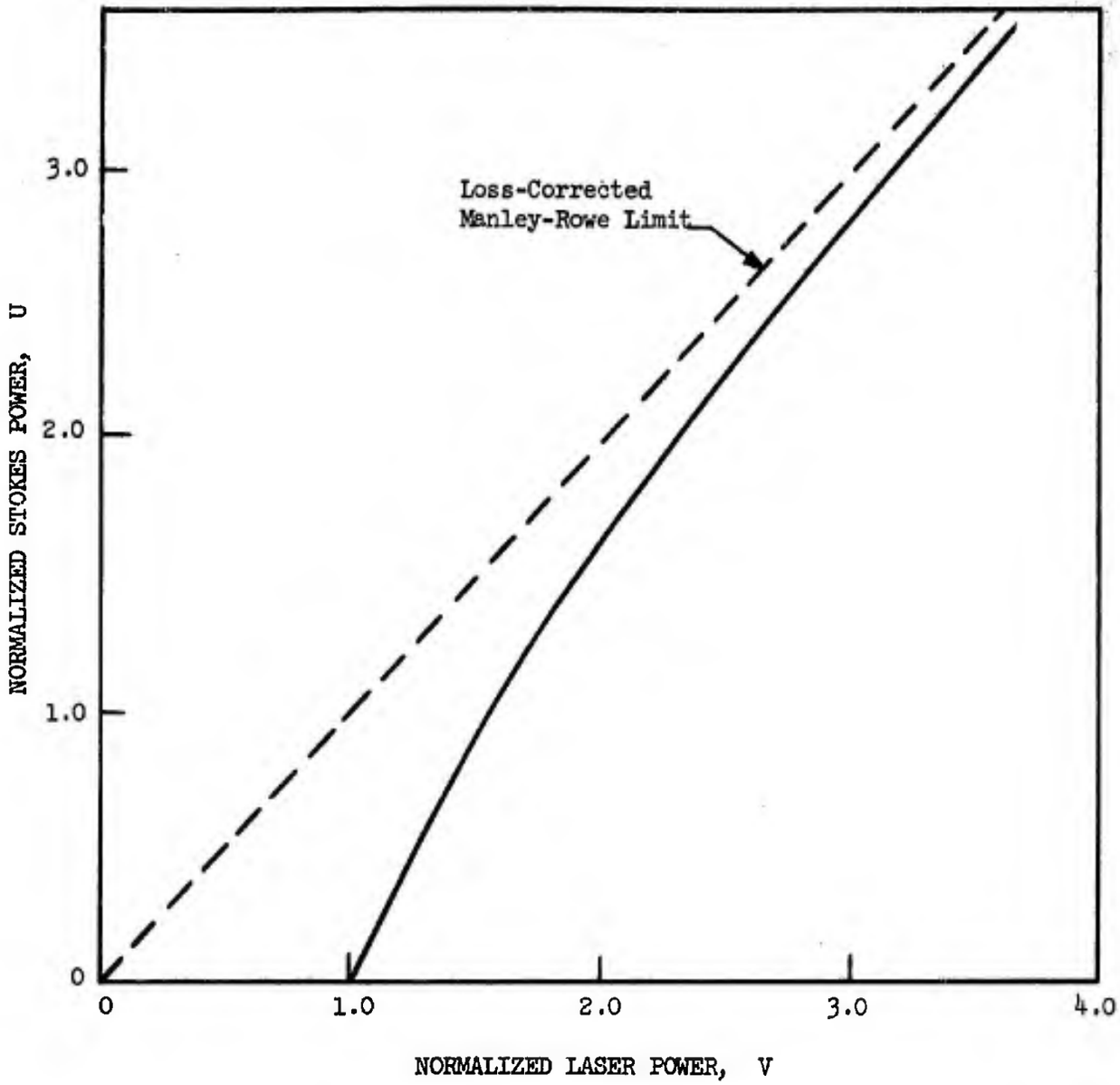

FIG. 5.2--Normalized Stokes power as a function of normalized laser power. As the normalized laser power, V , is increased beyond its threshold value, the Stokes power grows until the ratio of the normalized Stokes and laser powers equals unity. This corresponds to a ratio of unnormalized powers equal to the Manley-Rowe limit multiplied by the factor τ_{ph}/τ_R which corrects for loss in the resonator.

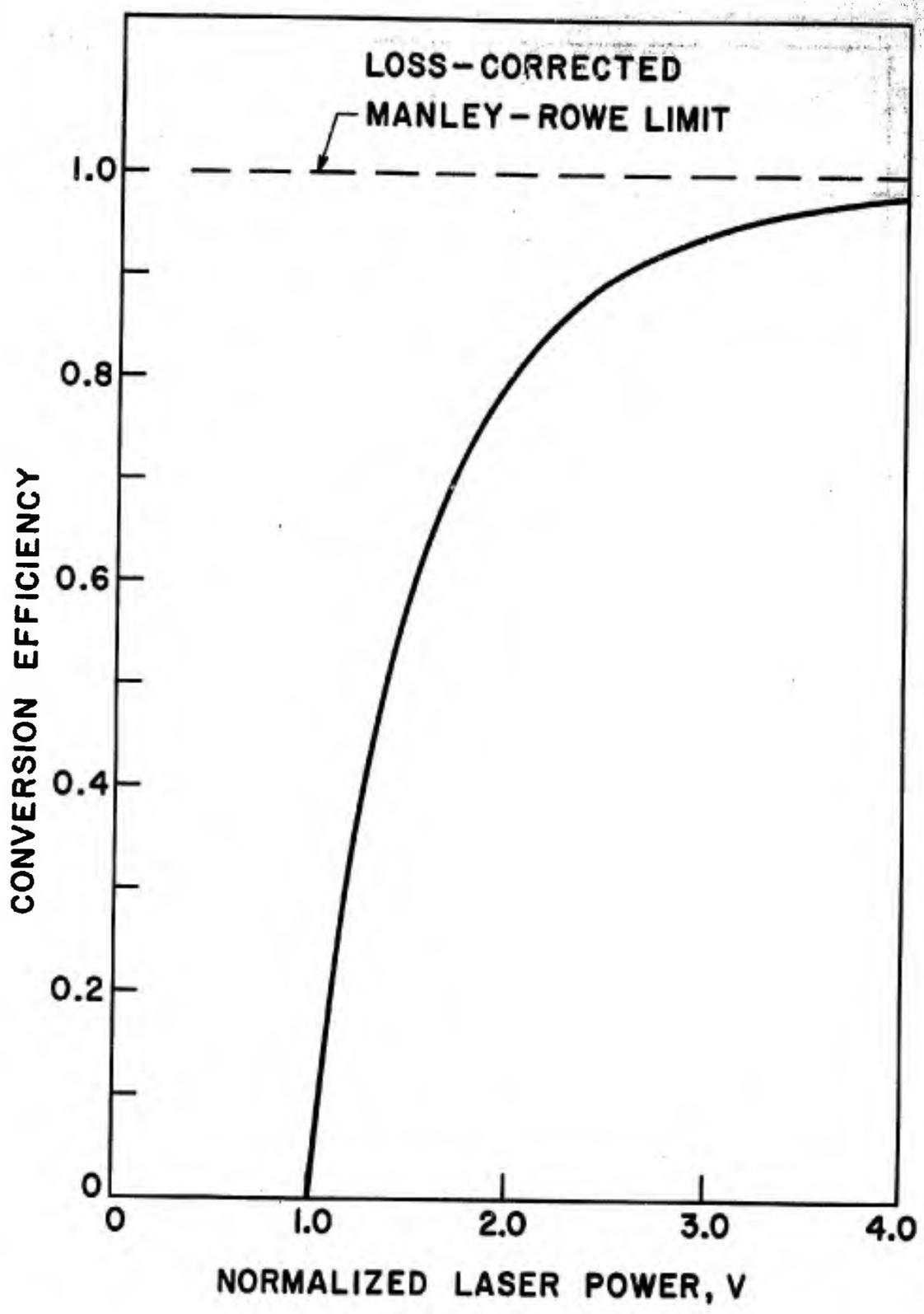

FIG. 5.3--Conversion efficiency as a function of normalized laser power. For laser powers which are several times threshold, the conversion efficiency approaches the Manley-Rowe limit multiplied by the correction factor τ_{ph}/τ_R which accounts for loss within the resonator.

large values of P_L , we obtain

$$\frac{P_s}{P_L} \approx \frac{\omega_s}{\omega_L} \frac{\tau_{ph}}{\tau_R} \quad . \tag{5.12}$$

Figure 5.3 shows that the above is a good approximation when the laser power is approximately a factor of three above threshold.

Conversion to the parametric effect by the substitution relation (4.32) indicates that the behavior described here carries over in toto, the only difference being that V and U given by (5.10) and (5.11) are each modified by the factor $\sqrt{\epsilon_\infty^V}/n_V$.

In summary, then, the tunable Raman laser is a threshold device which, if operated well above threshold, provides for the conversion of laser power into Stokes power in accordance with the loss-corrected Manley-Rowe parametric relationships.

CHAPTER VI

EXPERIMENTAL WORK

A. INTRODUCTION

In this chapter is described a two-part experimental program designed to determine the feasibility of the construction of a tunable Raman laser based on the theoretical work presented in Chapters II – IV.

The first part consists of a study of the stimulated Raman effect in a cavity with benzene as the Raman medium and a Q-switched ruby laser as the source. Although the particular vibration studied (992 cm^{-1}) is not infrared active and therefore does not allow the Stokes output to be tuned, it does permit verification of the design considerations since the theory is applicable to both cases.

In the second part of the program, the measurement of the tuning characteristic of an infrared-active vibrational mode in the crystal lithium niobate ($LiNbO_3$) is reported. This measurement is based on the detection of spontaneous Raman and parametric scattering of a low-level He-Ne gas laser beam, and provides direct verification of the tunability of the Stokes output.

With the above apparatus in operation, the 3450 cm^{-1} vibrational mode in H_2O was also examined to verify that a mode, although simultaneously Raman and infrared active, does not lead to a tunable Stokes output in an isotropic medium. (See Section III, B.4.)

B. STIMULATED RAMAN EFFECT IN AN OFF-AXIS RESONATOR

1. Description of Experimental Apparatus

The design of a tunable Raman laser requires the use of an off-axis cavity system as described in Fig. 5.1. In such a system a source laser beam makes a single pass through a Raman material, acting as a pump for the generation of Stokes cavity fields. In order to determine whether

the behavior of such a system is as described in Chapter V, the experimental configuration shown in Fig. 6.1 was assembled and a series of measurements was performed with benzene as the Raman medium and a Q-switched ruby laser as the source. These measurements are reported in considerable detail elsewhere,[46] and therefore only a brief description sufficient to indicate the basic features of interest is presented.

The Raman cell was placed within a resonator consisting of two plane dielectric mirrors separated by 50 cm. A typical set of measurements was made with a 20 cm cell fitted with Brewster windows to minimize reflections within the resonator. Both mirrors had a reflectivity of 98% at the Stokes wavelength, 7450 Å, and were partially cut away so that the exciting laser beam could pass through at a small angle without damaging the coatings. The entire Raman resonator assembly was mounted on an elevated table which permitted one end of the optical bench holding the laser to be rotated about a pivot point directly below the center of the Raman cell. Rotation of the laser beam about this point provided for angular control of the separation of the laser and Stokes beams as shown in Fig. 6.2.

The laser consisted of a $\frac{1}{2}$" × 3" Linde ruby rod with Brewster ends, and typically produced a pulse of 10 megawatts peak power with full width at half maximum of 30 nsec. The Q-switching was accomplished by means of a rotating prism. The beam was weakly focused with a 50 cm lens to increase the effective power density, producing beam diameters of 3-4 mm.

The laser and Stokes powers were monitored by reflecting a small percentage of the beam onto magnesium oxide screens and detecting the radiation with HPA 4203 PIN photodiodes.

2. Experimental Results

Typical experimental results and the corresponding theoretical curve are presented in Fig. 6.3. The data is seen to exhibit the main features of the stimulated Raman effect predicted in Chapter IV such as the existence of a threshold and an asymptotic approach (once loss is accounted for) to the Manley-Rowe limit at high excitation levels.

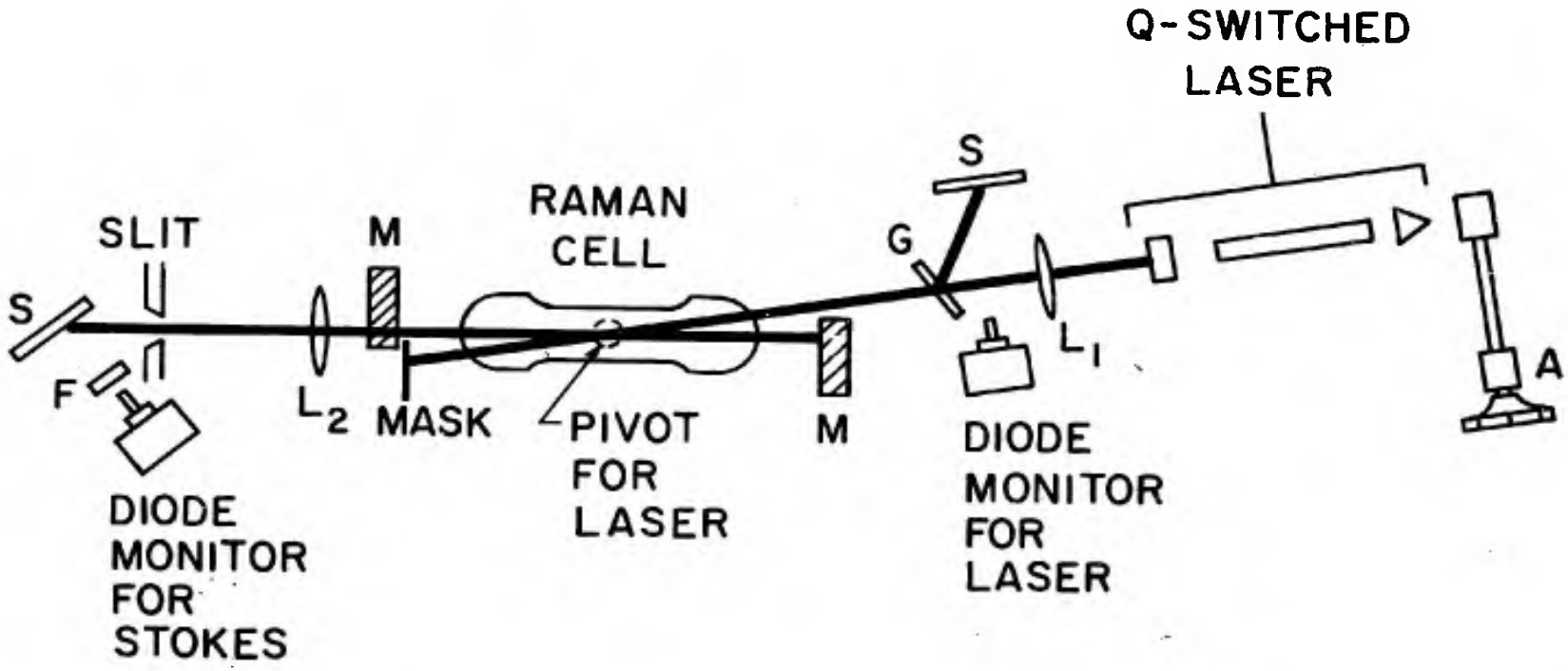

FIG. 6.1--Diagram of experimental apparatus. The cell of liquid is placed between mirrors, M , with reflectivities R . The ruby laser beam enters the cell at a small angle which is controlled by a mechanical track, A . The other items designated by letters are as follows: L_1 - 50 cm lens, L_2 - 24 cm lens, G - glass slide, S - M_gO screen, F - Spike filter for Stokes wavelength.

FIG. 6.2--Angular separation of the laser and Stokes beams. This photograph was taken from above the Stokes resonator and shows the two separate beams emerging from the Raman cell at the right.

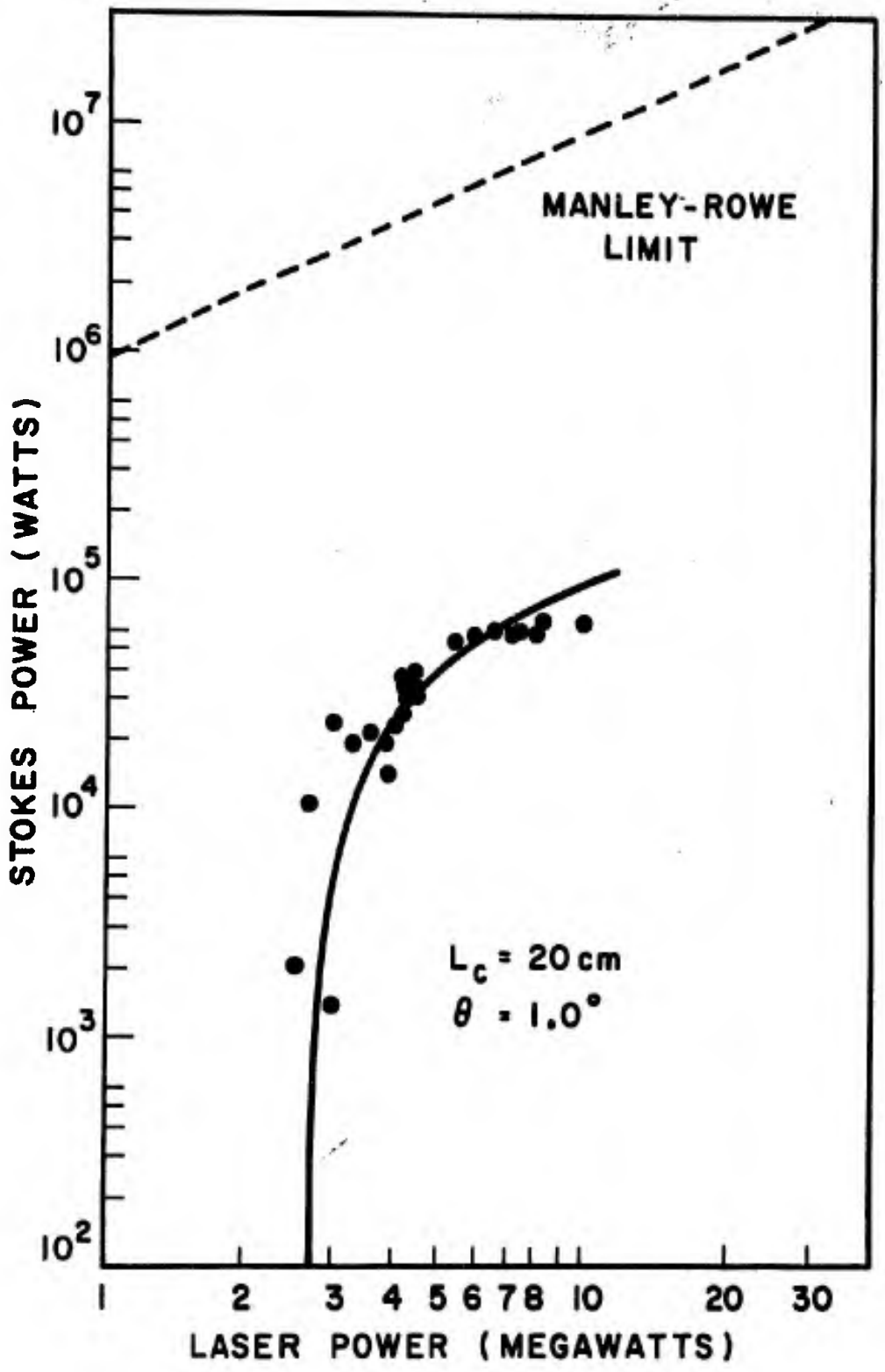

FIG. 6.3--Comparsion of theory and experiment. Stokes output power is plotted as a function of laser power for a 20 cm cell of benzene showing the scatter of experimental data. The solid line is the theoretical curve.

The appropriate parameters for a quantitative comparison between theory and experiment are

$$A = 9.6 \times 10^{-2} \text{ cm}^2 ,$$

$$\chi_R''(\Omega) = 6.1 \times 10^{-13} \text{ esu} ,$$

$$\lambda_s = 7.45 \times 10^{-5} \text{ cm} ,$$

$$L_R = 50 \text{ cm (resonator length)}$$

$$L_c = 20 \text{ cm (Raman cell length)}$$

$$n_L = n_s = 1.49 ,$$

$$R = 0.98 .$$

The area A was determined by measurement of the beam diameter at the input to the Raman cell, and the value for $\chi_R''(\Omega)$ was taken from the literature.[89] Once the above factors are inserted into the equations describing the behavior of the resonator system, one parameter yet remains to be determined in order to fit the theoretical curve to the data, namely, the photon lifetime τ_{ph}. An indirect determination is obtainable from the experimental power conversion data in terms of the ratio of Stokes to laser power at saturation. [See Eq. (5.12).] Taking the ratio of P_s to P_L at saturation from the experimental data and using the mirror reflectivities to determine the resonator lifetime $\tau_R = 83$ nsec, we obtain a photon lifetime of $\tau_{ph} = 1.2$ nsec. An independent interferometer measurement on a similar system yielded a value of 3.3 nsec, indicating that the obtained value is reasonable.

With the above values, (5.10) yields a threshold power

$$P_L = \frac{\lambda_s \, n_L \, n_{eff}^2 \, A \, L_R}{64\pi^3 \, \tau_{ph} \, \chi_R''(\Omega) \, L_c} = 2.63 \text{ Megawatts} ,$$

a value in good agreement with the experimental data. The above expression has been generalized from (5.10) to take into account the fact that the Raman cell does not fill the resonator, e.g., $n_{eff}^2 = 1 + (L_c/L_R)(n_s-1)$. The good agreement between theory and experiment thus indicates that the stimulated Raman effect in an off-axis resonator system is described properly by the theory.

Further evidence of the well-behaved properties of the resonator Stokes is contained in the time behavior of the resonator output shown in Fig. 6.4. This is a tracing of a photograph taken on a Tektronix 519 oscilloscope with a horizontal scale of 10 nsec/cm. For this photograph, the Stokes resonator was excited by a single-longitudinal-mode Q-switched laser which produced a relatively smooth output pulse in comparison with the oscillations which characterized the resonator Stokes. The frequency of the oscillatory behavior is that corresponding to interference of axial modes in the Stokes resonator, and the duration of the oscillations indicates that at least two such modes existed for a 30 nsec time interval. Thus the off-axis system does indeed act as a driven resonator with a well-defined longitudinal mode structure.

All the results discussed above, when taken together, indicate that the off-axis Raman system behaves both qualitatively and quantitatively in the manner described by the theory developed for the tunable Raman laser in Chapter V. The information presented there can therefore be taken as the basis for design considerations.

C. RAMAN AND PARAMETRIC SCATTERING FROM $LiNbO_3$

1. Introduction

In this section the theory developed for the tunable Stokes effect is applied to a specific example, that of the crystal $LiNbO_3$. This crystal was chosen for study because it possesses an optical vibrational mode at 628 cm^{-1} which is strongly Raman and infrared active.

In the experimental part of the study, the tuning concept is directly verified by means of a measurement of the Stokes tuning characteristic. The measurement technique, which consists of spontaneous Raman and

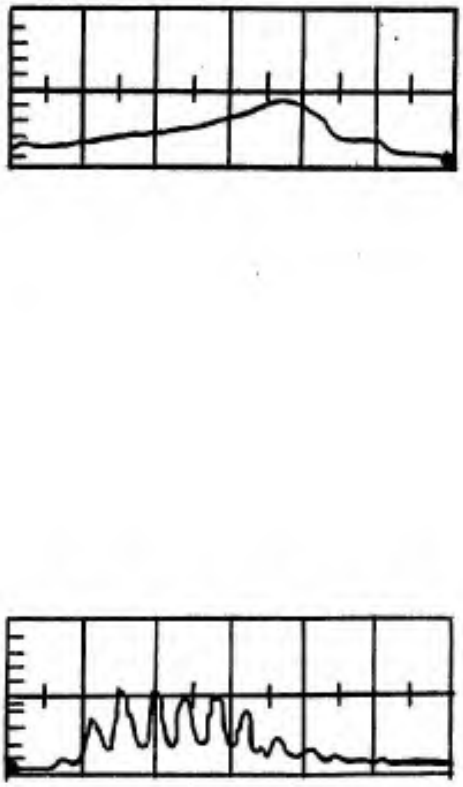

FIG. 6.4--Mode interference of the resonator Stokes. The upper trace shows the laser pulse shape. Note the absence of any repetitive perturbations on the pulse. The lower trace shows the oscillatory behavior which characterized the resonator Stokes with the frequency of oscillation corresponding exactly to the c/2L mode separation of the resonator. Time progresses from left to right with horizontal scale factors of 20 nsec/cm in the upper trace and 10 nsec/cm in the lower.

parametric scattering of a He-Ne gas laser beam, is itself of considerable interest. Application of the technique provides, in addition to the tuning characteristic, a plot of the dispersion characteristic of the vibrational mode in the mixed-mode region, a material property of interest in its own right. The dispersion characteristic measured in this manner is found to agree within experimental accuracy with the theoretical curve predicted on the basis of infrared reflectivity data. This method therefore provides a valuable alternative to the more difficult reflectivity measurements.

2. Crystal Structure, Mode Classification, and Raman and Infrared Activity

Lithium niobate is a negative uniaxial crystal $(n_o > n_e)$, trigonal in structure, belonging to the point group C_{3v} and space group R3c.[90] The ion positions in the unit cell are shown in Fig. 6.5.[91] As indicated in the figure, there are two formula units, and, therefore, ten atoms per unit cell. Thus there are thirty vibrational degrees of freedom giving rise to thirty phonon branches, three acoustic and twenty-seven optical. The labeling or classification of these branches is carried out according to the symmetries of the vibrations of the unit cell structure. Since information in the literature on Raman and infrared activity is presented in terms of the nomenclature used to classify the modes, a brief digression on this subject is useful at this point.

The method of classification is based on the fact that although the application of an allowed symmetry element transforms the non-vibrating structure into itself, in a vibrating structure the transformed displacements associated with a normal mode vibration are not necessarily the same as the non-transformed ones. In particular, with respect to a given symmetry operation the displacement coordinates may remain unchanged in sign (symmetric), be reversed in sign (antisymmetric), or in general change by more than just a sign.[92] It is these differences which form the basis for classification.

As far as notation is concerned, the classification of vibrations begins with a letter designation according to whether the vibrations are symmetric, antisymmetric, or degenerate with respect to axes of symmetry. Those symmetric with respect to an axis of symmetry are designated A-symmetry

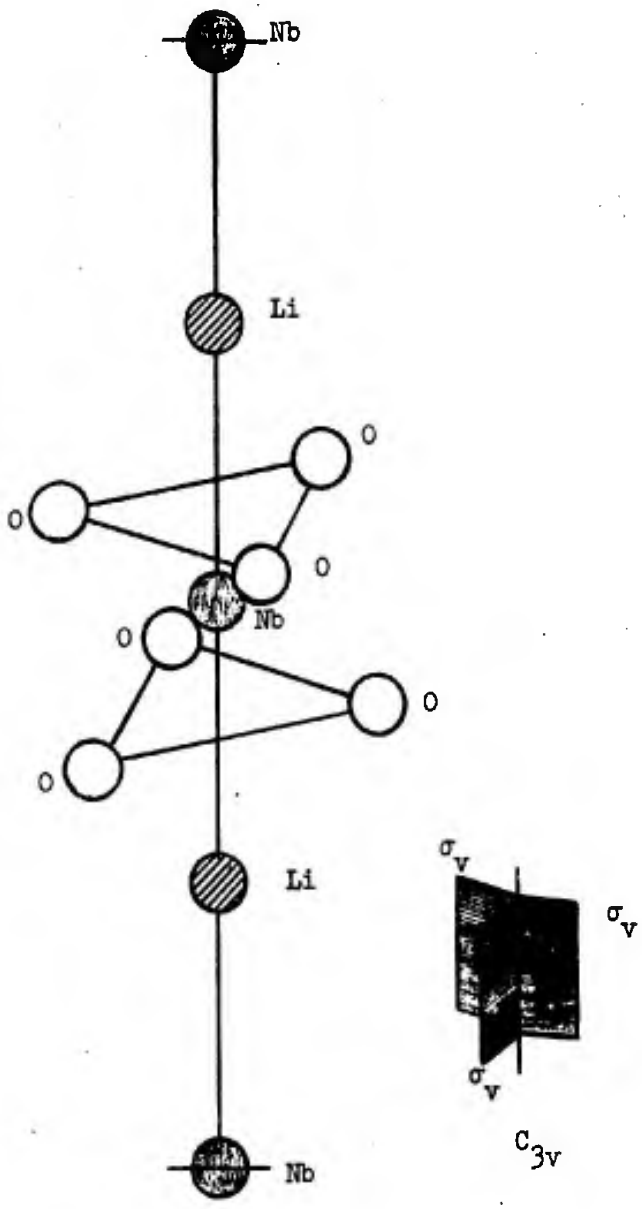

FIG. 6.5--Structure of $LiNbO_3$ unit cell. There are two formula units, and, therefore, ten atoms per unit cell. The unit cell belongs to the point group C_{3v}, indicating symmetries corresponding to a cyclic 3-fold rotation axis with 3 vertical symmetry planes σ_v through the axis arranged 120° apart.

vibrations; those antisymmetric with respect to an axis of symmetry are designated B-symmetry vibrations; and those that are degenerate with respect to an axis of symmetry are designated by E if doubly degenerate and by F if triply degenerate.[93] For n-fold degenerate vibrations, there are n distinct normal vibrations each of which has the same vibrational character and frequency. Further subscript notation, e.g., A_1, B_{3u}, is used to label symmetries with respect to other symmetry elements such as mirror planes. For a given point group the type of modes and their infrared and Raman activity can be determined by reference to Herzberg.[94]

The unit cell structure of $LiNbO_3$ has point group symmetry C_{3v}. As given in Herzberg,[94] there are, therefore, three species or types of normal vibrations. Two are non-degenerate species symmetric with respect to the three-fold rotation axis C_3: of these, one is symmetric with respect to the three mirror planes σ_v, the other antisymmetric. They are labeled as A_1 and A_2 modes, respectively. The third species consists of doubly-degenerate E modes.

Reference to Table 55 in Herzberg then yields the infrared and Raman activity or lack of it (i.e., the selection rules) for the given point group. The pertinent table entries for the C_{3v} group are as shown below.

TABLE VI.1

Infrared and Raman Selection Rules

M_x	M_y	M_z	α_{xx}	α_{yy}	α_{zz}	α_{xy}	α_{xz}	α_{yz}
E	E	A_1	A_1,E	A_1,E	A_1	E	E	E

In the notation of Herzberg, the quantities M and α refer to the dipole moment and polarizability, respectively. If a mode appears as an entry under any component of M, then that mode is infrared active, i.e., capable of absorbing infrared radiation. If a mode appears as an entry under any component of α, then that mode is Raman active. For the case at hand we see that the A_1 and E vibrations are simultaneously

Raman and infrared active, while the A_2 vibrations, since absent from the table, are Raman and infrared inactive.

The number of modes falling into each category depends on the number and particular configuration of the atoms within the unit cell. The enumeration of the modes is generally carried out with the aid of group theory, and is available in the literature. For $LiNbO_3$ the thirty phonon branches consist of three acoustic branches (one A_1 mode and one doubly-degenerate E mode) and twenty-seven optical branches. The twenty-seven optical branches consist of four totally symmetric vibrations of the A_1 type which are simultaneously Raman and infrared active $(E \| c)$, five vibrations of the A_2 type which are Raman and infrared inactive, and nine doubly-degenerate vibrations of the E type which are simultaneously Raman and infrared active $(E \perp c)$.

Published data on the Raman and infrared spectra for light polarized parallel to the c-axis are reproduced in Figs. 6.6 and 6.7. Based on this data, the 628 cm^{-1} A_1-symmetry mode was chosen for study because of its relatively large frequency shift in the Raman spectrum, its isolation from nearby modes, and its relatively strong Raman and infrared cross sections.[95,96]

3. Outline of Experimental Program

An experiment to observe spontaneous Raman and parametric scattering was set up according to the basic design indicated in Fig. 6.8. Before discussing the experiment itself, it is useful to summarize for the $LiNbO_3$ case the expectations based on the theory developed in Chapter IV.

In the region of large angle scattering corresponding to large k'_v, the predominant Stokes scattering mechanism is expected to be the pure Raman scattering process described by the relation

$$\tilde{P}'_s = \chi_R |\tilde{E}_L|^2 \tilde{E}_s \quad .$$

The summetry properties of such a process are determined by the symmetry properties of the fourth rank Raman susceptibility tensor χ_R. This information has been conveniently tabulated for all the vibrations in all the crystal classes in the form of a Raman tensor $R^T_{\sigma\rho}$ which relates the incident and scattered intensities as indicated in Table VI.2.

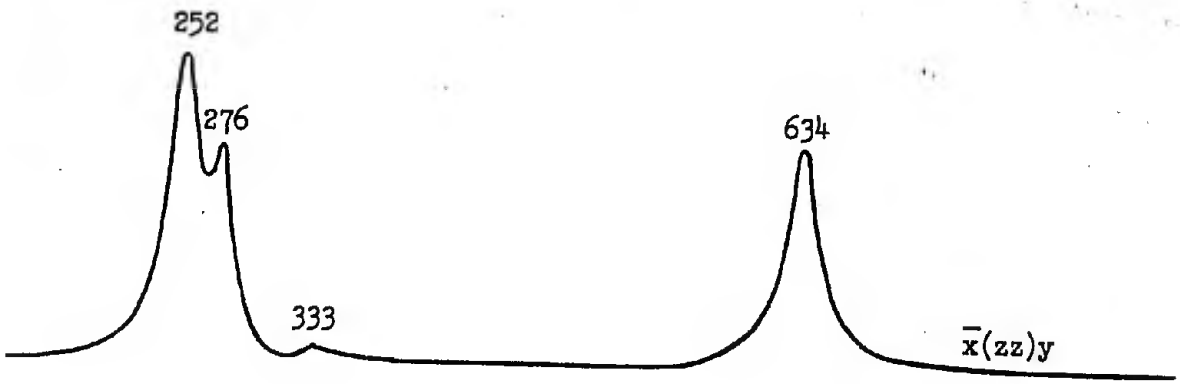

FIG. 6.6--Raman spectrum of $LiNbO_3$ for the propagation directions and polarizations indicated by the notation $\bar{x}(zz)y$. The inner two letters, from left to right, indicate the polarizations of the incident and scattered beams, respectively; the outer two letters, from left to right, indicate the propagation directions of the incident and scattered beams. The overbar indicates a negative direction.

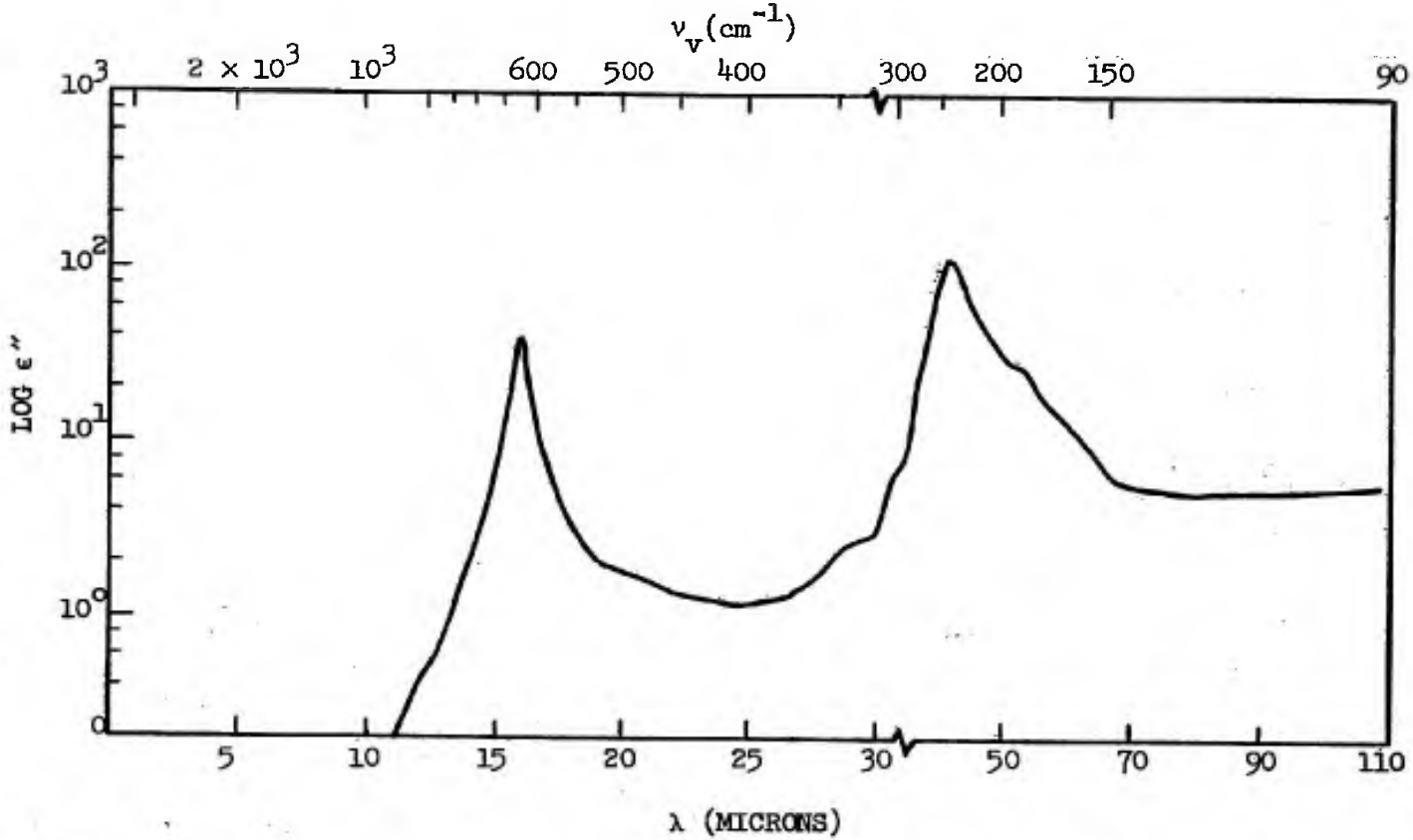

FIG. 6.7--Infrared absorption spectrum of $LiNbO_3$ for E‖c (extraordinary wave). For this polarization the spectrum is due to the A_1-symmetry modes, the infrared properties of which can be summarized in terms of the mode frequencies, strengths, and bandwidths, respectively, which are listed below:

ν_j (cm^{-1})	s_j	γ_j (cm^{-1})
248	16.0	21
274	1.0	14
307	0.16	25
628	2.55	34
692*	0.13	49

$\epsilon_\parallel(\infty) = 4.6$

*The observed mode at 692 cm^{-1} is in addition to the four fundamental A_1-symmetry modes predicted by group theory, and has been assigned by Barker and Louden as corresponding to a second order phonon combination band. Its contribution to $\epsilon_\parallel$ must be taken into account in the same manner as that of the fundamental modes.

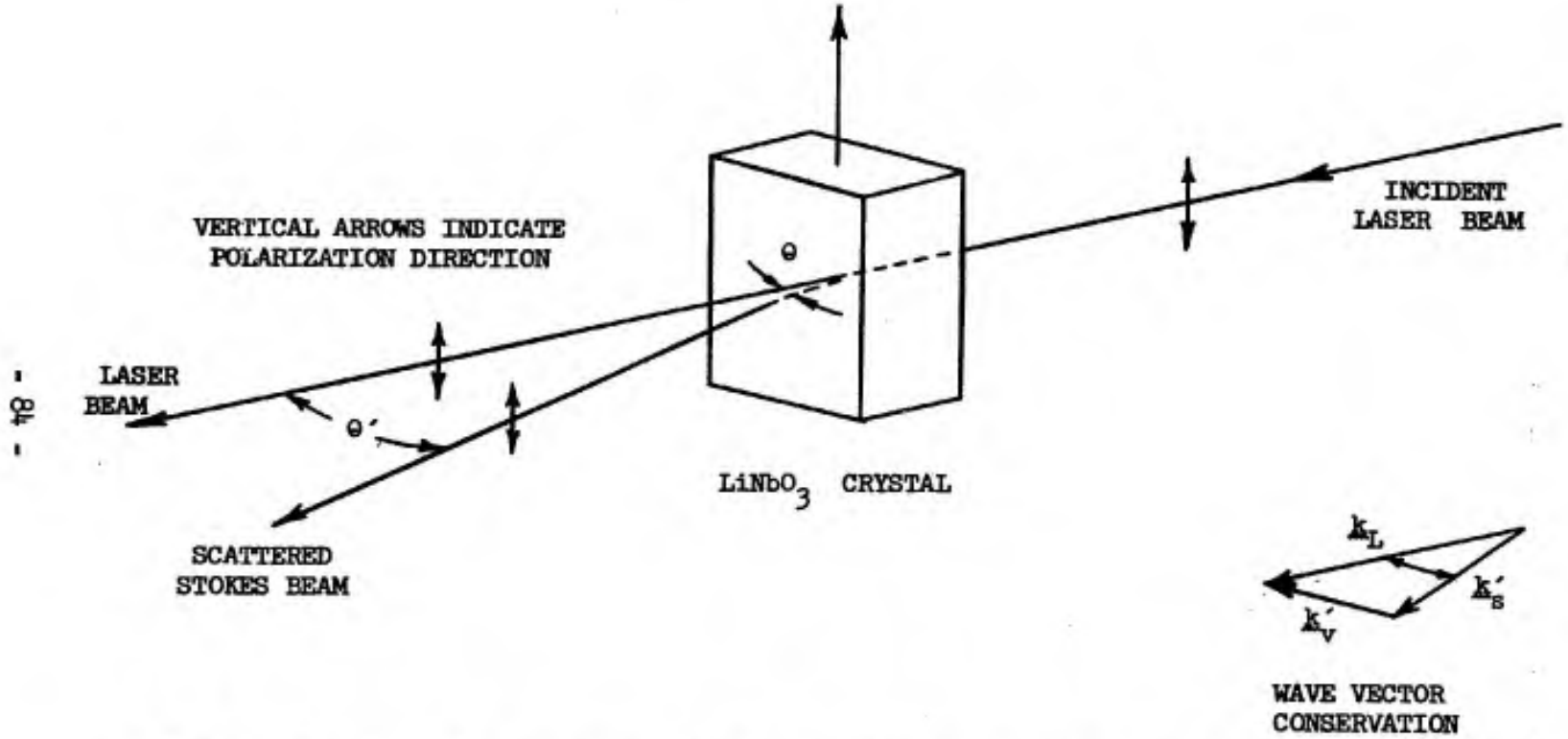

FIG. 6.8--Experimental arrangement for the observation of spontaneous Raman and parametric scattering. A vertically-polarized incident laser beam passes through a lithium niobate ($LiNbO_3$) crystal as an extraordinary wave ($E \parallel c$), exciting optical vibration modes in the crystal. Light scattered at the Stokes frequency at angle θ' is detected to determine the angular dependence of the frequency shift. For the A_1-symmetry mode of interest the scattered Stokes light is also vertically polarized.

TABLE VI.2

Raman tensor $R^{\tau}_{\sigma\rho}$ for the Point Group C_{3v} .[97]

$$R[A_1(z)] = \begin{bmatrix} a & 0 & 0 \\ 0 & a & 0 \\ 0 & 0 & b \end{bmatrix} \quad R[E(y)] = \begin{bmatrix} c & 0 & 0 \\ 0 & -c & d \\ 0 & d & 0 \end{bmatrix} \quad R[E(-x)] = \begin{bmatrix} 0 & -c & -d \\ -c & 0 & 0 \\ -d & 0 & 0 \end{bmatrix}$$

The z-axis is assumed to be parallel to the c-axis. The tensor element $R^{\tau}_{\sigma\rho}$ signifies that σ-polarized incident light produces ρ-polarized Stokes light with participation of a τ-polarized phonon. (The x,y, or z in parentheses after the letter representing the mode symmetry corresponds to the phonon polarization direction τ .)

TABLE VI.3

Linear Electro-Optic Tensor $z_{\rho\sigma\tau}$.[98]

The z-axis is assumed to be parallel to the c-axis. The tensor element $z_{\rho\sigma\tau}$ signifies that σ-polarized incident light produces ρ-polarized Stokes light with participation of a τ-polarized infrared wave associated with the lattice mode. The non-zero tensor elements are as follows:

$$z_{xzx} = z_{yzy} = z_{zxx} = z_{zyy}$$

$$z_{yyy} = -z_{xxy} = -z_{xyx} = -z_{yxx}$$

$$z_{xxz} = z_{yyz}$$

$$z_{zzz}$$

From the table it is seen that Stokes light scattered from the A_1 mode due to incident laser light polarized in the z-direction is itself also polarized in the z-direction.

In this region of the dispersion characteristic the difference between the laser and Stokes frequencies is expected to occur at the transverse optical mode vibrational frequency, $\Omega = 628\ cm^{-1}$.

As the region of small angle scattering is approached corresponding to small k_v' , the predominant Stokes scattering mechanism is expected to be the resonant parametric process described by the relation

$$\tilde{P}_s' = \chi_p \tilde{E}_v^* \tilde{E}_L \quad .$$

The symmetry properties in this case are determined by the symmetry properties of the third rank parametric susceptibility tensor, χ_p . By reference to the derivation of this tensor property it is seen that χ_{ijk} is derived in terms of the polarizability tensor Q_{ij} , and must therefore be symmetric in the first two indices, i.e., $\chi_{ijk} = \chi_{jik}$. As a result, the symmetry properties of the parametric tensor are those of the linear electro-optic tensor, $z_{\rho\sigma\tau} = z_{\sigma\rho\tau}$. (See Table VI.3.) From the table it is seen that the scattering of an incident field polarized in the z-direction by a mode which produces a z-polarized infrared wave yields Stokes light polarized in the z-direction. Since for both cases of scattering from the A_1-symmetry mode of interest, the polarization directions of the incident and scattered light and of the phonon are all parallel to the c-axis, the one-dimensional derivations of the previous chapters are directly applicable.

For the parametric scattering case, the difference between the laser and Stokes frequencies is expected to follow the infrared dispersion characteristic. As discussed in Fig. 3.3, the infrared dispersion characteristic is given by

$$k_v^{o2} = \frac{\omega_v^2 \epsilon_v}{c^2} = 4\pi^2 \nu_v^2 \epsilon_v \quad ,$$

where k_v^o is the optical mode wave vector, frequency ν_v is measured in cm^{-1}, and ϵ_v is the complex dielectric constant given by

$$\epsilon_v = \epsilon_\infty^v + \sum_j \frac{\Delta \epsilon_j \nu_j^2}{\nu_j^2 - \nu_v^2 + i\nu\gamma_j} \quad .$$

In the above expression ϵ_∞^v is the frequency-independent contribution to the dielectric constant due to the ultraviolet electronic resonances, and the ν_j , $\Delta\epsilon_j$, and γ_j are the mode frequencies, strengths, and bandwidths, respectively.

Since $LiNbO_3$ is a uniaxial crystal, there are two expressions of the form (2), one for propagation with $E \perp c$ (ordinary), and one for $E \| c$ (extraordinary). For the case under consideration we are interested in the dispersion characteristic for extraordinary waves which is determined by the A_1-symmetry modes, as discussed in Fig. 6.6. The parameter values listed there, when substituted into the above two equations, result in the theoretical dispersion characteristic shown in Fig. 6.9 as a solid curve.

4. Experimental Results

The experimental arrangement for detecting the spontaneous Stokes light is described in Fig. 6.10.

The data from the experiment yields a plot of the Stokes frequency shift as a function of the angular separation θ between Stokes and laser beams (Fig. 6.11). Of course, to obtain the angle θ inside the crystal, one must first correct the measured angle θ' by Snell's law as indicated in Fig. 6.12.

In order to plot the data on a $\nu_v - k_v'$ dispersion diagram, wave vector conservation (Fig. 4.3) is invoked to obtain the relationship between k_v' and θ ,

$$\begin{aligned} k_v'^2 &= k_L^2 + k_s'^2 - 2k_L k_s' \cos\theta \\ &= 4\pi(\nu_L n_L - \nu_s n_s)^2 + 8\pi^2 \nu_L \nu_s n_L n_s (1 - \cos\theta) \quad , \end{aligned} \tag{6.1}$$

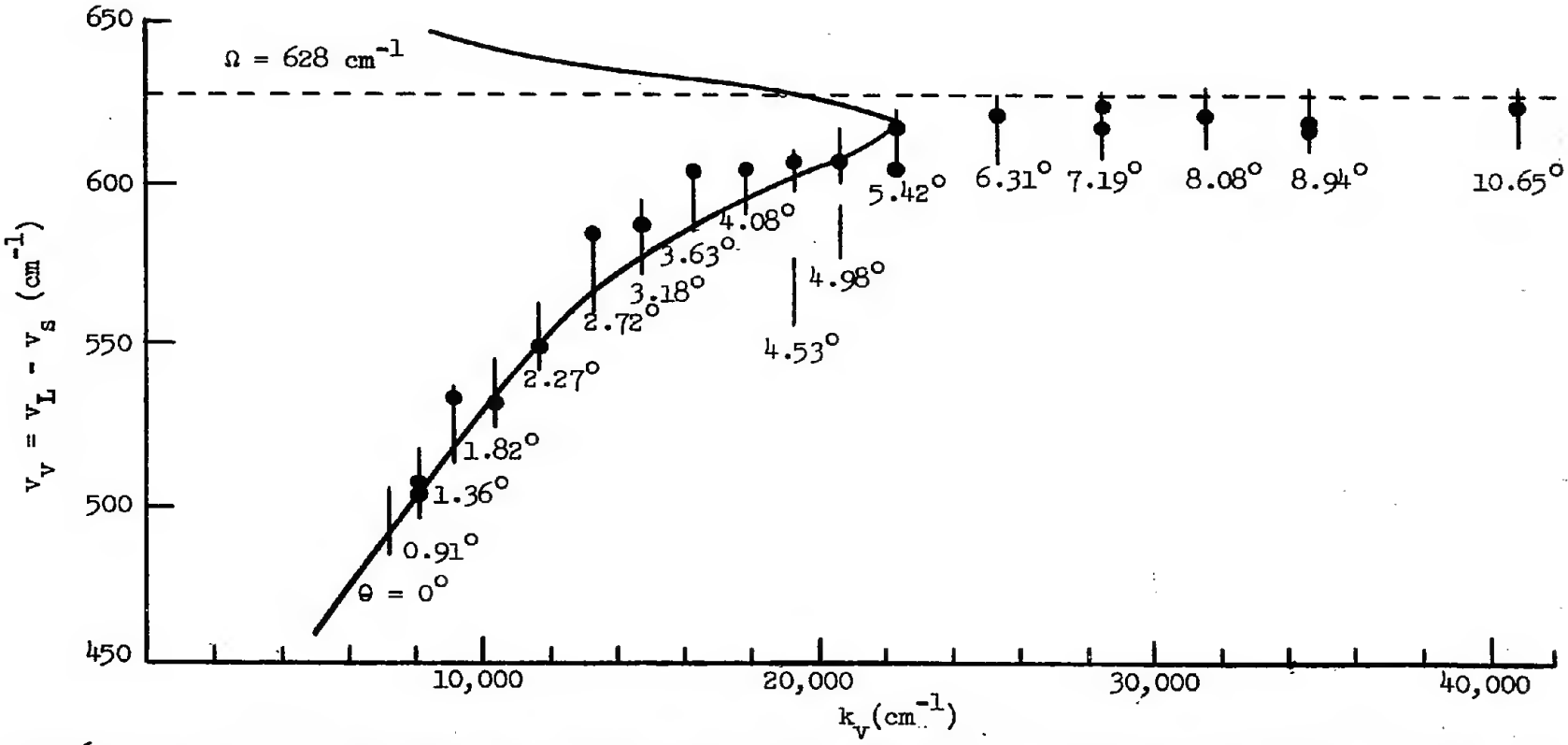

FIG. 6.9--Dispersion diagram for observed Stokes light. The solid curve is the theoretical infrared dispersion characteristic based on infrared reflectivity measurements, the short intersecting vertical lines are frequency - wave vector conservation curves for a given angular separation θ between Stokes and laser beams, and the circles correspond to experimentally-observed Stokes frequency shifts.

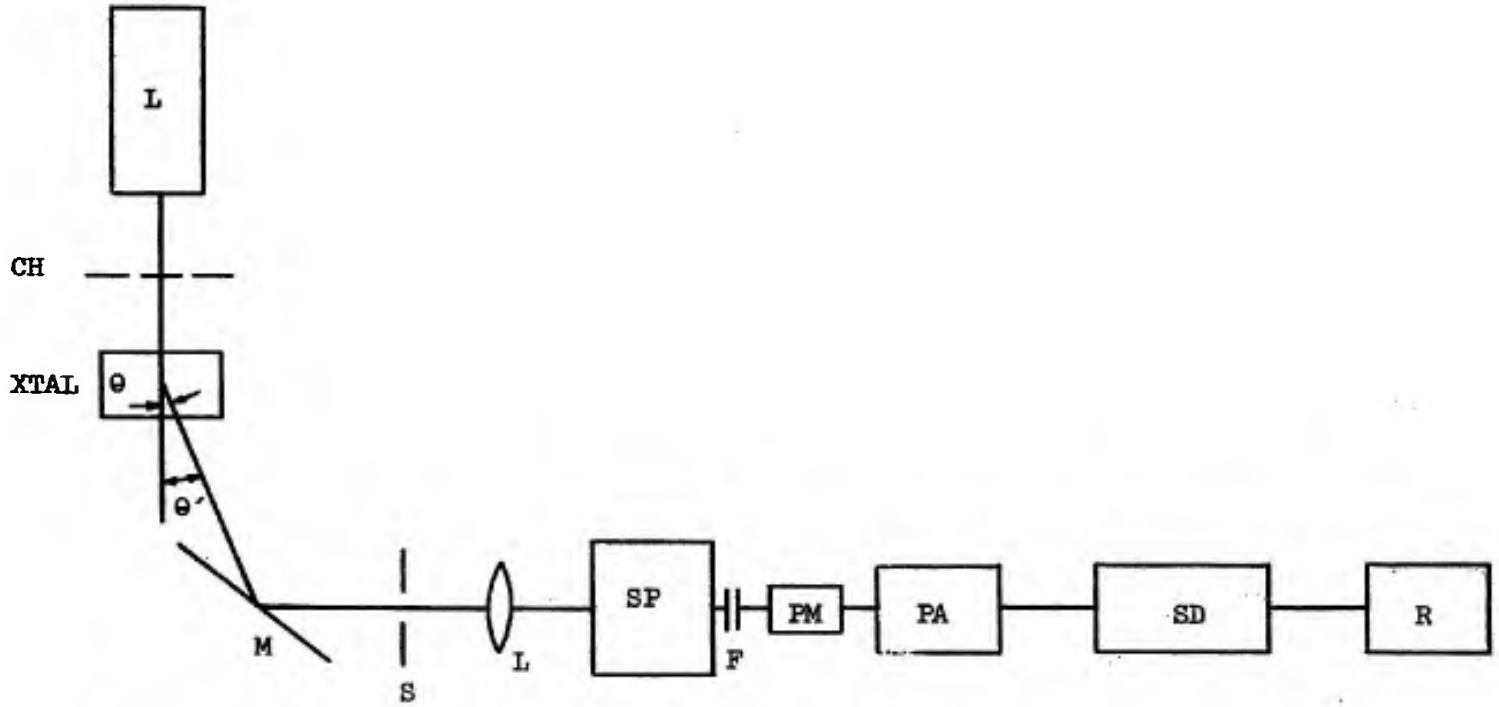

FIG. 6.10--Experimental apparatus for observation of spontaneous Raman and parametric scattering. A 50 milliwatt 6328 Å laser beam emerges from source L and passes through a 1000 cps chopper, CH, to fall on a 0.5 cm thick $LiNbO_3$ crystal, XTAL. Stokes light emerging from XTAL at angle θ′ is directed by an adjustable mirror, M , through a slit, S , which defines an acceptance angle inside the crystal of 0.2°. The scattered light is then collected by a lens, L , which images the crystal on the slit of a grating spectrometer, SP . The output from SP passes through two 2-58 Corning filters, F , and is detected by an EMI 9558B photomultiplier tube, PM , followed by a PAR CR-4 low-noise preamp, PA , and PAR JB-5 synchronous detector, SD , finally to be recorded on a strip-chart recorder, R .

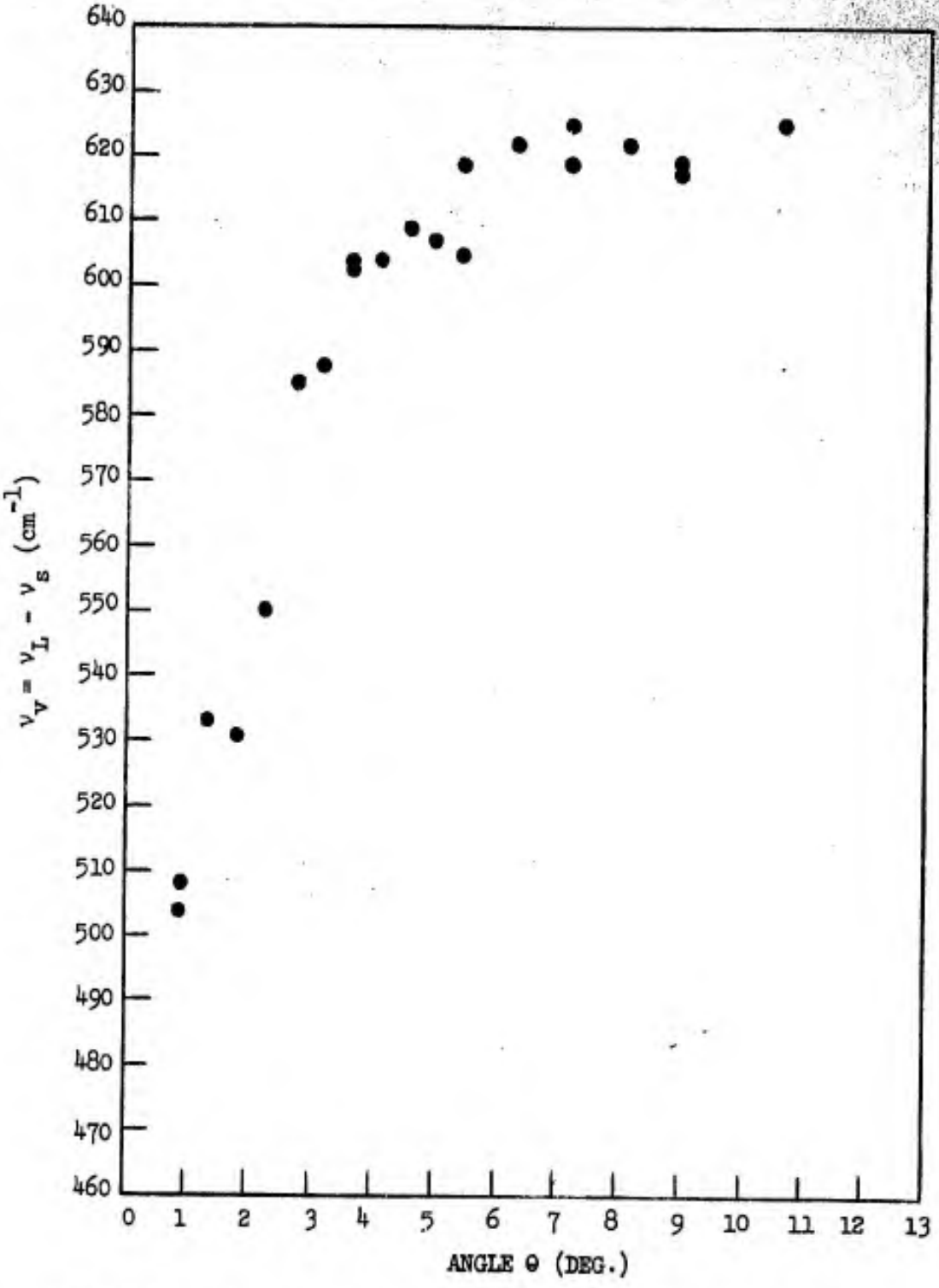

FIG. 6.11 Stokes frequency shift as a function of the angular separation θ between Stokes and laser beams.

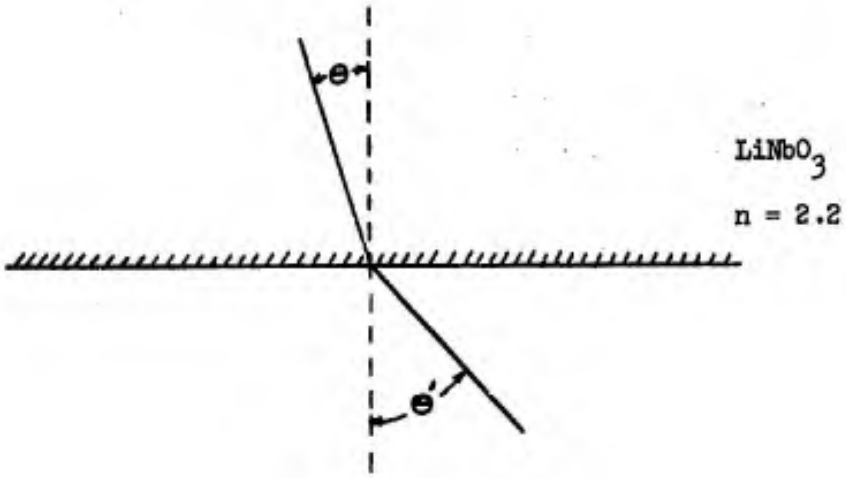

θ′	1	2	3	4	5	6	7	8	9	10.	11	12	14	16
θ	0.46	0.91	1.36	1.82	2.27	2.72	3.18	3.63	4.08	4.53	4.98	5.42	6.31	7.19

θ′	18	20	22	24
θ	8.08	8.94	9.80	10.65

FIG. 6.12--Snell's law correction to observed angle θ', $n \sin \theta = \sin \theta'$.

where ν_L, ν_s are the laser and Stokes frequencies in cm^{-1}, and n_L, n_s are the corresponding refractive indices. From the data of Boyd, et al. (plotted in Fig. 6.13), we find that $n_L = 2.200$ and n_s in the region of interest can be approximated by

$$n_s = 2.191 + 8.204 \times 10^{-6}(\nu_s - 14706) \quad . \tag{6.2}$$

With $\nu = \nu_L - \nu_s$, a computer plot of (6.1) incorporating the information in (6.1) yields a family of curves for various angles which allow the data points to be plotted on the dispersion diagram as shown in Fig. 6.9.

The data points are found to be in agreement with the expectations based on the theory developed in Chapter IV. The Stokes output is observed to follow the infrared dispersion characteristic in the region where parametric scattering is dominant and asymptotically to approach a purely vibrational dispersion curve in the region where pure Raman scattering is dominant. No appreciable change in the scattered intensity was observed during the transition.

The observed tuning range for the Stokes output extended from 6536 Å to 6586 Å, a range of 50 Å. (As is seen from Fig. 6.9, this is approximately the maximum tuning range possible for this transition, since at $\theta = 0^\circ$ the minimum theoretical frequency shift is set by high frequency dispersion at 492 cm^{-1}.) The results thus indicate that Stokes tuning over a relatively broad range is possible, thus substantiating the tunability concept.

D. FEASIBILITY OF THE CONSTRUCTION OF A TUNABLE RAMAN LASER BASED ON THE 628 cm^{-1} TRANSITION IN $LiNbO_3$

As far as the construction of a tunable Raman laser is concerned, the primary requirement which must be met is that the resonator gain at the Stokes frequency must be sufficient to overcome the losses, i.e., the threshold condition $V = 1$ in Eq. (5.10) must be met, implying

$$\frac{\mathcal{P}_L}{A} \geq \frac{n_L n_s^2 \lambda_s}{64\pi^3 \tau_{ph} \chi_R''(\Omega)} \quad . \tag{6.3}$$

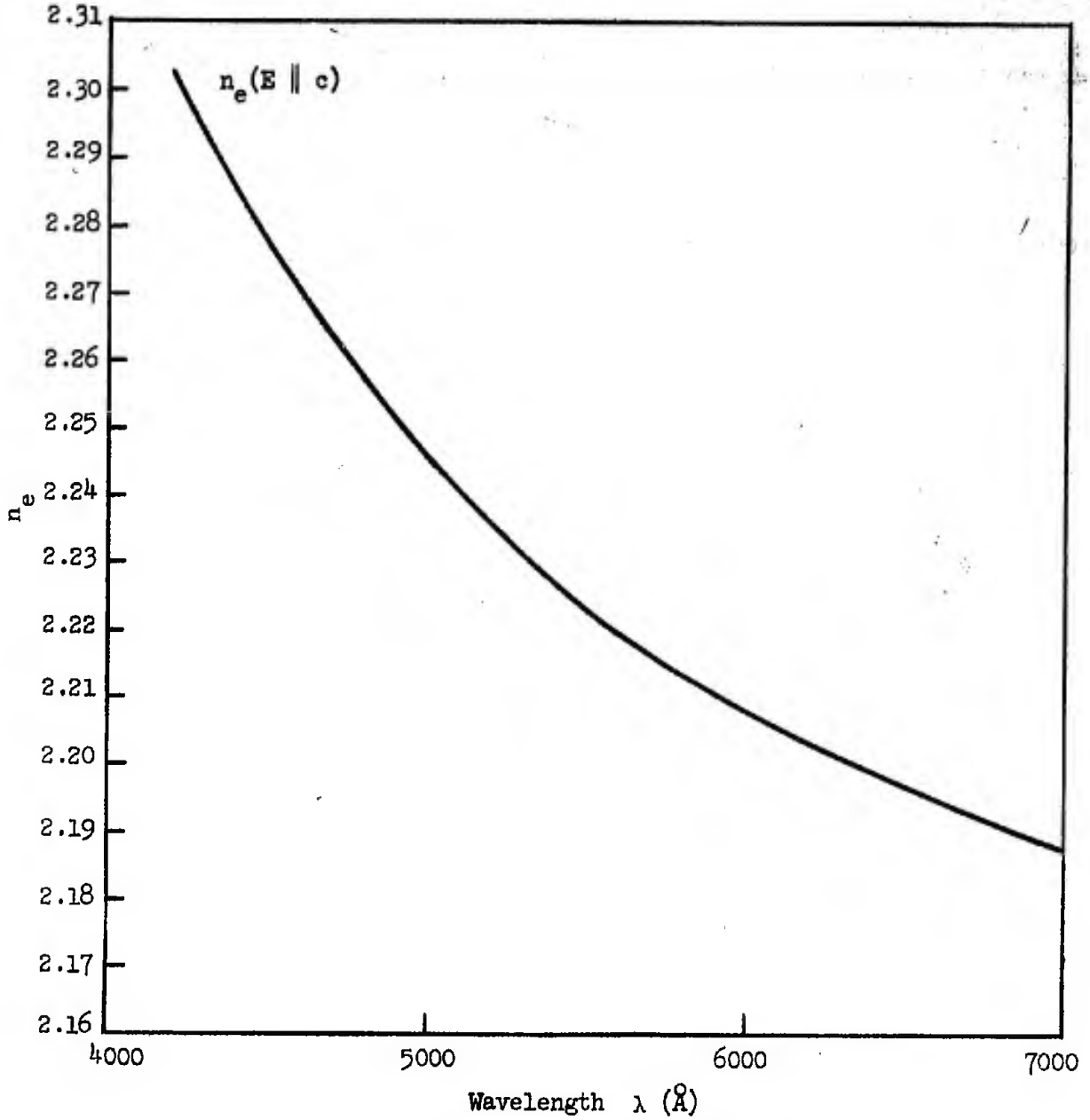

FIG. 6.13--Extraordinary refractive index n_e for $LiNbO_3$.

Introducing the one-way loss per pass ϵ, which for small losses is related to the photon lifetime, τ_{ph}, by

$$\tau_{ph} = \frac{L}{c/n_s} \frac{1}{\epsilon} ,$$

we can express the threshold condition (6 3) in the alternative form

$$g_s L = \epsilon , \tag{6.4}$$

where g_s is the Stokes power gain,

$$g_s = \frac{64\pi^3 \chi_R''(\Omega)}{c n_L n_s \lambda_s} \frac{P_L}{A} . \tag{6.5}$$

Stated in this form, the threshold condition is simply the requirement that the single pass gain at the Stokes frequency must be sufficient to overcome the single pass loss.

The threshold condition in terms of the laser power per unit area then, is, from (6.4) and (6.5),

$$\frac{P_L}{A} \geq \left[\frac{c n_L n_s \lambda_s \epsilon}{64\pi^3 L |\chi_R''(\Omega)|_{C_6H_6}} \right] \frac{|\chi_R''|_{C_6H_6}}{|\chi_R''|_{LiNbO_3}} . \tag{6.6}$$

Here we have chosen to express the threshold condition in terms of the ratio of benzene (992 cm^{-1}) to $LiNbO_3$ peak susceptibilities.

In the construction of a device, two design parameters which can be controlled are the crystal length and the choice of mirrors. Concerning the crystal length, if mirror losses predominate, then ϵ is a fixed quantity (i.e., independent of crystal length), and by (6.4) a long crystal is indicated. Once scattering and absorption losses predominate, however, further lengthening of the crystal is of no avail, since these losses are proportional to the crystal length. With typical scattering losses of 1-2% cm^{-1} and mirror losses of 1% per mirror, crystals on the order of 3-4 cm constitute a reasonable choice.

As far as the choice of mirrors is concerned, experiments with plano-concave and plane-parallel resonators in systems similar to the one proposed here indicate that, of the two, measured losses are those expected from mirror reflectivity calculations only for the plano-concave resonator.[99] For a plane-parallel resonator, on the other hand, additional losses of ten percent per pass beyond that expected from mirror reflectivities are encountered. Therefore, a plane-parallel resonator is to be avoided.

As a value for the loss parameter ϵ which is probably the lowest that can be achieved with the present state of the art, we take the results of Ashkin and Boyd.[100] There an experimentally-determined value of $\epsilon = 0.011$ for a 0.55 cm crystal was obtained by direct measurement of the width of the Fabry-Perot cavity resonances. The cavity in this case consisted of multiple-layer dielectric coatings deposited directly on the faces of the crystal which had been fabricated with curved surfaces (4 cm radius of curvature). The width of the Fabry-Perot resonances was measured for an extraordinary wave propagating along the a axis by the technique of applying a swept transverse electric field along the optic z axis such that the resonator acts as a scanning interferometer.

For the other parameters, assuming a ruby laser pump source, $n_L \approx n_s \approx 2.2$, $\lambda_s = 7.26 \times 10^{-5}$, $\chi_R''(\Omega)_{C_6H_6} = 6.1 \times 10^{-13}$ esu . The threshold condition (6.6) then reduces to

$$\frac{\rho_L}{A} \geq 17.4 \frac{|\chi_R''|_{C_6H_6}}{|\chi_R''|_{LiNbO_3}} \frac{Mw}{cm^2} \quad . \tag{6.7}$$

The ratio of susceptibilities is available from spontaneous Raman scattering data.[101] The wavelength-integrated Raman intensity for benzene is found to be approximately 1/60 that of $LiNbO_3$. Since the intensity is proportional to the product of the peak susceptibility, χ_R'' , and the width of the Raman line, γ , the ratio of the peak susceptibilities is therefore given by the ratio of the observed intensities divided by the

ratio of the bandwidths, or

$$\frac{|\chi_R''|_{C_6H_6}}{|\chi_R''|_{LiNbO_3}} = \frac{1}{60} \times \frac{30}{2.3} = 0.22 \quad ,$$

where the Raman linewidths are those quoted in reference 101. The threshold power per unit area given by (6.7) is therefore by this calculation ~ 4 Mw/cm^2 .

In the above threshold calculation, it is assumed that the applied laser beam which acts as a pump for the stimulated Raman process has a given uniform intensity or power per unit area within the Raman medium. Such an assumption is reasonable in the case of an unfocused or weakly-focused beam. If the beam is strongly focused in order to reach threshold with relatively low powers, however, then the intensity distribution is highly nonuniform with the beam concentrated near the focus. In this case the threshold condition is determined by the integrated path gain through the focal region. For this calculation we assume that the laser beam profile is gaussian, which is typical of the output of gas lasers. The calculation is performed in Appendix E. Two important results are:

(a) once the beam is focused sufficiently to bring the effective interaction length or focal region inside the crystal, further focusing does not materially increase the integrated path gain – therefore, in order to lessen the possibility of damage to the Raman medium, as little focusing as necessary is to be used;

(b) if a gaussian laser beam is brought to focus inside the medium, the threshold condition is expressed in terms of the total power rather than the power per unit area. The threshold laser power $\mathcal{P}_L$ required for the integrated single pass gain to overcome the single pass loss ϵ is given by

$$\mathcal{P}_L = \frac{\lambda_L \epsilon}{2\pi K n_L} \quad . \tag{6.8}$$

For the $LiNbO_3$ case at hand with K given by (4.33), the threshold power P_L given by (6.8) is ~ 10 watts.

The calculations presented above coupled with previous considerations indicate that the construction of a tunable Raman laser based on the 628 cm^{-1} transition is feasible with crystals and components representative of the best of the state-of-the-art. As higher quality large crystals become available, the construction of such a device will be undertaken.

CHAPTER VII

CONCLUSIONS

The primary contributions of this work are

(a) the conception of the tunable Raman laser as a device capable of yielding continuously tunable coherent optical radiation over a range of tens of angstroms;

(b) the development of the theory describing the tunable Raman effect;

(c) the verification of the theory by a series of experiments culminating in the observation of tunable Stokes emission from the crystal lithium niobate. As predicted by theory, in experiments with benzene, water, and lithium niobate, tunable Stokes emission is observed only for the $LiNbO_3$ case which satisfies the dual requirement that the vibration involved in the Raman scattering event must be infrared active and the medium must lack a center of symmetry. In accordance with theory, the tuning characteristic obtained as a result of phase matching is observed to follow the infrared dispersion characteristic;

(d) the design of a tunable Raman laser system based on the use of an off-axis resonator;

(e) verification of the tunable Raman laser design by stimulated Raman experiments with benzene which, although not tunable, permits substantiation of the design considerations shown to be applicable to both tunable and non-tunable cases;

(f) the presentation of calculations indicating that the construction of a tunable Raman laser based on the 628 cm^{-1} line in $LiNbO_3$ is feasible provided a crystal and components with characteristics corresponding to the best of the state-of-the-art can be assembled together. Construction of such a device in the future is envisioned as high quality crystals become available.

APPENDIX A

SUBSTANCES FOUND TO EXHIBIT STIMULTED RAMAN EFFECT

LIQUIDS	FREQ. SHIFT (cm^{-1})	REFERENCES
Bromoform	222	C
Tetrachloroethylene	447	J
Carbon Tetrachloride	460	L
Hexafluorobenzene	515	L
Bromoform	539	C
Trichlorethylene	640	C
Carbon Disulfide	656	C
Chloroform	667	C
Orthoxylene	730	B
α Dimethyl Phenethylamine	836	I
Dioxan	836	C
Morpholine	841	L
Thiophenol	916	L
Nitro Methane	927	L
Deuterated Benzene	944	A
Cumene	990	L
1:3 Di Bromobenzene	990	J
Benzene	992	A,C
Pyridine	992	A
Aniline	997	H
Styrene	998	D,H
m Toluidine	999	L
Bromogenzene	1000	H
Chlorobenzene	1001	L
Benzonitrile	1002	H
T: Butyl Benzene	1002	J
Ethyl Benzene	1002	B
Toluene	1004	A,C
Fluorobenzene	1012	E
γ Picoline	1016	L
m Cresol	1029	L
Meta-Dichlorobenzene	1030	L
1: Fluoro 2: Chlorobenzene	1030	J
Iodo Benzene	1070	L
Benzoyl Chloride	1086	L
Benzaldehyde	1086	L
Anisole	1097	L
Pyrrole	1178	L
Furan	1180	L
Styrene	1315	D,H

Nitrobenzene	1344	A,C
1: Bromonaphthalene	1368	A
1: Chloronaphthalene	1368	H
2: Ethyl Naphthalene	1381	J
m Nitro Toluene	1389	L
Quinolene	1427	L
Furan	1522	L
Methyl Salicylate	1612	L
Cinnamaldehyde	1624	H
Styrene	1629	D,H
3: Methyl Butadiene	1638	G
Pentadiene	1655	G
Isoprene	1792	I
1: Hexyne	2116	L
Ortho-Dichlorobenzene	2202	L
Benzonitrile	2229	H
1:2 Dimethyl Aniline	2292	L
Methyl Cyclohexane	2817	L
Methanol	2831	C
cis trans 1:3 Dimethyl Cyclohexane	2844	J
Tetrahydrofuran	2849	H
Cyclohexane	2852	A,C
cis 1:2 Dimethyl Cyclohexane	2854	J
α Dimethyl Phenethylamine	2856	I
Dioxan	2856	C
Cyclohexane	2863	A,C
Cyclohexanone	2863	B
cis trans 1:3 Dimethyl Cyclohexane	2870	J
cis 1:4 Dimethyl Cyclohexane	2873	J
Cyclohexane	2884	A,C
Dichloro Methane	2902	L
Morpholine	2902	L
2: Octene	2908	J
2:3 Dimethyl 1:5 Hexadiene	2910	J
Limonene	2910	I
Orthoxylene	2913	B
1: Hexyne	2915	L
cis 2: Heptene	2920	J
Mesitylene	2920	I
2: Bromopropane	2920	J
Acetone	2921	B,C
Ethanol	2921	C
Carvone	2922	I
cis 1:2 Dimethyl Cyclohexane	2927	J
Dimethyl Formamide	2930	C
2: Chloro 2 Methyl Butane	2931	J
2: Octene	2931	J
cis trans 1:3 Dimethyl Cyclohexane	2931	J
Metaxylene	2933	B
1:2 Diethyl Tartrate	2933	I
Orthoxylene	2933	B
Piperidine	2933	B

1:2 Diethyl Benzene	2934	J
2 Chloro 2 Methyl Butene	2935	J
1: Bromopropane	2935	J
Piperidine	2936	B
Tetrahydrofuran	2939	H
Piperidine	2940	B
Cyclohexanone	2945	B
2: Nitropropane	2948	J
1:2 Diethyl Carbonate	2955	L
1:2 Dichloro Ethane	2956	L
Trans Dichlorethylene	2956	C
1: Bromopropane	2962	J
2 Chloro 2 Methyl Butane	2962	J
α Dimethyl Phenethylamine	2967	I
Dioxan	2967	C
Cyclohexanol	2982	L
Cyclopentane	2982	L
Cyclopentanol	2982	L
Bromo-Cyclopentane	2982	L
Ortho-Dichlorobenzene	2982	L
Para Chlorotoluene	2982	L
α Picoline	2982	L
Paraxylene	2988	B
Orthoxylene	2992	B
Di Butyl n Phthalate	2992	L
1:1:1 Trichloroethane	3018	C
Ethylene Chlorhydrin	3022	L
Iso Phorone	3022	L
Nitroso Dimethylamine	3022	L
Propylene Glycol	3022	L
Cyclohexane	3038	L
Styrene	3056	D,H
Benzene	3064	A,C
T: Butyl Benzene	3064	J
1: Fluoro 2: Chlorobenzene	3084	J
Turpentine	3090	L
Pseudo Cumene	3093	L
Acetic Acid	3162	L
Acetonyl Acetone	3162	L
Methyl Methacrylate	3162	L
γ Picoline	3182	L
Aniline	3300	H
Water	3651	L

SOLIDS

Quartz	128	K
α Sulphur	216	H
Quartz	466	K
α Sulphur	470	H
Calcium Tungstate	911	H
Stilbene	997	I

Polystyrene	1001	C
Calcite	1084	C
Diamond	1332	H
Naphthalene	1380	H
Stilbene	1591	I
Tryglycine Sulphate	2422	L
Tryglycine Sulphate	2702	L
Tryglycine Sulphate	3022	L
Polystyrene	3054	C

GASES

Oxygen	1552	H
Methane	2916	F
Deuterium	2991	F
Hydrogen	4155	F

REFERENCES

A. G. Eckhardt, R. W. Hellwarth, F. J. McClung, S. E. Schwarz, and D. Weiner, "Stimulated Raman Scattering from Organic Liquids," Phys. Rev. Letters 9, 455 457 (December 1962).

B. M. Geller, D. P. Bortfeld, and W. R. Sooy, "New Woodbury-Raman Laser Materials," Appl. Phys. Letters 3, 36-40 (August, 1963).

C. S. Kern and B. Feldman, "Stimulated Raman Emission," M.I.T. Lincoln Lab. Solid-State Res. Rept. 3, p. 18 (1964).

D. D. P. Bortfeld, M. Geller, and G. Eckhardt, "Combination Lines in the Stimulated Raman Spectrum of Styrene," J. Chem. Phys. 40, 1770-1771 (March 15, 1964).

E. J. A. Calviello and Z. H. Heller, "Raman Laser Action in Mixed Liquids," Appl. Phys. Letters 5, 112-113 (September 1964).

F. R. W. Minck, R. W. Terhune, and W. G. Rado, "Laser-Stimulated Raman Effect and Resonant Four-Photon Interactions in Gases H_2 , D_2 , and CH_4 ," Appl. Phys. Letters 3, 181-184 (November 15, 1963).

G. V. A. Subov, M. M. Sushchinskii, and I. K. Shuvalton, "Investigation of the Excitation Threshold of Induced Raman Scattering," J. Exptl. Theoret. Phys. (USSR) 47, 784-786 (August 1964).

H. G. Eckhardt, "Selection of Raman Laser Materials," IEEE J. Quant. Electr. QE-2, 1-8 (January 1966).

I. D. L. Weinberg, "Stimulated Raman Emission in Crystals and Organic Liquids," M.I.T. Lincoln Lab. Solid-State Res. Rept. 2, p. 31 (1965).

J. J. J. Barrett and M. C. Tobin, "Stimulated Raman Emission Frequencies in 21 Organic Liquids," J. Opt. Soc. Amer. 56, 129-130 (January 1966).

K. P. E. Tannenwald and J. B. Thaxter, "Stimulated Brillouin and Raman Scattering in Quartz at 2.1° to 293° Kelvin," Science 134, 1319-1320 (December 9, 1966).

L. M. D. Martin and E. L. Thomas, "Infrared Difference Frequency Generation," IEEE J. Quant. Electr. QE-2, (August 1966).

APPENDIX B

REALITY PROOF FOR MATRIX ELEMENT PRODUCTS

Following is a proof that the matrix elements products $(\mu_i)_{12}(\mu_j)^*_{12}$, $(\alpha_{ij})_{12}(\alpha_{k\ell})^*_{12}$, and $(\mu_i)_{12}(\alpha_{jk})^*_{12}$ are real. From the definition of a matrix element we have

$$(\mu_i)_{12}(\alpha_{jk})^*_{12} = \langle 1|\mu_i|2\rangle\langle 1|\alpha_{jk}|2\rangle^* = \langle 1|\mu_i|2\rangle\langle 2|\alpha_{jk}|1\rangle \quad ,$$

where the second equality follows from the hermitian property of the operator μ_i. To the above we add and subtract the term $\langle 1|\mu_i|1\rangle\langle 1|\alpha_{jk}|1\rangle$, yielding

$$(\mu_i)_{12}(\alpha_{jk})^*_{12} = \sum_{n=1}^{2} \langle 1|\mu_i|n\rangle\langle n|\alpha_{jk}|1\rangle - \langle 1|\mu_i|1\rangle\langle 1|\alpha_{jk}|1\rangle \quad . \qquad (B.1)$$

Upon removal of the identify relation $I = \sum_{n=1}^{2} |n\rangle\langle n|$, (B.1) further reduces to

$$(\mu_i)_{12}(\alpha_{jk})^*_{12} = \langle 1|\mu_i\alpha_{jk}|1\rangle - \langle 1|\mu_i|1\rangle\langle 1|\alpha_{jk}|1\rangle \quad . \qquad (B.2)$$

In addition, by the rule for the hermitian conjugation of operators and the fact that μ_i and α_{jk} are individually hermitian, we have the relationship

$$(\mu_i\alpha_{jk})^\dagger = \alpha^\dagger_{jk}\,\mu^\dagger_i = \alpha_{jk}\,\mu_i \quad .$$

However, μ_i and α_{jk} are both functions of r alone and, hence, commuting observables. Therefore, the order of the operators may be reversed, yielding

$$(\mu_i\,\alpha_{jk})^\dagger = \mu_i\,\alpha_{jk} \quad ,$$

that is, the product is also hermitian.

Since the dipole moment, polarizability, and their product are hermitian, they are represented by hermitian matrices, the diagonal elements of which are real. Therefore, the product considered in (B.2) above, which is expressed entirely in terms of diagonal elements, must be real, thereby proving the assertion. The proof for the other products of interest follows identically.

APPENDIX C

STOKES WAVE VECTOR IN AN INFRARED-ACTIVE RAMAN-ACTIVE MEDIUM

Substitution of the assumed solutions

$$\tilde{E}_\nu = \tilde{\tilde{E}}_\nu e^{-i\underset{\sim}{k}_\nu \cdot \underset{\sim}{r}} \quad , \qquad \nu = v,\ L,\ s,$$

into the coupled-wave equations

$$\nabla \times (\nabla \times \tilde{E}_v) - \frac{\omega_v^2 \epsilon_v^*}{c^2} \tilde{E}_v^* = \frac{4\pi\omega_v^2}{c^2} \chi_P \tilde{E}_L^* \tilde{E}_s \quad ,$$

$$\nabla \times (\nabla \times \tilde{E}_s) - \frac{\omega_s^2 \epsilon_\infty^s}{c^2} \tilde{E}_s = \frac{4\pi\omega_s^2}{c^2} (\chi_P \tilde{E}_v^* \tilde{E}_L + \chi_R |\tilde{E}_L|^2 E_s) \quad ,$$

yields

$$\left(k_v^{*2} - \frac{\omega_v^2 \epsilon_v^*}{c^2}\right) \tilde{\tilde{E}}_v^* = \frac{4\pi\omega_v^2}{c^2} \chi_P \tilde{\tilde{E}}_L^* \tilde{\tilde{E}}_s \qquad (C.1)$$

$$\left(k_s^2 - \frac{\omega_s^2 \epsilon_\infty^s}{c^2}\right) \tilde{\tilde{E}}_s = \frac{4\pi\omega_s^2}{c^2} (\chi_P \tilde{\tilde{E}}_L \tilde{\tilde{E}}_v^* + \chi_R |\tilde{\tilde{E}}_L|^2 \tilde{\tilde{E}}_s) \quad . \qquad (C.2)$$

In the derivation of (C.1) and (C.2) exponential balance imposes the condition

$$\underset{\sim}{k}_v^* = \underset{\sim}{k}_L - \underset{\sim}{k}_s \quad ,$$

where $\underset{\sim}{k}_L$ is assumed real since laser depletion is ignored.

The substitution of (C.2) into (C.1) yields

$$k_s^2 = \frac{\omega_s^2 \epsilon_\infty^s}{c^2}\left[1 + \frac{4\pi}{\epsilon_\infty^s}\chi_R|\tilde{E}_L|^2 + \frac{16\pi^2 \omega_v^2 \chi_P^2 |\tilde{E}_L|^2}{c^2 \epsilon_\infty^s (k_v^{*2} - k_v^{o*2})}\right] ,$$

where $k_v^{o*2} = \frac{\omega_v^2}{c^2}\epsilon_v^*$ is the dispersion relationship for an infrared wave as obtained from a measurement of the absorption and dispersion properties of the medium in the absence of laser and Stokes fields. [See discussion leading to Eq. (3.11).]

Since the nonlinear susceptibilities χ_R and χ_P are small, the square root can be taken by means of the approximation $\sqrt{1 + x} \approx 1 + x/2$, giving

$$k_s = \frac{\omega_s \sqrt{\epsilon_\infty^s}}{c} + \frac{2\pi\omega_s \chi_R |\tilde{E}_L|^2}{c\sqrt{\epsilon_\infty^s}} + \frac{8\pi^2 \omega_v^2 \omega_s \chi_P^2 |\tilde{E}_L|^2}{c^3 \sqrt{\epsilon_\infty^s}\,(k_v^{*2} - k_v^{o*2})} .$$

APPENDIX D

COMPARISON OF RAMAN AND NEAR-RESONANT PARAMETRIC GAINS

The resonant Raman and near-resonant parametric gains are given by Eqs. (4.16) and (4.29), respectively:

$$\alpha_R(\Omega) = \frac{4\pi^2 \chi_R''(\Omega) \left|\tilde{E}_L\right|^2}{n_s \lambda_s} \quad , \tag{D.1}$$

$$\alpha_{PR} = \frac{16\pi^4 \chi_P'^2 \left|\tilde{E}_L\right|^2}{n_s n_v \lambda_s \lambda_v \alpha_v} \quad , \tag{D.2}$$

where α_v is the infrared wave loss constant $\alpha_v \triangleq |k_v^{o''}|$.

The infrared wave propagation constant, given by Eqs. (3.1) and (4.8), is

$$k_v^{o2} = \frac{\omega_v^2 \epsilon_v}{c^2} = \frac{\omega_v^2}{c^2} (\epsilon_v^\infty + 4\pi \chi_v) \quad .$$

In the region outside the line, $\chi_v = \chi_v' + i\chi_v''$ is small relative to ϵ_v^∞ , and therefore the square root expansion $\sqrt{1 + x} \approx 1 + x/2$ can be used to obtain

$$\alpha_v = \frac{4\pi^2 |\chi_v'|}{\lambda_v \sqrt{\epsilon_\infty^v}} \quad . \tag{D.3}$$

Taking into account the Lorentzian lineshape factors for the susceptibilities given in Eqs. (4.5) – (4.7), and invoking the near-resonance condition $\Omega^2 - \omega^2 \approx 2\Omega(\Omega - \omega)$, the susceptibility terms which appear in

the above equations can be written in the form

$$\chi_V'' \approx \chi_V''(\Omega) \frac{\gamma^2/4}{(\Omega - \omega_V)^2} \quad , \qquad (D.4)$$

$$\chi_P' \approx \chi_P''(\Omega) \frac{\gamma/2}{(\Omega - \omega_V)} \quad ,$$

where outside the line $(\Omega - \omega_V)^2 \gg \gamma^2/4$.

Combination of (D.1) – (D.4) then leads to the result

$$\frac{\alpha_{PR}}{\alpha_R(\Omega)} \approx \frac{\sqrt{\epsilon_\infty}}{n_V} \frac{[\chi_P''(\Omega)]^2}{\chi_R''(\Omega)\,|\chi_V''(\Omega)|} \quad .$$

APPENDIX E

STOKES GAIN AND THRESHOLD IN A FOCUSED GAUSSIAN BEAM

In this appendix we consider the effect of focusing of the laser beam on the Raman gain of a system. The beam profile will be taken to be that of the lowest order gaussian mode after some preliminary justification of this choice.

Wave Equation

We begin with the wave equation for the electric field in a medium of refractive index n, assuming no sources present,

$$\nabla^2 \underset{\sim}{E} - \frac{n^2}{c^2} \frac{\partial^2 \underset{\sim}{E}}{\partial t^2} = 0 \quad . \tag{E.1}$$

For an optical beam with finite transverse dimensions propagating in the z direction, we assume a solution of the form

$$\underset{\sim}{E} = \frac{1}{2} \underset{\sim}{\tilde{E}}(x,y,z)\, e^{i(\omega t - kz)} + \text{c.c.} \quad , \tag{E.2}$$

where $k = 2\pi n/\lambda$, λ is the free space wavelength, c.c. denotes complex conjugate, and $\underset{\sim}{\tilde{E}}(x,y,z)$ is a slowly varying function of the spatial coordinates. If it is further assumed that slow spatial variations in the z direction can be neglected with respect to those in the transverse plane, i.e., $\partial^2 \underset{\sim}{E}/\partial z^2 \ll \partial^2 \underset{\sim}{E}/\partial x^2$, $\partial^2 \underset{\sim}{E}/\partial y^2$, substitution of (E.2) into (A.1) yields

$$\frac{\partial^2 \underset{\sim}{E}}{\partial x^2} + \frac{\partial^2 \underset{\sim}{E}}{\partial y^2} - 2ik \frac{\partial \underset{\sim}{E}}{\partial z} = 0 \quad . \tag{E.3}$$

Fundamental Gaussian Mode

For a simple beam we look for a solution with cylindrical symmetry and with peak intensity along the z axis. By substitution it can be shown that the following expression which meets these requirements is an

acceptable solution,

$$\underset{\sim}{\tilde{E}} = \underset{\sim}{A} \frac{\exp\left[-\dfrac{r^2}{w_0^2(1+\xi^2)}(1+i\xi)\right]}{1 - i\xi} \quad .$$

The corresponding beam intensity (proportional to $|\underset{\sim}{\tilde{E}}|^2$) can be written in the form

$$I(r,z) = B \frac{e^{-2r^2/w^2}}{(w/w_0)^2} \quad , \qquad \text{(E.4)}$$

where all the pertinent quantities are described in the caption accompanying Fig. E.1.

With the beam intensity given by (E.4), it is a simple matter to express the intensity in terms of the total power P carried by the beam;

$$P = 2\pi \int_0^\infty r\, I(r,z)\, dr = \frac{2\pi B}{(w/w_0)^2} \int_0^\infty r\, e^{-2r^2/w^2}\, dr = \frac{\pi w_0^2 B}{2} \quad .$$

Therefore, we have

$$\boxed{I(r,z) = \frac{2P}{\pi w(z)^2} e^{-2r^2/w(z)^2}} \quad . \qquad \text{(E.5)}$$

In order to select mirrors for cavities to contain such beams, it is also necessary to know the radii of curvature of surfaces of constant phase,

$$R = z(1 + 1/\xi^2) \quad .$$

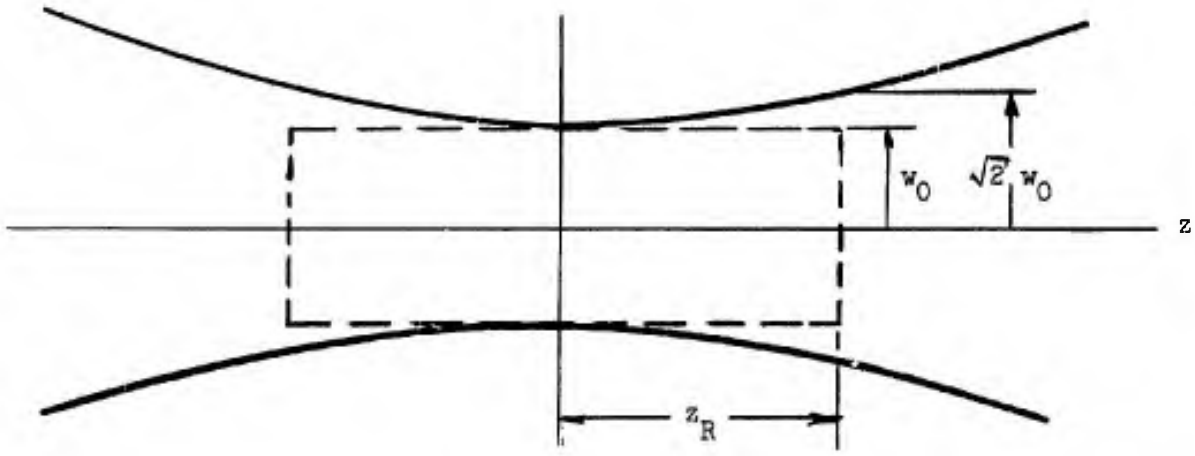

FIG. E.1—Gaussian beam profile. The quantity $w = w_0\sqrt{1 + \xi^2}$ is the beam radius or "spot size" which is the radius at which the intensity drops to $e^{-2} = 0.135$ its on-axis value, w_0 is the beam radius at the "waist" where the beam contracts to its minimum diameter, $\xi = z/z_R$ is the normalized axial distance measured from the beam waist position, and $z_R = \pi w_0^2 n/\lambda$ is the distance along the axis at which the beam intensity drops to one-half its value at the waist as a result of the beam spreading to twice the area of the waist. The quantity z_R is often called the "Rayleigh Range", a term borrowed from antenna theory.

In the region of the waist ($\xi^2 \ll 1$) the beam radius is essentially constant and the wavefronts of equal phase are nearly planar (infinite radius of curvature). In this region, therefore, the beam can be considered to be a columnar beam with gaussian intensity distribution and constant phase in the transverse plane. At distances far from the waist ($\xi^2 \gg 1$) , the beam maintains its gaussian intensity distribution in the transverse plane, but now appears as a diverging beam of half angle $\theta = \lambda/\pi w_0 n$ with spherical wavefronts appearing to emanate from a point source at $z = 0$.

The above is a description of the lowest order or "fundamental" gaussian mode solution to (E.3). The solution is applicable both to beams propagating freely in a medium and to beams confined in an optical resonator. Beams of more complicated transverse structure can be described in terms of a superposition which includes higher order modes consisting of products of hermite and gaussian functions. For further information and discussion see Kogelnik and Li [Proc. IEEE 54, 1312 (1966)].

Focused Gaussian Beam

The effect of using a converging lens to focus a gaussian beam is simply to alter the beam parameters such that the beam waist and Rayleigh range near the focus take on values appropriate to the degree of focusing; in particular, the beam maintains its gaussian intensity distribution. Therefore, the previous considerations apply equally to a focused or unfocused beam. The parameters applicable to a focused gaussian beam are presented and discussed in Figs. E.2 and E.3.

Stokes Gain and Threshold

The growth equation for the Stokes intensity I_s in the presence of a laser beam is given by Eq. (4.31),

$$\frac{dI_s}{dz} = g_s I_s \quad , \tag{E.6}$$

where g_s is the Stokes gain per unit length which is proportional to the laser intensity,

$$g_s = K I_L \quad . \tag{E.7}$$

If the laser beam is assumed to be a focused gaussian beam without depletion, the integrated Stokes gain over a length L centered on the waist, along the axis where the intensity is greatest, is, from (E.5) – (E.7),

$$\bar{g}_s L \triangleq \int_{-L/2}^{L/2} g_s(z)dz = K \int_{-L/2}^{L/2} I_L(0,z)dz = \frac{4Kn_L P_L}{\lambda_L} \tan^{-1}\left(\frac{L}{2z_R}\right) ,$$

where the subscript L refers to the laser.

In order for stimulated Stokes emission to occur in a cavity the single pass gain $\bar{g}\,L$ must overcome the single pass loss ϵ, yielding a threshold laser power,

$$\boxed{(P_L)_{th} = \frac{\lambda_L \epsilon}{4Kn_L} \frac{1}{\tan^{-1}(L/2z_R)}} \quad . \tag{E.8}$$

The significance and interpretation of the above expression is contained in the caption accompanying the plot in Fig. E.4.

FIG. E.2--Focused gaussian beam diameter. Placement of a converging lens of focal length f in the waist region of a gaussian beam of diameter $d_0 = 2w_0$ brings the beam to focus (in air) with a diameter

$$d_0' = 2w_0' = \frac{4}{\pi}\left(\frac{f}{d_0}\right)\lambda \quad .$$

If the beam passes through an air-dielectric interface before coming to focus (e.g., focusing in a crystal), the spot size w_0' at the focused waist remains the same size as when focused in air although the position of the waist shifts its location in accordance with geometrical optics.

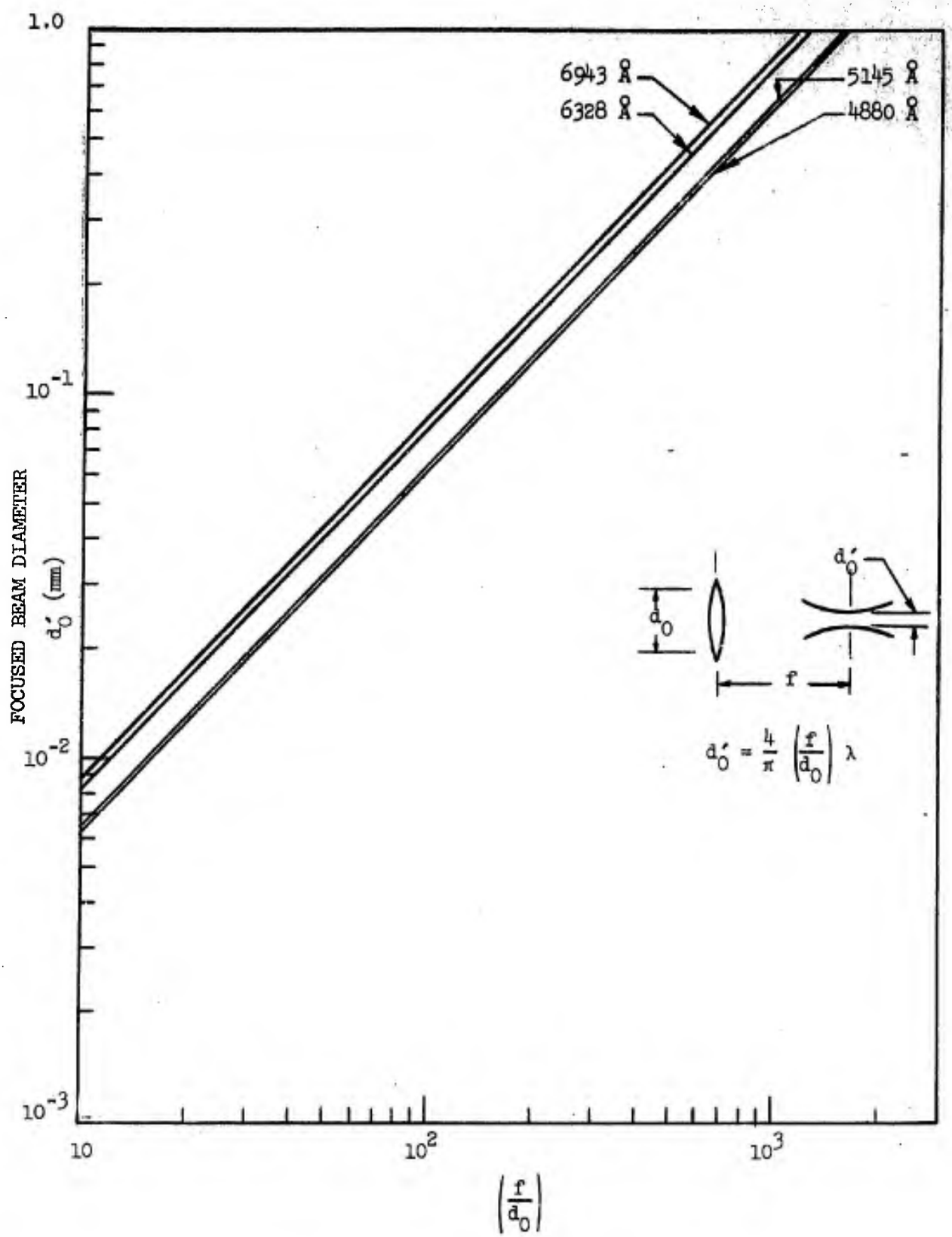
1.0
10^{-1}
10^{-2}
10^{-3}
FOCUSED BEAM DIAMETER
d_0' (mm)
6943 Å
6328 Å
5145 Å
4880 Å
d_0
d_0'
f
$d_0' = \frac{4}{\pi}\left(\frac{f}{d_0}\right)\lambda$
10
10^2
10^3
$\left(\frac{f}{d_0}\right)$

FIGURE E.2

FIG. E.3--Focused gaussian beam "interaction length" $2z_R$. Placement of a converging lens of focal length f in the waist region of a gaussian beam of diameter $d_0 = 2w_0$ brings the beam to focus in air with a Rayleigh Range

$$z'_R = \frac{4}{\pi}\left(\frac{f}{d_0}\right)^2 \lambda \quad .$$

If the beam passes through an air-dielectric interface before coming to focus as in a crystal, the Rayleigh Range is increased over that in air by the factor n where n is the index of refraction of the medium in which the beam is focused.

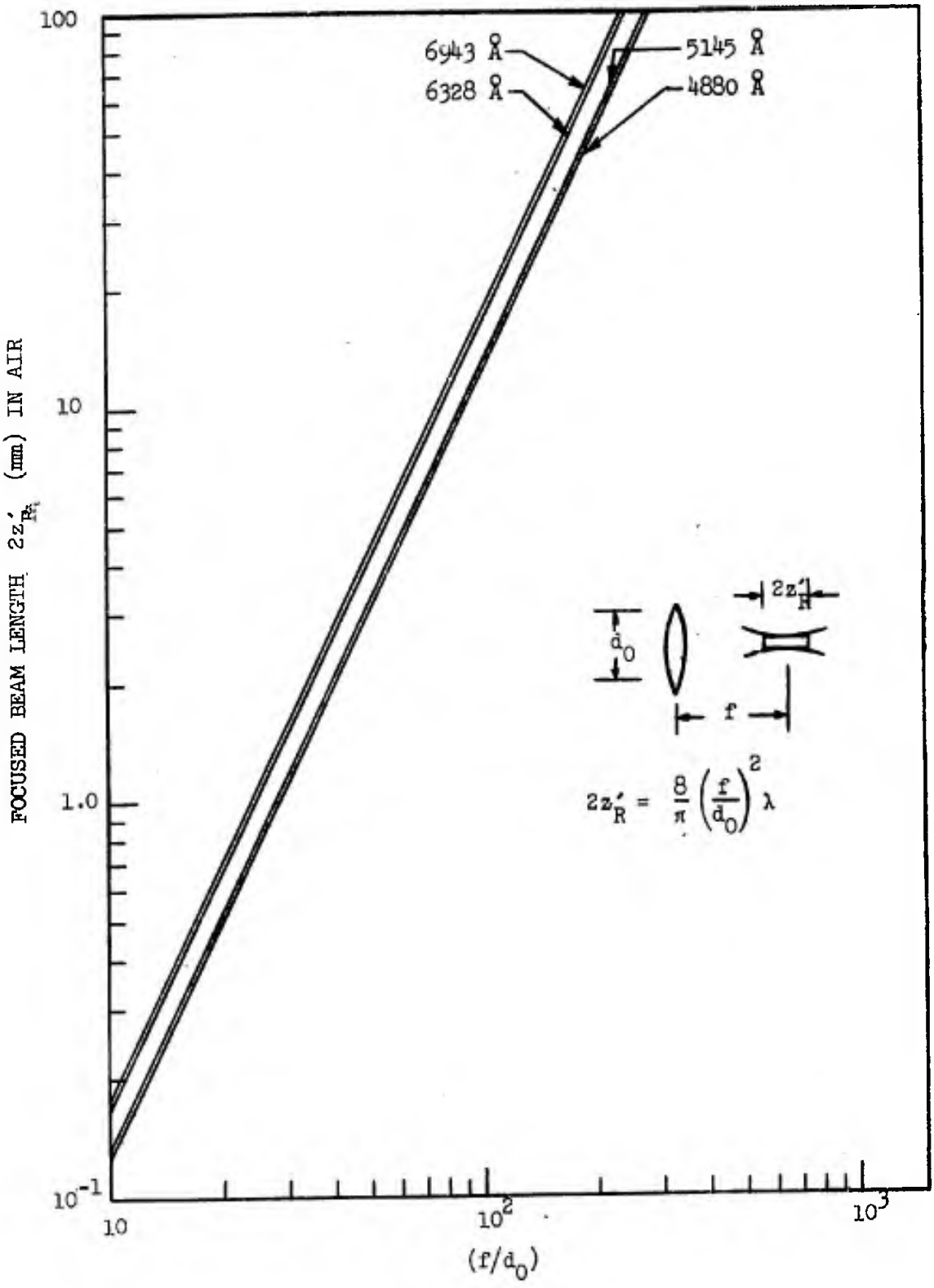
100
10
1.0
10^{-1}
10
10^2
10^3
(f/d_0)
FOCUSED BEAM LENGTH $2z'_R$ (mm) IN AIR
6943 Å
6328 Å
5145 Å
4880 Å
$2z'_R$
d_0
f
$2z'_R = \frac{8}{\pi}\left(\frac{f}{d_0}\right)^2 \lambda$

FIGURE E.3

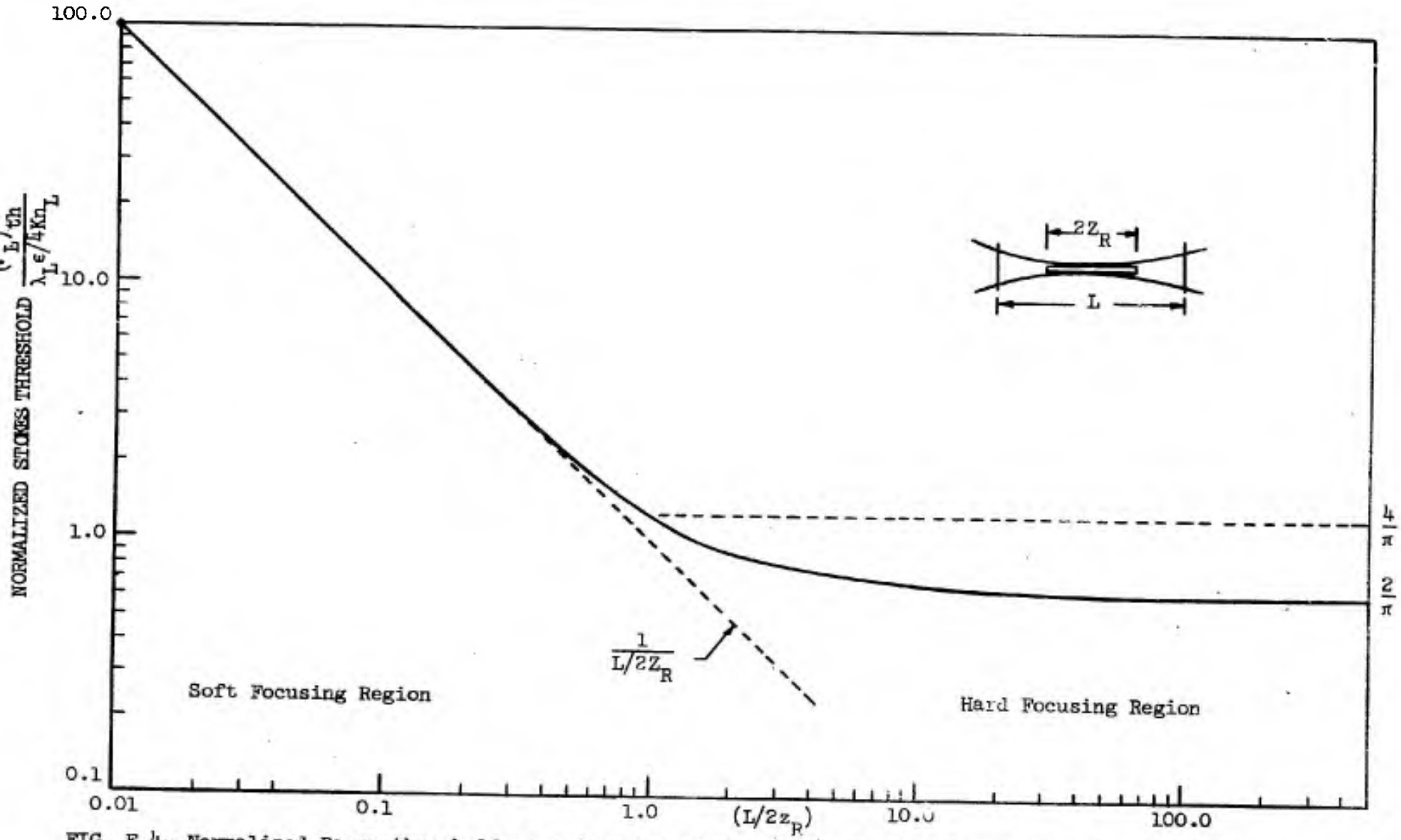

FIG. E.4--Normalized Raman threshold as a function of the degree of focusing. Once the Rayleigh Range z_R is brought within the Raman medium by focusing $(L/2z_R = 1)$, further focusing can, at most, reduce the threshold by another factor of 2.

REFERENCES

1. C. V. Raman and R. S. Krishnan, Nature 121, 501 (1928).
2. G. Landsberg and L. Mandelstam, Naturwissenschaften 16, 557 (1928).
3. E. J. Woodbury and W. K. Ng, Proc. IRE (Corres.) 50, 2367 (1962).
4. G. Eckhardt, R. W. Hellwarth, F. J. McClung, S. E. Schwarz, and D. Weiner, Phys. Rev. Letters 9, 455 (1962).
5. E. J. Woodbury, in Quantum Electronics Proceedings of the Third International Congress, ed. by P. Grivet and N. Bloembergen, Columbia University Press, New York, vol. 2, 1576 (1964).
6. M. Geller, D. P. Bortfeld, and W. R. Sooy, Appl. Phys. Letters 3, 36 (1963).
7. B. P. Stoicheff, Phys. Letters 7, 186 (1963).
8. G. Eckhardt, D. P. Bortfeld, and M. Geller, Appl. Phys. Letters 3, 136 (1963).
9. R. W. Minck, R. W. Terhune, and W. G. Rado, Appl. Phys. Letters 3, 181 (1963).
10. R. W. Hellwarth, Phys. Rev. 130, 1850 (1963).
11. R. W. Hellwarth, Appl. Optics 2, 847 (1963).
12. H. J. Zeiger and P. E. Tannenwald, Quantum Electronics Proceedings of the Third International Congress, ed. by P. Grivet and N. Bloembergen, Columbia University Press, New York, vol. 2, 1588 (1964).
13. E. Garmire, F. Pandarese, and C. H. Townes, Phys. Rev. Letters 11, 160 (1963).
14. G. Eckhardt, IEEE J. Quant. Electr. QE-2, 1 (1966).
15. M. D. Martin and E. L. Thomas, IEEE J. Quant. Electr. QE-2, 196 (1966).
16. N. Bloembergen and Y. R. Shen, Phys. Rev. Letters 13, 720 (1964).
17. P. Lallemand and N. Bloembergen, Appl. Phys. Letters 6, 210 (1965).
18. P. Lallemand and N. Bloembergen, Appl. Phys. Letters 6, 212 (1965).

19. N. Bloembergen and P. Lallemand, Physics of Quantum Electronics Conference Proceedings, ed. by P. L. Kelley, B. Lax, and P. E. Tannenwald, McGraw-Hill Book Company, New York, 137 (1966).
20. F. J. McClung, W. G. Wagner, and D. Weiner, Physics of Quantum Electronics Conference Proceedings, ed. by P. L. Kelley, B. Lax, and P. E. Tannenwald, McGraw-Hill Book Company, New York, 155 (1966).
21. G. Bret and G. Mayer, Physics of Quantum Electronics Conference Proceedings, ed. by P. L. Kelley, B. Lax, and P. E. Tannenwald, McGraw-Hill Book Company, New York, 155 (1966).
22. F. J. McClung, W. G. Wagner, and D. Weiner, Phys. Rev. Letters 15, 96 (1965).
23. D. Weiner, S. E. Schwarz, and F. J. McClung, J. Appl. Phys. 36, 2395 (1965).
24. F. J. McClung and D. Weiner, J. Opt. Soc. Am. 54, 641 (1964).
25. T. C. Damen, R.C.C. Leite, and S.P.S. Porto, Phys. Rev. Letters 14, 9 (1965).
26. H. Takuma and D. A. Jennings, Appl. Phys. Letters 4, 185 (1964).
27. J. H. Dennis and P. E. Tannenwald, Appl. Phys. Letters 5, 58 (1964).
28. D. P. Bortfeld and W. R. Sooy, Appl. Phys. Letters 7, 283 (1965).
29. R. Y. Chiao, E. Garmire, and C. H. Townes, Phys. Rev. Letters 13, 479 (1964).
30. N. F. Pilipetskii and A. R. Rustamov, JETP Letters 2, 55 (1965).
31. P. L. Kelley, Phys. Rev. Letters 15, 1005 (1965).
32. Y. R. Shen and Y. J. Shaham, Phys. Rev. Letters 15, 1008 (1965).
33. P. Lallemand and N. Bloembergen, Phys. Rev. Letters 15, 1010 (1965).
34. C. C. Wang, Phys. Rev. Letters 16, 344 (1966).
35. E. Garmire, R. Y. Chiao, and C. H. Townes, Phys. Rev. Letters 16, 347 (1966).
36. N. Bloembergen and P. Lallemand, IEEE J. Quant. Electr. QE-2, 246 (1966).
37. D. H. Close, C. R. Giuliano, R. W. Hellwarth, L. D. Hess, F. J. McClung, and W. G. Wagner, IEEE J. Quant. Electr. QE-2, 553 (1966).
38. A. Javan and P. L. Kelley, IEEE J. Quant. Electr. QE-2, 470 (1966).

39. R. Y. Chiao, M. A. Johnson, S. Krinsky, H. A. Smith, C. H. Townes, and E. Garmire, IEEE J. Quant. Electr. QE-2, 467 (1966).

40. C. C. Wang, Phys. Rev. 152, 149 (1966).

41. R. W. Hellwarth, Phys. Rev. 152, 152 (1966).

42. B. G. Huth, N. V. Karlov, R. H. Pantell, and H. E. Puthoff, Microwave Laboratory Report No. 1445, Stanford University (1966).

43. B. G. Huth, N. V. Karlov, R. H. Pantell, and H. E. Puthoff, Microwave Laboratory Report No. 1447, Stanford University (1966).

44. B. G. Huth, N. V. Karlov, R. H. Pantell, and H. E. Puthoff, Pres. 24th Conference on Electron Device Research, Pasadena, Calif., June, 1966.

45. B. G. Huth, N. V. Karlov, R. H. Pantell, and H. E. Puthoff, Proc. Sixth International Conference on Microwave and Optical Generation and Amplification, Cambridge, England, September, 1966.

46. B. G. Huth, N. V. Karlov, R. H. Pantell, and H. E. Puthoff, IEEE J. Quant. Electr. QE-2, 763 (1966). See also B. G. Huth, Microwave Laboratory Report No. 1542, Stanford University (1967).

47. L. E. Hargrove, R. L. Fork, and M. A. Pollack, Appl. Phys. Letters 5, 4 (1964).

48. K. Gürs and R. Muller, Optical Masers (Microwave Research Institute Symposia Series), Polytechnic Press, vol. 13, 243 (1963).

49. H. W. Mocker and R. J. Collins, Appl. Phys. Letters 7, 270 (1965).

50. A. Yariv, J. Appl. Phys. 36, 388 (1965).

51. M. H. Crowell, IEEE J. Quant. Electr. QE-1, 12 (1965).

52. M. DiDomenico, Jr., J. Appl. Phys. 35, 2870 (1964).

53. S. E. Harris and O. P. McDuff, IEEE J. Quant. Electr. QE-1, 245 (1966).

54. R. H. Pantell and R. L. Kohn, IEEE J. Quant. Electr. QE-2, 306 (1966).

55. R. H. Pantell, B. G. Huth, H. E. Puthoff, R. L. Kohn, Microwave Laboratory Report No. 1443, Stanford University (1966).

56. R. H. Pantell, B. G. Huth, H. E. Puthoff, R. L. Kohn, Appl. Phys. Letters 9, 104 (1966).

57. R. Loudon, Proc. Phys. Soc. 82, 393 (1963).

58. R. H. Pantell and H. E. Puthoff, Proposal to the Office of Naval Research for Continuation of Microwave Research under Contract Nonr 225(48), NR 373-361, for Period 1 January 1965 – 31 December 1965, Microwave Laboratory Proposal, Stanford University (1964).
59. C. Kittel, Quantum Theory of Solids (John Wiley and Sons, Inc., New York, 1963), pp. 37 ff.
60. J. J. Hopfield, Phys. Rev. 112, 1555 (1958).
61. K. Huang, Proc. Roy. Soc. (London) A208, 352 (1951).
62. M. Born and K. Huang, Dynamical Theory of Crystal Lattices (Clarendon Press, Oxford, 1954), pp. 82 ff.
63. A. S. Barker, Jr., Phys. Rev. 136, A1290 (1964).
64. B. G. Huth, R. H. Pantell, and H. E. Puthoff, Pres. Spring Meeting Electrochemical Society, San Francisco, Calif. (May, 1965).
65. H. E. Puthoff, R. H. Pantell, and B. G. Huth, Microwave Laboratory Report No. 1363, Stanford University (1965).
66. H. E. Puthoff, R. H. Pantell, and B. G. Huth, J. Appl. Phys. 37, 860 (1966).
67. C H. Henry and J. J. Hopfield, Phys. Rev. Letters 15, 964 (1965).
68. S.P.S. Porto, B. Tell, and T.C. Damen, Phys. Rev. Letters 16, 450 (1966).
69. W. L. Faust and C. H. Henry, Phys. Rev. Letters 17, 1265 (1966).
70. H. E. Puthoff, R. H. Pantell, B. G. Huth, and M. Chacon, Microwave Laboratory Report No. 1529, Stanford University (1967).
71. E. T. Jaynes, Microwave Laboratory Report No. 502, Stanford University (1958).
72. E. T. Jaynes and F. W. Cummings, Proc. IEEE 51, 89 (1963).
73. G. Eckhardt, IEEE J. Quant. Electr. QE-2, 1 (1966).
74. M. Born and M. Bradburn, Proc. Roy. Soc.A 188, 161 (1947).
75. H. Smith, Phil. Trans. Roy. Soc. A 241, 105 (1948).
76. M. Born and K. Huang, Dynamical Theory of Crystal Lattices (Clarendon Press, Oxford, 1954), pp. 367 ff.
77. J. F. Nye, Physical Properties of Crystals (Clarendon Press, Oxford, 1957), pp. 74, 182.
78. R. H. Pantell and H. E. Puthoff, Quantum Analysis, Stanford University Classnotes, 1967.

79. N. Bloembergen, Nonlinear Optics (W. A. Benjamin, Inc., New York, 1965), p. 68.
80. Reference 79, pp. 68, 192.
81. G. Herzberg, Infrared and Raman Spectra of Polyatomic Molecules, vol. 2, (D. Van Nostrand Company, Inc., New York, 1945).
82. C. Kittel, Quantum Theory of Solids (John Wiley and Sons, Inc., New York, 1963), pp. 37 ff.
83. J. J. Hopfield, Phys. Rev. 112, 1555 (1958).
84. K. Huang, Proc. Roy. Soc. (London) A208, 352 (1951).
85. M. Born and K. Huang, Dynamical Theory of Crystal Lattices (Clarendon Press, Oxford, 1954), pp. 82 ff.
86. A. S. Barker, Jr., Phys. Rev. 136, A1290 (1964).
87. P. N. Butcher, R. Loudon, and T. P. McLean, Proc. Phys. Soc. 85, 565 (1965).
88. J. C. Slater, Microwave Electronics (D. Van Nostrand, Inc., Princeton, 1950), p. 66.
89. T. C. Damen, R.C.C. Leite, and S.P.S. Porto, Phys. Rev. Letters 14, 9 (1965).
90. Y. Shiozaki and T. Mitsui, J. Phys. Chem. Solids 24, 1057 (1963).
91. A. S. Barker, Jr., and R. Loudon, private communication.
92. G. Herzberg, Infrared and Raman Spectra of Polyatomic Molecules, vol. 2 (D. Van Nostrand Company Inc., New York, 1945), p. 82.
93. Ibid., p. 105, 106.
94. Ibid., p. 109.
95. J. D. Axe and D. F. O'Kane, Appl. Phys. Letters 9, 58 (1966).
96. R. F. Schaufele and M. J. Weber, Phys. Rev. 152, 705 (1966).
97. R. Loudon, Adv. in Physics 13, 423 (1964).
98. P. N. Butcher, Nonlinear Optical Phenomena, Bulletin 200, Engineering Experiment Station, Ohio State University, Columbus, Ohio (1965).
99. A. Ashkin, G. D. Boyd, and J. M. Dziedzic, IEEE J. Quant. Electr. QE-2, 109 (1966).
100. G. D. Boyd and A. Ashkin, Phys. Rev. 146, 187 (1966).
101. I. P. Kaminow and W. D. Johnston, Jr., to be published.